Fermilab

FERMILAB-PUB-08-003-A-CD

The SEGUE Stellar Parameter Pipeline. II. Validation with Galactic Globular and Open Clusters

Young Sun Lee, Timothy C. Beers, Thirupathi Sivarani

Department of Physics & Astronomy, CSCE: Center for the Study of Cosmic Evolution, and JINA: Joint Institute for Nuclear Astrophysics, Michigan State University, East Lansing, MI 48824, USA

lee@pa.msu.edu, beers@pa.msu.edu, thirupathi@pa.msu.edu

Jennifer A. Johnson, Deokkeun An

Department of Astronomy, Ohio State University, Columbus, OH 43210

jaj@astronomy.ohio-state.edu, deokkeun@astronomy.ohio-state.edu

Ronald Wilhelm

Department of Physics, Texas Tech University, Lubbock, TX 79409

ron.wilhelm@ttu.edu

Carlos Allende Prieto, Lars Koesterke

Department of Astronomy, University of Texas, Austin, TX 78712

callende@astro.as.utexas.edu

Paola Re Fiorentin

Max Planck Institut für Astronomie, Königstuhl 17, 69117 Heidelberg, Germany

fiorent@mpia-hd.mpg.de

Coryn A.L. Bailer-Jones

Max Planck Institut für Astronomie, Königstuhl 17, 69117 Heidelberg, Germany

calj@mpia-hd.mpg.de

John E. Norris

Research School of Astronomy and Astrophysics,
Australian National University, Weston, ACT 2611, Australia

jen@mso.anu.edu.au

Brian Yanny

Fermi National Accelerator Laboratory,
Batavia, IL 60510

yanny@fnal.gov

Constance Rockosi

Department of Astronomy,
University of California, Santa Cruz, CA 95064

crockosi@ucolick.org

Heidi J. Newberg

Department of Physics & Astronomy,
Rensselaer Polytechnical Institute, Troy, NY 12180

newbeh@rpi.edu

Kyle M. Cudworth

Yerkes Observatory,
The University of Chicago, Williams Bay, WI 53191

kmc@yerkes.uchicago.edu

Kaike Pan

Apache Point Observatory,
Apache Point Observatory, P. O. Box 59, Sunspot, NM 88349

kpan@apo.nmsu.edu

ABSTRACT

We validate the performance and accuracy of the current SEGUE (Sloan Extension for Galactic Understanding and Exploration) Stellar Parameter Pipeline (SSPP), which determines stellar atmospheric parameters (effective temperature, surface gravity, and metallicity) by comparing derived overall metallicities and radial velocities from selected likely members of three globular clusters (M 13, M 15, and M 2) and two open clusters (NGC 2420 and M 67) to the literature values. Spectroscopic and photometric data obtained during the course of the original Sloan Digital Sky Survey (SDSS-I) and its first extension (SDSS-II/SEGUE) are used to determine stellar radial velocities and atmospheric parameter estimates for stars in these clusters. Based on the scatter in the metallicities derived for the members of each cluster, we quantify the typical uncertainty of the SSPP values, $\sigma([\mathrm{Fe/H}]) = 0.13$ dex for stars in the range of 4500 K $\leq T_{\rm eff} \leq$ 7500 K and $2.0 \leq \log g \leq 5.0$, at least over the metallicity interval spanned by the clusters studied ($-2.3 \leq$ [Fe/H] < 0). The surface gravities and effective temperatures derived by the SSPP are also compared with those estimated from the comparison of the color-magnitude diagrams with stellar evolution models; we find satisfactory agreement. At present, the SSPP underestimates [Fe/H] for near-solar-metallicity stars, represented by members of M 67 in this study, by $\sim$ 0.3 dex.

Subject headings: methods: data analysis — stars: abundances, fundamental parameters — surveys — techniques: spectroscopic

1. Introduction

The Sloan Extension for Galactic Understanding and Exploration (SEGUE) is one of three key projects (LEGACY, SUPERNOVA SURVEY, and SEGUE) in the current extension of the Sloan Digital Sky Survey, known collectively as SDSS-II. The SEGUE program is in the process of obtaining *ugriz* imaging of some 3500 square degrees of sky outside of the SDSS-I footprint (Fukugita et al. 1996; Gunn et al. 1998, 2006; York et al. 2000; Stoughton et al. 2002; Abazajian et al. 2003, 2004, 2005; Pier et al. 2003), with special attention being given to scans of lower Galactic latitudes ($|b| < 35°$) in order to better probe the disk/halo interface of the Milky Way. SEGUE is also obtaining $R \simeq 2000$ spectroscopy over the wavelength range $3800 - 9200$ Å for some 250,000 stars in 200 selected areas over the sky available from Apache Point, New Mexico.

The SEGUE Stellar Parameter Pipeline (hereafter, SSPP) processes the wavelength- and flux-calibrated spectra generated by the standard SDSS spectroscopic reduction pipeline (Stoughton et al. 2002), obtains equivalent widths and/or line indices for 77 atomic or molecular absorption lines, and estimates $T_{\rm eff}$, log g, and [Fe/H] through the application of a number of approaches. The current techniques employed by the SSPP include a minimum distance method (Allende Prieto et al. 2006), neural network analysis (Bailer-Jones 2000; Willemsen et al. 2005; Re Fiorentin et al. 2007), auto-correlation analysis (Beers et al. 1999), and a variety of line index calculations based on previous calibrations with respect to known standard stars (Beers et al. 1999; Cenarro et al. 2001a,b; Morrison et al. 2003). The SSPP employs five different methods for estimation of $T_{\rm eff}$, eight for estimation of log g, and nine for estimation of [Fe/H]. Details of the methods used are discussed in detail by Lee et al. (2007a, hereafter Paper I). The use of multiple methods allows for empirical determinations of the internal errors for each parameter, based on the range of reported values – typical internal errors for stars in the temperature range 4500 K $\leq T_{\rm eff} \leq$ 7500 K are $\sim$ 73 K, $\sim$ 0.19 dex, and $\sim$ 0.10 dex, in $T_{\rm eff}$, log g, and [Fe/H], respectively. Allende Prieto et al. (2007, hereafter Paper III) point out that the internal uncertainties provided by the SSPP underestimate the typical random errors at high signal-to-noise (S/N) ratios because most methods in the SSPP make use of similar parameter indicators (e.g., hydrogen lines for effective temperature) and similar atmospheric models. Paper III empirically determines empirically external uncertainties of $\sim$ 130 K, $\sim$ 0.21 dex, and $\sim$ 0.11 dex, for $T_{\rm eff}$, log g, and [Fe/H], respectively, by comparison with high-resolution spectroscopy ($7000 < R < 45,000$) of brighter SDSS-I/SEGUE that have been obtained with 8m$-$10m class telescopes. Somewhat larger errors apply to stars with temperatures near the extremes of the range above. The present study of Galactic globular and open cluster stars tests the SSPP's ability to derive accurate results for stars with a wide range of temperatures and gravities appropriate for metal-poor and near-solar-metallicity stellar populations in the Galaxy, and demonstrates that the derived metallicity scale is identical for dwarfs and giants.

Although the SSPP will continue to evolve in the near future, it has been frozen for now at the version used for obtaining results for stars with suitable data from SDSS Data Release 6 (DR-6; Adelman-McCarthy et al. 2007b). Previous versions of the SSPP have already been used for the analysis of SDSS-I observations. For example, Allende Prieto et al. (2006) report on the application of one of the methods included in the SSPP to some 20,000 F- and G-type stars from SDSS-I DR-3 (Abazajian et al. 2005). Beers et al. (2006) have compiled a list of over 6000 stars with [Fe/H] < -2.0 (including several hundred with [Fe/H] < -3.0), based on application of the present SSPP to some 200,000 stars from SDSS-I DR-5 (Adelman-McCarthy et al. 2007a). Carollo et al. (2007) reports on an analysis of the kinematics of relatively bright stars from SDSS-I that have been used as calibration objects

during the main survey.

In this paper, the second in the SSPP series, we show that estimates of the atmospheric parameters and radial velocities obtained by the SSPP for stars with a reasonable likelihood of membership in previously studied Galactic globular and open clusters are sufficiently accurate to justify the use of the present SSPP parameters for carrying out detailed studies of the halo and thick-disk populations of the Milky Way. In deriving the overall iron abundance for each cluster, we assume it comprises a chemically homogenous population.

In §2, the photometric and spectroscopic data obtained for M 13, M 15, M 2, NGC 2402, and M 67 are described. Section 3 presents the methods used to separate likely cluster members from field stars in the directions toward these clusters. Best estimates of the overall [Fe/H] and radial velocity of each cluster are derived in §4. In §5 we compare the SSPP determinations of $T_{\rm eff}$ and log g for selected member stars in each cluster with their expected positions on color-magnitude diagrams. A summary and brief conclusions are provided in §6.

2. Photometric and Spectroscopic Data

Galactic globular and open clusters are nearly ideal testbeds for validation of the stellar atmospheric parameters estimated by the SSPP. In most clusters, it is expected that their member stars were born simultaneously out of well-mixed, uniform-abundance gas at the same location in the Galaxy. Therefore, with the exception of effects due to post main-sequence evolution, primordial variations in carbon and nitrogen, or contamination from binary companions that have transferred material, the member stars should exhibit very similar elemental abundance patterns. Three of the clusters in our study, M 13, M 15, and M 2, have well-known CN variations that extend to the main-sequence turnoffs (Smith & Briley 2006 for M13; Cohen, Briley, & Stetson 2005 for M15; Smith & Mateo 1990 for M2). However, these abundance variations can be ignored when deriving metallicities from regions of the spectra that do not include CH, CN, or NH features, as is the case with most of our techniques (those that may be affected by the presence of such features are automatically de-selected in the determination of the adopted [Fe/H]).

True cluster members should exhibit small radial velocity differences with respect to their parent clusters. Furthermore, it is possible to examine theoretical predictions of temperatures and surface gravities for member stars that lie along the cluster main sequence (MS), red giant branch (RGB), or horizontal branch (HB) in color-magnitude diagrams (CMDs). As part of tests of the SEGUE star-selection algorithm (Adelman-McCarthy et

al. 2007b) and the SSPP, and during normal SEGUE operation, we have obtained *ugriz* photometry and medium-resolution (2.3 Å; $R = 2000$) spectroscopy for large numbers of stars along lines of sight toward the globular clusters M 13, M 15, and M 2 and the open clusters NGC 2420 and M 67. Below we discuss these photometric and spectroscopic data in more detail.

2.1. Photometric Data

The SDSS obtains scans of the sky using the ARC 2.5m telescope on Apache Point, New Mexico. These data are collected in five broad bands (u, g, r, i, z) with central wavelengths 3551, 4686, 6166, 7480, and 8932 Å (Fukugita et al. 1996), respectively, using an imaging array of 30 (6×5) 2048×2048 Tektronix CCDs (Gunn et al. 1998). The pixel size is 24 μm, corresponding to $0.396''$ on the sky. A series of software procedures, collectively known as the SDSS PHOTO pipeline (Lupton et al. 2001), processes and reduces the scanned images shortly after data are obtained. As part of these procedures, the instrumental fluxes and astrometric positions (Pier et al. 2003), as well as a determination of whether an object is likely to be stellar (i.e., a *point source*), or not (an *extended* source) are obtained. Afterwards, the photometric data are further calibrated by matching to brighter known standards observed with a smaller calibration telescope on Apache Point (Hogg et al. 2001; Smith et al. 2002; Tucker et al. 2006). The processed photometric data have been shown to exhibit 2% relative and absolute errors (0.02 magnitudes) in g, r, and i, and $3\% - 5\%$ errors in u and z for all stellar objects brighter than $g = 20$ (Stoughton et al. 2002; Abazajian et al. 2004, 2005; Ivezic et al. 2004). The first-pass photometric data for each of the clusters used in the present study were secured by querying the DR-3 (Abazanjian et al. 2005), DR-5 (Adelman-McCarthy et al. 2007a), and DR-6 (Adelman-McCarthy et al. 2007b) releases from the SDSS Catalog Archive Server (CAS).

Figure 1 illustrates one of the primary challenges in working with data for clusters obtained with SDSS – the automated PHOTO pipeline (Lupton et al. 2001) was not designed to adequately deal with crowded fields such as the central regions of globular clusters. As a result, essentially all of the stars in this region (which are by definition the most likely ones to be cluster members) do not have reported apparent magnitudes in the SDSS CAS. To circumvent this limitation as much as possible, we have instead performed crowded field photometry for the center of the clusters, using the DAOPHOT/ALLFRAME suite of programs (Stetson 1987; Stetson 1994) in IRAF[1]. A full description of the methods used and the pho-

[1]IRAF is distributed by the National Optical Astronomy Observatories, which is operated by the Associ-

tometric measures obtained is provided by Johnson et al. (2007). Briefly, DAOPHOT was run on each image, and the five images of each field (one for each filter) were then simultaneously run through ALLFRAME. DAOGROW (Stetson 1990) was used to derive aperture corrections to the point-spread-function photometry for the SDSS aperture radius of 7.4 arcsecs. Finally, the zeropoint term from the *tsField* files was applied to calibrate the data. This procedure also permits a check on the techniques used by the SDSS PHOTO pipeline in regions outside the cluster where the areal density of sources on the sky is sufficiently low that it may be used.

After completing the above procedures, we finally combine the results from the PHOTO pipeline with those from the crowded-field photometry to obtain an almost complete catalog of *ugriz* photometry for stars in the region of each of our program clusters. All photometric data are corrected for extinction and reddening by application of the Schlegel, Finkbeiner, & Davis (1998) maps. The average reddening ($E(B-V)$) for stars in the direction of these clusters is 0.017, 0.110, 0.045, 0.041, 0.032 for M 13, M 15, M 2, NGC 2420, and M 67, respectively. Comparing with the literature values listed in Table 1, most of the average reddenings of the clusters agree within about 0.02 mags.

2.2. Spectroscopic Data

The spectroscopy discussed in the present paper was obtained during the course of SEGUE tests and normal SEGUE observations. In normal SEGUE operation mode, a pair of plug-plates (referred to as the "bright" and "faint" plates) are obtained over the 3° field of the ARC 2.5m. A total of 640 optical fibers are employed to obtain $R = 2000$ spectra for on the order of 600 program stars for each plate (the remaining fibers are used for spectrophotometric and reddening calibration objects and observations of the night sky). The exposure time depends on observation conditions. For a bright plate, exposures are set to achieve a total $(S/N)^2 > 15/1$ from the two blue-side CCDs on the SDSS spectrographs; the exposure for a faint plate is set such that a total $(S/N)^2 > 50/1$ for all four (red and blue CCDs) on the SDSS spectrographs is achieved. In order to identify and remove cosmic ray hits, each plate must have at least three exposures; the integration time for any single exposure is not longer than 30 minutes. For the purposes of targeting objects on these plates, the boundary between the bright and faint plates is set at $r \sim 18.0$. The data thus obtained are processed through the SDSS spectroscopic pipeline software (SPECTRO2D and

---

ation of Universities for Research in Astronomy, Inc. under cooperative agreement with the National Science Foundation.

SPECTRO1D), which produces wavelength and flux-calibrated spectra, and also obtains estimates of radial velocities and line indices (Stoughton et al. 2002). Tests of the quality of stellar radial velocities from the SSPP (which uses initial estimates from the SDSS processing pipelines) indicate precisions better than 5 km s^{-1} are achieved for brighter stars, with zero-point offsets of no more than a few km s^{-1}, respectively (Paper III). These errors degrade for fainter stars, as expected.

An initial set of candidate member stars of the globular and open clusters studied in the present paper were selected on the basis of photometric and astrometric data (proper motions) from the literature. The central cores of the clusters were not targeted because the PHOTO pipeline does not resolve the very crowded fields into single star detections, and also due to limitations on the separations of the fibers during the spectroscopic follow-up stage. The primary method for selecting member candidates was performed by plotting a photometric CMD for a given cluster, and choosing stars from regions of this diagram that correspond to location on the MS turnoff or RGB of the cluster. An additional list of bright stars for M 15 and M 2 with previously available proper motions consistent with membership in the clusters was provided by Cudworth (1976 and private communication) and Cudworth & Rauscher (1987). Other stars in the fields of these clusters were used to fill spectroscopic fibers using the default SEGUE target selection algorithm (Adelman-McCarthy et al. 2007b). While many of these additional targets turned out to be stars from the general field populations, a significant fraction turned out serendipitously to be members of the clusters.

For M 13, three specially designed plates were obtained. Two of the three plates followed the standard SEGUE target selection procedure (Adelman-McCarthy et al. 2007b) of sampling stars with a variety of spectral types based on the SDSS imaging and PHOTO processing. An additional set of likely M 13 members, including several stars that were saturated in the SDSS image ($r < 14.5$) and with coordinates from Cudworth & Monet (1979) and Cudworth (private communication), were added to the target list with high priority (bumping ordinary SEGUE targets), in order to obtain spectra of several likely giant-branch and horizontal-branch members.

In the case of NGC 2420, the stars chosen for spectroscopy were primarily targeted from the SDSS photometry obtained by the PHOTO pipeline, using the normal SEGUE target selection algorithm. Additional stars with apparent magnitudes in the range $14.5 < g < 20.5$ that fell within 0.5 degrees from the center of NGC 2420 were also targeted for spectroscopy. However, due to crowding, if two objects were within $55''$ of one another, then only one received a fiber. Thus, not every star in the central region of NGC 2420 was targeted. There were about 480 objects selected in this way, including a number of non-cluster members that

are located in the NGC 2420 field.

For M 67, the initial targets came from the SDSS imaging data processed by the PHOTO pipeline. However, for this cluster, many candidate members with positions, magnitudes, and colors from the WEBDA (http: //www.univie.ac.at/webda/) catalogs were added to the target lists. The bright targets (with $r < 14$) saturate the SDSS imaging camera, so these were added from the literature (Sanders 1989; Fan et al. 1996). Such bright stars normally saturate a regular SDSS spectroscopic exposure, so there were exposed for shorter than normal. About 200 very bright stars between about $12 < g < 14$ were targeted.

In total, we obtained SDSS spectroscopy for 1920, 1280, 640, 1280, and 640 targets, including sky spectra and calibration object spectra, in the fields of M 13, M 15, M 2, NGC 2420, and M 67 respectively. The reduced spectra were then processed through the SSPP in order to estimate $T_{\rm eff}$, log g, and [Fe/H], among other quantities. Table 1 summarizes the global properties of the clusters under consideration in this paper, taken from the compilation of Harris (1996) for the globular clusters and from WEDBA or Gratton (2000) for the open clusters.

2.3. Radial Velocities

There are two estimated radial velocities provided from the SDSS spectroscopic pipeline. One is an absorption redshift obtained by cross-correlating the spectra with templates that were obtained from SDSS commissioning spectra (Stoughton et al. 2002). Another comes from matching the spectra with ELODIE template spectra (Prugniel & Soubiran 2001). In most cases the velocity based on the ELODIE template matches appears to be the best available estimate, as spectra of "quality assurance" stars with multiple measurements show the most repeatable values for this estimator. However, this is not always the case. We proceed to select the best available velocity in the following manner. If the velocity determined by comparison with the ELODIE templates has a reported error of 20 km s^{-1} or less then this velocity is adopted. If the error from the ELODIE template comparison is larger than 20 km s^{-1}, and the relative offset between the two radial velocities is less than 40 km s^{-1}, we take an average of the two. If none of the criteria above are satisfied, which happens only rarely, and mainly for quite low S/N spectra, or for hot/cool stars without adequate templates, we obtain the calculated radial velocity from a custom routine that examines the wavelengths of a number of prominent absorption features. If none of these methods yield a reasonable estimate of radial velocity, or it appears spurious (i.e., falls outside of the range $\pm$1000 km s^{-1}), we simply ignore the star in subsequent analyses. A more detailed description of the procedures used for determination of the best available radial velocity, and of zero-point

offsets of the radial velocities, can be found in Paper I.

3. Membership Selection from the Spectroscopic Samples

Owing to an insufficient number of stars with available spectroscopy for each cluster, it is not possible to obtain a well-defined Color Magnitude Diagram (CMD) based solely on spectroscopically confirmed member stars. Thus, we make use of photometric data in the field of each cluster, and describe below how we obtain a relatively clean CMD for individual clusters, and select likely member stars from the spectroscopic data.

3.1. Likely Member Star Selection for Globular Clusters

One of the primary issues that one needs to address when creating a CMD, or selecting likely member stars, for a star cluster is removal of contamination from field stars. In order to approximately isolate the likely cluster members from the field stars we have made use of the CMD mask algorithm described by Grillmair et al. (1995). We illustrate the basic idea by application of this algorithm to the M 13 field shown in Figure 1. We first select all stars inside the estimated tidal radius ($25.2'$; Harris 1996), shown as the innermost green circle in Figure 1. This is regarded as the cluster region. The red dots represent stars with available photometry from the SDSS PHOTO pipeline (Lupton et al. 2001); the black dots are stars with photometry obtained from DAOPHOT. The blue open circles indicate stars with available spectroscopy. We then choose an annulus outside the cluster region, indicated on the Figure as the region between the two black circles, as the field or background region.

We next obtain CMDs of each region, spanning $-1.0 \leq (g-r)_0 \leq 1.5$ and $12 \leq g_0 \leq 22$, and then subdivide these diagrams such that the size of each sub-grid is 0.2 mag wide in g_0 and 0.05 mag wide in $(g-r)_0$ color. The total number of sub-grids for the CMDs in each region is thus 2500 (50×50). Figure 2 shows the resulting CMDs of the cluster (left panel) and field (right panel) regions, overplotted with squares representing the selected sub-grids, obtained as described below.

We first calculate the signal-to-noise (s/n) in each preliminary sub-grid by application of Eqn. (1) over the entire CMD region shown in Figure 2. Here we assume that the field stars outside the tidal radius are uniformly distributed throughout the annulus area.

$$s/n(i,j) = \frac{n_c(i,j) - g n_f(i,j)}{\sqrt{n_c(i,j) + g^2 n_f(i,j)}}. \quad (1)$$

In the above, n_c and n_f refer to the number of stars in each sub-grid with color index i and magnitude index j, counted within the cluster region and field region, respectively. The parameter g represents the ratio of the cluster area to the field area.

The following procedures are followed in order to find the optimal range of colors and magnitudes that correspond to the likely members of each cluster. First, we sort the elements of $s/n(i,j)$ in descending order, so that we obtain a one-dimensional array of $s/n(i,j)$ with index l; the array element with the highest $s/n(i,j)$ corresponds to $l = 1$. The next step is to obtain star counts in gradually larger regions of the CMDs. The accumulated area is represented as $a_k = ka_l$, where $a_l = 0.01$ mag^2, which is the same for all sub-grids, and is the area of a single sub-grid in the CMD array, and the k is the number of sub-grids to combine. Finally, the cumulative signal-to-noise ratio, $S/N(a_k)$, as a function of a_k, is calculated from:

$$S/N(a_k) = \frac{N_c(a_k) - gN_f(a_k)}{\sqrt{N_c(a_k) + g^2 N_f(a_k)}} \tag{2}$$

where,

$$N_c(a_k) = \sum_{l=1}^{k} n_c(l), \quad N_f(a_k) = \sum_{l=1}^{k} n_f(l) \tag{3}$$

The parameter $n_c(l)$ denotes the number of stars within the cluster region having ordered color-magnitude index l; $n_f(l)$ represents the same quantity for the field region. Based on the maximum value of $S/N(a_k)$, a threshold value of s/n is picked in order to select high-contrast surface-density areas (i.e, high s/n) between the cluster and field regions. These are considered to be the sub-grids that contain likely cluster members. After removing single-star events in areas of the CMDs where the field-star density is low, all stars in sub-grids with $s/n(i,j)$ greater than the threshold value of s/n are selected. These stars are considered as the photometrically likely member stars for a given cluster.

The red squares shown in the left panel of Figure 2 are the sub-grids with s/n greater than the threshold value; the corresponding sub-grids in the field region are shown as green squares in the right panel of this Figure. Figure 3 depicts the CMD of the selected likely members of M 13 from the photometric data, shown as black dots. The same procedures are performed to differentiate the likely member stars of M 15 and M 2 from the photometric sample.

We now proceed to select the stars that are likely members of the globular clusters from the available spectroscopic sample. This step begins by selection of the stars within the cluster tidal radii that pass the photometric criterion for membership, based on their location on the cluster CMDs according to the algorithm described above.

Figure 3 displays the cleaned CMD of M 13, overplotted with the likely members from the spectroscopic sample (shown as red circles). The same procedures are carried out to identify likely member stars of M 15 and M 2 from their spectroscopic data. Based on these cuts, at this stage of the analysis there are 296 (338) likely members for M 13, 124 (160) for M 15, and 21 (22) for M 2 identified. In the above, the first listed numbers indicate the stars with available estimates of [Fe/H] from the SSPP, while the quantities in parentheses represent the number of stars with available radial velocities (RVs). Additional cuts, based on the derived metallicity estimates and RVs, are described in §4.

3.2. Likely Member Star Selection for Open Clusters

Since the fields of nearby open clusters are not as crowded as those of globular clusters, the signal-to-noise ratio between the cluster region and the background region is not sufficiently high to select likely cluster members by means of the CMD mask algorithm. As an alternative, we first obtain a fiducial line for an open cluster (including its main sequence and sub-giant branch, if it exists) by use of an robust polynomial fitting procedure. As an example, Figure 4 shows the CMD of the NGC 2420 field inside a radius of 0.3 degrees from the center of the cluster. According to the open cluster catalog of Dias et al. (2002), the apparent diameter of this cluster is only $5^{'}$ on the sky, but we prefer to adopt a $20^{'}$ radius, in order to include as many member stars as possible. The red line is the fiducial line derived from the robust polynomial fit. The blue lines are the upper and lower limits (fiducial $\pm$ 0.06 dex in $(g-r)_0$), determined by eye. Stars from the spectroscopic sample that fall within the $20^{'}$ radius and inside the blue limit lines in Figure 4 are identified.

A similar procedure is applied to M 67, except that a $30^{'}$ (apparent diameter of $25^{'}$; Dias et al. 2002) radius and fiducial $\pm$ 0.10 mag in $(g-r)_0$ is used. Based on this selection method, there are 195 (234) and 61 (64) for NGC 2420 and M 67, respectively. The first listed numbers indicate the stars with available estimates of [Fe/H] from the SSPP, while the quantities in parentheses represent the number of stars with available radial velocities (RVs) . Additional cuts, based on the derived metallicity estimates and RVs, are described below.

4. Determination of Overall Metallicities and Radial Velocities of the Clusters

In order to investigate the accuracy of our derived metallicities and RVs, we now consider the global distribution of these parameters obtained from the current version of the SSPP for the likely cluster members. In this section, we describe a method to best isolate "true member stars" from the spectroscopic samples described above. We then use these subsamples to determine our best estimates of the overall metallicities and RVs of the clusters considered in this study.

4.1. Selection of True Members

We establish the criteria for carrying out metallicity and RV cuts as follows.

The left panel of Figure 5 illustrates the [Fe/H] distribution for three different subsamples of stars. The first, shown as the black dot-dashed line, represents the distribution of derived metallicities for the 1547 stars with available estimates of [Fe/H] along the line of sight to M 13. Note that this distribution includes numerous stars that cannot be considered members of the cluster, as they cover a much wider range of [Fe/H] than might be expected if they were drawn exclusively from the cluster member population. The dot-dashed line in the right panel of Figure 5 shows the RV distribution of these same stars.

The red dashed line in the left panel of Figure 5 is the distribution of [Fe/H] for the 296 likely members selected from the spectroscopic sample as described above. We obtain a Gaussian fit to the *highest peak* of the distribution of these stars (solid blue line in Figure 5), and obtain an estimate of the mean (<[Fe/H]>) and standard deviation (σ) for this distribution. Similar fits are obtained for the distribution of RVs for the likely members shown in the right panel of Figure 5. On the basis of these fits, we now trim likely outliers by application of a 2-σ clipping procedure, for example:

$$< [\mathrm{Fe/H}] > -2\sigma_{[\mathrm{Fe/H}]} \leq [\mathrm{Fe/H}]_\star \leq < [\mathrm{Fe/H}] > +2\sigma_{[\mathrm{Fe/H}]} \quad (4)$$

$$< \mathrm{RV} > -2\sigma_{\mathrm{RV}} \leq \mathrm{RV}_\star \leq < \mathrm{RV} > +2\sigma_{\mathrm{RV}} \quad (5)$$

In the above, $[\mathrm{Fe/H}]_\star$ and $\mathrm{RV}_\star$ correspond to the values of these parameters for each star under consideration. The stars surviving both of these clips are considered true cluster members for the purpose of this study. Note that at no point have we considered the external "known" values of [Fe/H] and RV for the clusters as a whole.

Based on the application of these membership cuts, we now have a total of 169 stars identified as true members of M 13, 63 stars as true members of M 15, 9 stars as true members of M 2, 195 stars as true members of NGC 2420, and 51 stars as true members of M 67. The distribution of [Fe/H] and RV for the surviving members of M 13 are shown as green histograms in the left and right panels of Figure 5, respectively. Similar plots for M 15, M 2, NGC 2420, and M 67 are shown in Figures 6, 7, 8, and 9, respectively. The distribution of [Fe/H] for the selected true member stars of each cluster, as a function of $T_{\rm eff}$, is shown in Figure 10.

Table 2 summarizes the results of the above exercise. Column (1) lists the cluster name. Columns (2) and (3) are the lower and upper limits for the 2-σ cuts on [Fe/H], respectively. Columns (4) and (5) are the corresponding adopted limits on RV used for these cuts.

Tables 4−8 list the observed and derived quantities for all of the individual stars considered as true member stars in the analysis of each cluster. The columns are as defined in the table notes for Table 4.

4.2. Determination of Overall Estimates of Mean Cluster Metallicity and Radial Velocity

We now obtain final estimates of the cluster metallicities and RVs based on Gaussian fits to the surviving true member stars for each cluster, as shown by the blue curves in Figures 5−9. Table 2 summarizes these determinations. The mean metallicity and 1-σ spread of the metallicities of the true member stars are listed in columns (6) and (7), respectively. Similar quantities for the RVs are listed in columns (8) and (9). Column (10) lists the total number of true member stars associated with each cluster, based on our analysis. External estimates of the metallicities and RVs for these clusters, adopted from the Harris (1996) compilation for M 13, M 15, and M 2 and from WEBDA (and references therein) for NGC 2420 and M 67, are listed in columns (11) and (12). Column (13) lists metallicity estimates for these clusters obtained from high-resolution spectroscopy of a limited number of brighter stars by Kraft & Ivans (2003) for M 15 and M 13, Ivans (private communication) for M 2, and Gratton (2000) for NGC 2420 and M 67.

For M 13, our estimate of the mean abundance, $<$[Fe/H]$> = -1.56$, is very close to the Harris (1996) estimate ($[{\rm Fe/H}]_{\rm H} = -1.54$). However, the recent study of Kraft & Ivans (2003) reported a revised cluster abundance for M 13, derived from high-resolution spectroscopy of 28 giants. Their value indicates a metallicity for M 13 that is a bit lower than that given by Harris, $[{\rm Fe/H}]_{\rm HR} = -1.63$, and is lower by 0.07 dex than our estimate. Cohen &

Meléndez (2005) reported [Fe/H] = −1.50 from a high-resolution (R = 35,000) analysis of a sample of 25 stars, consisting of stars from the giant branch to near the main-sequence turnoff. Our derived spread in the metallicities of the M 13 true member stars (0.16 dex) is also satisfyingly low, especially considering the wide range of temperatures for true members that are considered here. Our estimate of the mean radial velocity, <RV> = −245.1 km s^{-1}, with a standard deviation of 8.7 km s^{-1}, is in good agreement with that given by Harris (−245.6 km s^{-1}). It is important to note that, as mentioned in Paper I, we have already added +7.3 km s^{-1} to all DR-6 (Adelman-McCarthy et al. 2007b) stellar radial velocities. Before the adjustment of this offset, an average offset of −8.6 km s^{-1} for M 13 and −6.8 km s^{-1} for M 15 is obtained. Thus, together with an offset of −6.6 km s^{-1} that was obtained from a preliminary result of a high-resolution spectroscopic analysis of SDSS-I/SEGUE stars (Paper III) before DR-6 (Adelman-McCarthy et al. 2007b), we derived an average offset of −7.3 km s^{-1}. However, a recent high-resolution spectroscopic analysis of SDSS-I/SEGUE stars indicates an offset of about −6.9 km s^{-1}, resulting in an average of −7.4 km s^{-1}, Hence, in future data releases (e.g, DR-7), this very minor difference might be reflected. For the analysis of our clusters, all radial velocities have been corrected by +7.3 km s^{-1}, in order to be consistent with DR-6.

Our estimate of the mean abundance of M 15, <[Fe/H]> = −2.12, is close to the value listed by Harris ([Fe/H]$_{\rm H}$ = −2.26). While Kraft & Ivans (2003) obtained [Fe/H]$_{\rm HR}$ = −2.42, based on high-resolution spectroscopy for nine giants in this cluster, Otsuki et al. (2006) reported [Fe/H] = −2.29 from an analysis of high-resolution spectra for six giants belonging to this cluster. Our derived spread in the metallicities of true member stars in M 15 is quite low (0.14 dex). Our estimate of the mean radial velocity, <RV> = −107.4 km s^{-1}, with a standard deviation of 10.5 km s^{-1}, agrees very well with that of the Harris (1996) value (−107.0 km s^{-1}).

There are only a very small number of true member stars (9) for M 2. Their average metallicity, <[Fe/H]> = −1.58, is similar to the Harris (1996) value ([Fe/H]$_{\rm H}$ = −1.62), and is in very good agreement with the value obtained by Ivans (private communication) ([Fe/H]$_{\rm HR}$ = −1.56). The estimated spread in our derived metallicities, 0.08 dex, is quite small. Our estimate of the mean radial velocity, <RV> = +0.4 km s^{-1}, with a standard deviation of 7.7 km s^{-1}, is higher (by about 6 km s^{-1}) than that provided by Harris (−5.3 km s^{-1}). Clearly, for the purposes of validation of the SSPP, it would be highly desirable to obtain a larger number of member stars in M 2; a new plate (640 spectra) will be obtained in the near future. Note that M 2 presents a special challenge, since its mean metallicity is quite close to that expected for members of the field halo population, while its radial velocity is buried in the peak of foreground disk stars. Our stringent criterion for true cluster members should remain effective, however, since few non-cluster members will fulfill both the RV and

metallicity criteria.

There are 130 true member stars selected for the open cluster NGC 2420. The mean iron abundance of the selected true member stars is <[Fe/H]> = −0.46, which is in excellent agreement with the value ([Fe/H] = −0.44) determined by Gratton (2000) from high-resolution spectroscopy of one member star. Friel & Janes (1993) reported [Fe/H] = −0.42 for nine member stars, based on medium- and low-resolution spectroscopic data. Friel et al. (2002) determined [Fe/H] = −0.38 ± 0.07, based on medium-resolution spectra of 20 member stars. Most of these literature values are within the spread of our derived value. The derived spread in the metallicities of true member stars (0.12 dex) is very low. The radial velocity for NGC 2420 listed in Table 2, (+74.0 km s^{-1}), is an average of the values +84.0 km s^{-1}, +71.1 km s^{-1}, and +67.0 km s^{-1} from Friel (1989), Scott et al. (1995), and Rastorguev et al. (1999), respectively. This value agrees very well with our derived estimate of +74.8 km s^{-1}, with a standard deviation of 6.2 km s^{-1}.

For M 67, 51 stars are identified as true member stars. A mean metallicity of <[Fe/H]>= −0.35 is derived, with a small spread of 0.15 dex. This derived <[Fe/H]> differs by 0.37 dex from that of Gratton (2000), [Fe/H] = +0.02, who derived this value from a high-resolution study of one member star. Randich et al. (2007) analyzed 10 member stars of this cluster, based on high-resolution ($R \sim 45,000$) spectroscopy, and derived [Fe/H] = +0.03 ± 0.01. [Fe/H] = +0.02 ± 0.03 was determined by Yong et al. (2005) from a high-resolution spectroscopic analysis of three member stars. However, based on medium-resolution spectra of 25 members, Friel et al. (2002) reported [Fe/H] = −0.15 ± 0.05. Other catalogs of open clusters (e.g., Twarog et al. 1997; Chen et al. 2003) also report a solar metallicity for this cluster. The literature values based on high-resolution spectroscopic analyses clearly suggest that the present SSPP tends to under-estimate [Fe/H] by about 0.3 dex for near-solar-metallicity stars. This is perhaps related to the difficulties arising from the strong atomic and molecular lines (and possibly unreliable synthetic spectra) for metal-rich stars. As mentioned by Gratton (2000), it might be desirable to re-calibrate the metallicity scale used for the analysis of medium-resolution spectra for stars with the solar iron abundance to better match the results obtained from high-resolution analyses. The radial velocity of +32.9 km s^{-1} for M 67 from the literature listed in Table 2 (the average of the Scott et al. 1995; Friel & Janes 1993; Rastorguev et al. 1999 values) agrees with our derived mean radial velocity of +34.9 km s^{-1} within the standard deviation of our measurements, 5.6 km s^{-1}.

Thus, taking into account only the scatter in the metallicities and radial velocities calculated from the members of each cluster, we are able to derive estimates of typical external uncertainties for the SSPP values, σ([Fe/H]) = 0.13 dex, and σ(RV) = 7.7 km s^{-1}

(after 5σ clipping is applied).

5. A Comparison of Derived $T_{\rm eff}$ and log g for True Cluster Members with Color-Magnitude Diagrams

In the previous section, we have considered the accuracy with which the SSPP obtains estimates of metallicity and radial velocity. We now consider the accuracy with which the SSPP obtains estimates of effective temperatures, $T_{\rm eff}$, and surface gravities, log g. One excellent "global" test of these estimates is to examine the locations of the true member stars on the observed CMD (based on the totality of likely photometric member data) for each cluster. One can also compare with corresponding theoretical CMDs.

Figures 11−15 show plots of the SSPP-estimated temperatures and gravities for true member stars superposed on the photometrically cleaned CMDs for each of our clusters. Note that in order to obtain the theoretical temperature scales (shown along the top of the left-hand panels in each Figure), we make use of a linear relation between $(g-r)_0$ color and $T_{\rm eff}$ by performing a least square fit in this plane to the theoretical models of Girardi et al. (2004). We choose the isochrones from this study that have the closest [Fe/H] to the derived metallicity of each cluster, and adopt an age of 13.5 Gyr for the globular clusters, 2.2 Gyr for NGC 2420, and 4.3 Gyr for M 67 (adopting the ages from WEBDA for the open clusters). A similar procedure is applied for transforming the g_0 magnitude to a theoretical log g scale (shown along the far right axis in the right-hand panels of each Figure). Distance moduli from the Harris (1996) compilation for the globular clusters and WEBDA for the open clusters (also listed in Table 1 of this study) are used in order to compute apparent magnitudes.

In these Figures, we plot the SSPP-estimated parameters for true member stars in different colors, corresponding to different ranges of temperature and surface gravity (as shown in the legend for each plot). Each color represents a range of 500 K in $T_{\rm eff}$ and 0.5 dex in log g. The effective temperature estimated by the SSPP appears in excellent agreement for most of the true member stars, with only a few exceptions. Such stars could either be outright errors in SSPP predictions, or could just be foreground/background stars that survived the various membership cuts we have applied. Inspection of the Figures also reveals the presence of a few stars close to the main-sequence TO in M 13 and M 15 that appear to have slightly lower SSPP-estimated log g than expected from the theoretical scale. The surface gravities of stars along the RGB appear to be very well estimated. Such behavior is perhaps to be expected, since the stars close to the TO region are at the low end of the S/N range that we accept for analysis, and thus are subject to greater errors in the determination

of their atmospheric parameters. The RGB stars are among the brightest, and hence are likely to have the best-determined estimates.

Inspection of Figure 14 for NGC 2420 indicates that gravity estimates for most of the main-sequence stars are well-estimated from the SSPP, with the exception of the faintest stars. These stars have only low S/N spectra available, resulting in higher uncertainties in determinations of their surface gravities. It should also be recalled that surface gravity is a difficult parameter to estimate, especially from spectra of the resolving power obtained by the SDSS. Overall, we are pleased to see as good a behavior in the estimates of this parameter as is demonstrated in Figures 11−15.

In addition, using the derived relations between $(g-r)_0$ and $T_{\rm eff}$, and g_0 and $\log g$ from the isochrones, we predicted $T_{\rm eff}$ and $\log g$ from the observed $(g-r)_0$ and g_0, respectively. Table 3 lists the averages and standard deviations of the residuals of the effective temperatures and surface gravities between the SSPP estimates and the calculated values. Even though we have employed a simple relationship between $(g-r)_0$ with $T_{\rm eff}$, we see good agreement between the SSPP estimates and the theoretical values in $T_{\rm eff}$. Although, as expected, we notice a rather large offset and scatter in the gravity, indicating a more complex function is needed, the scatters are still within each bin size (0.5 dex) in Figures 11−15. M 2 exhibits a larger scatter in both $T_{\rm eff}$ and $\log g$ than the other clusters, owing to the small number of member stars selected.

6. Summary and Conclusions

Based on photometric and spectroscopic data reported in SDSS-I and SDSS-II/SEGUE, we have examined estimates of stellar atmospheric parameters and heliocentric radial velocities obtained by the SEGUE Stellar Parameter Pipeline (SSPP) for likely members of three Galactic globular clusters, M 13, M 15, and M 2, and two open clusters, NGC 2420 and M 67, and compared them with those obtained by external estimates for each cluster as a whole.

From the derived scatters in the metallicities and radial velocities obtained for the likely members of each cluster, we quantify the typical external uncertainties of the SSPP-determined values, $\sigma([{\rm Fe/H}]) = 0.13$ dex, and $\sigma({\rm RV}) = 7.7$ km s^{-1}, respectively. These uncertainties apply for stars in the range of 4500 K $\leq T_{\rm eff} \leq$ 7500 K and $2.0 \leq \log g \leq 5.0$, at least over the metallicity interval spanned by the clusters studied ($-2.3 \leq [{\rm Fe/H}] < -0.4$). Therefore, the metallicities and radial velocities obtained by the SSPP appear sufficiently accurate to be used for studies of the kinematics and chemistry of the metal-poor and

moderately metal-rich stellar populations in the Galaxy. We have also confirmed that $T_{\rm eff}$ and log g are sufficiently well-determined by the SSPP to distinguish between different luminosity classes through a comparison with theoretical predictions.

A comparison of the analysis of the available high-resolution spectroscopy of SDSS-I/SEGUE stars (Paper III) with the SSPP predictions indicates that the uncertainty in radial velocities adopted by the SSPP is no more than 5 km s^{-1} (after adjusting for an empirical offset of +7.3 km s^{-1}). The empirically determined precisions in estimated atmospheric parameters are $\sim$ 130 K for effective temperature, $\sim$ 0.21 dex for surface gravity, and $\sim$ 0.11 dex for [Fe/H]. These errors apply to the brightest stars obtained by SDSS-I/SEGUE observations, on the order of $14.0 \leq g \leq 15.5$, and are expected to degrade somewhat for fainter stars. We also found that the SSPP tends to underestimate [Fe/H] for near-solar-metallicity stars (represented by members of M 67 in this study), by $\sim$ 0.3 dex.

In future papers we will compare the predictions of the SSPP with intermediate-metallicity clusters ([Fe/H] ~ -0.7) and with additional near-solar-metallicity populations, as sampled by metal-rich globular clusters and nearby open clusters. Additionall metal-poor clusters will also be examined. Further refinements in the SSPP, which hopefully will be better able to recover accurate abundances for near-solar-metallicity stars, are anticipated.

Funding for the SDSS and SDSS-II has been provided by the Alfred P. Sloan Foundation, the Participating Institutions, the National Science Foundation, the U.S. Department of Energy, the National Aeronautics and Space Administration, the Japanese Monbukagakusho, the Max Planck Society, and the Higher Education Funding Council for England. The SDSS Web Site is http://www.sdss.org/.

The SDSS is managed by the Astrophysical Research Consortium for the Participating Institutions. The Participating Institutions are the American Museum of Natural History, Astrophysical Institute Potsdam, University of Basel, University of Cambridge, Case Western Reserve University, University of Chicago, Drexel University, Fermilab, the Institute for Advanced Study, the Japan Participation Group, Johns Hopkins University, the Joint Institute for Nuclear Astrophysics, the Kavli Institute for Particle Astrophysics and Cosmology, the Korean Scientist Group, the Chinese Academy of Sciences (LAMOST), Los Alamos National Laboratory, the Max-Planck-Institute for Astronomy (MPIA), the Max-Planck-Institute for Astrophysics (MPA), New Mexico State University, Ohio State University, University of Pittsburgh, University of Portsmouth, Princeton University, the United States Naval Observatory, and the University of Washington.

Y.S.L., T.C.B., and T.S. acknowledge partial funding of this work from grant PHY 02-16783: Physics Frontiers Center / Joint Institute for Nuclear Astrophysics (JINA), awarded

by the U.S. National Science Foundation. NASA grants (NAG5-13057, NAG5-13147) to C.A.P. are thankfully acknowledged. J.E.N acknowledges support from Australian Research Council Grant DP0663562. C.B.J and P.R.F acknowledge support from the Deutsche Forschungsgemeinschaft (DFG) grant BA2163.

REFERENCES

Abazajian, K., et al. 2003, AJ, 126, 2081

Abazajian, K., et al. 2004, AJ, 128, 502

Abazajian, K., et al. 2005, AJ, 129, 1755

Adelman-McCarthy, J. K., et al. 2007a, ApJS, in press

Adelman-McCarthy, J. K., et al. 2007b, ApJS, accepted

Allende Prieto, C., et al. 2007, AJ, submitted (Paper III)

Allende Prieto, C., Beers, T. C., Wilhelm, R., et al. 2006, ApJ, 636, 804

Bailer-Jones, C. A. L. 2000, A&A, 357, 197

Beers, T. C., et al. 2006, BAAS, 38, 168.08

Beers, T. C., Rossi, S., Norris, J. E., Ryan, S. G., & Shefler, T. 1999, ApJ, 506, 892

Carollo, D., et al. 2007, Nature, submitted (astro-ph/0706.3005)

Cenarro A.J., Cardiel N., Gorgas J., Peletier R.F., Vazdekis A., & Prada F. 2001a, MNRAS, 326, 959

Cenarro A. J., Gorgas J., Cardiel N., Pedraz S., Peletier R.F., & Vazdekis, A. 2001b, MNRAS, 326, 981

Chen, L., Hou, J.L., & Wang, J.J. 2003, AJ, 125, 1397,

Cohen, J. G., Briley, M. M., & Stetson, P. B. 2005, AJ, 130, 1177

Cudworth, K. M. 1976, AJ, 81, 519

Cudworth, K. M. & Monet, D. G. 1979, AJ, 84, 774

Cudworth, K. M. & Rauscher, B. 1987, AJ, 93, 856

Dias, W. S., Alessi, B. S., Moitinho, A., & Lepine, J. R. D. 2002, A&A, 389, 871

Fan, X., et al. 1996, AJ, 112, 628

Friel, E. D.1989, PASP, 101, 244

Friel, E. D. & Janes, K. A. 1993, A&A, 267, 75

Friel, E. D., Janes, K. A., Tavarez, M., Scott, J., et al. 2002, AJ, 124, 2693

Fukugita, M., Ichikawa, T., Gunn, J.E., Doi, M., Shimasaku, K., & Schneider, D.P. 1996, AJ, 111, 1748

Girardi, L., Grebel, E. K., Odenkirchen, M., & Chiosi, C. 2004, A&A, 422, 205

Gratton, R. 2000, in Stellar Clusters and Associations: Convection, Rotation, and Dynamos, ASP Conference Series (eds. R. Pallavicini, G. Micela, & S. Sciortino), 198, p. 225

Grillmair, C. J., Freeman, K. C., Irwin, M., & Quinn, P. J. 1995, AJ, 109, 2553

Gunn, J. E., et al. 1998, AJ, 116, 3040

Gunn, J. E., et al. 2006, AJ, 131, 2332

Harris, W. E. 1996, AJ, 112, 1487

Hogg, D.W., Finkbeiner, D.P., Schlegel, D.J., & Gunn, J.E. 2001, AJ, 122, 2129

Ivezic, Z., et al. 2004, Astron. Nach., 325, 583

Johnson, J. A. et al. 2007, in preparation

Kraft, R. P. & Ivans, I. I. 2003, PASP, 115, 143

Lee, Y. S., et al. 2007a, AJ, submitted (Paper I)

Lupton, R., et al. 2001, in ASP Conf. Ser. 238, Astronomical Data Analysis Software and Systems X, ed. F. R. Harnden, Jr., F. A. Primini, and H. E. Payne (San Francisco: Astr. Soc. Pac.), p. 269

Morrison, H. L., Norris, J., Mateo, M., et al. 2003, AJ, 125, 2502

Moultaka, J., Ilovaisky, S. A., Prugniel, P., & Soubiran, C. 2004, PASP, 116, 693

Otsuki, K., Honda, S., Aoki, W., Kajino, T., & Mathews, G. 2006, ApJ, 641L, 117

Pier, J.R., Munn, J.A., Hindsley, R.B., Hennessy, G.S., Kent, S.M., Lupton, R.H., & Ivezic, Z. 2003, AJ, 125, 1559

Prugniel, Ph. & Soubiran, C., 2001, A&A, 369,1048

Randich, S., Sestito, P., Primas, F., Pallavicini, R., & Pasquini, L., 2006, A&A, 450, 557

Rastorguev, A.S., Glushkova, E.V., Dambis, A.K., & Zabolotskikh M.V. 1999, Astron. Letters, 25, 689

Re Fiorentin, P., Bailer-Jones, C. A. L., Lee, Y. S. et al. 2007, A&A, 467, 1373

Sanders, W. L. 1989, Rev., Mex. Astron. Astro. 17, 31

Schlegel, D. J., Finkbeiner, D. P., & Davis, M., 1998, ApJ, 500, 525

Scott, J. E., Friel, E. D., & Janes, K. A. 1995, AJ, 109, 1706

Smith, G. H & Briley, M. M. 2006, PASP, 118, 740

Smith, G. H. & Mateo, M. 1990, ApJ, 353, 533

Smith, J.A., et al 2002, AJ, 123, 2121

Stetson, P. B. 1987, PASP, 99, 191

Stetson, P. B. 1990, PASP, 102, 932

Stetson, P. B. 1994, PASP, 106, 250

Stoughton, C., et al. 2002, AJ, 123, 485

Twarog, B.A., Ashman, K.M., & Anthony-Twarog, B.J. 1997, AJ, 114, 2556

Tucker, D., et al. 2006, AN, 327, 821

Willemsen, P.G., Hilker, M., Kayser, A., & Bailer-Jones, C. A. L. 2005, A&A, 436, 379

Yong, D., Carney, B. W., & Teixera de Almeida, M. L. 2005, AJ, 130, 597

York, D. G., et al. 2000, AJ, 120, 1579

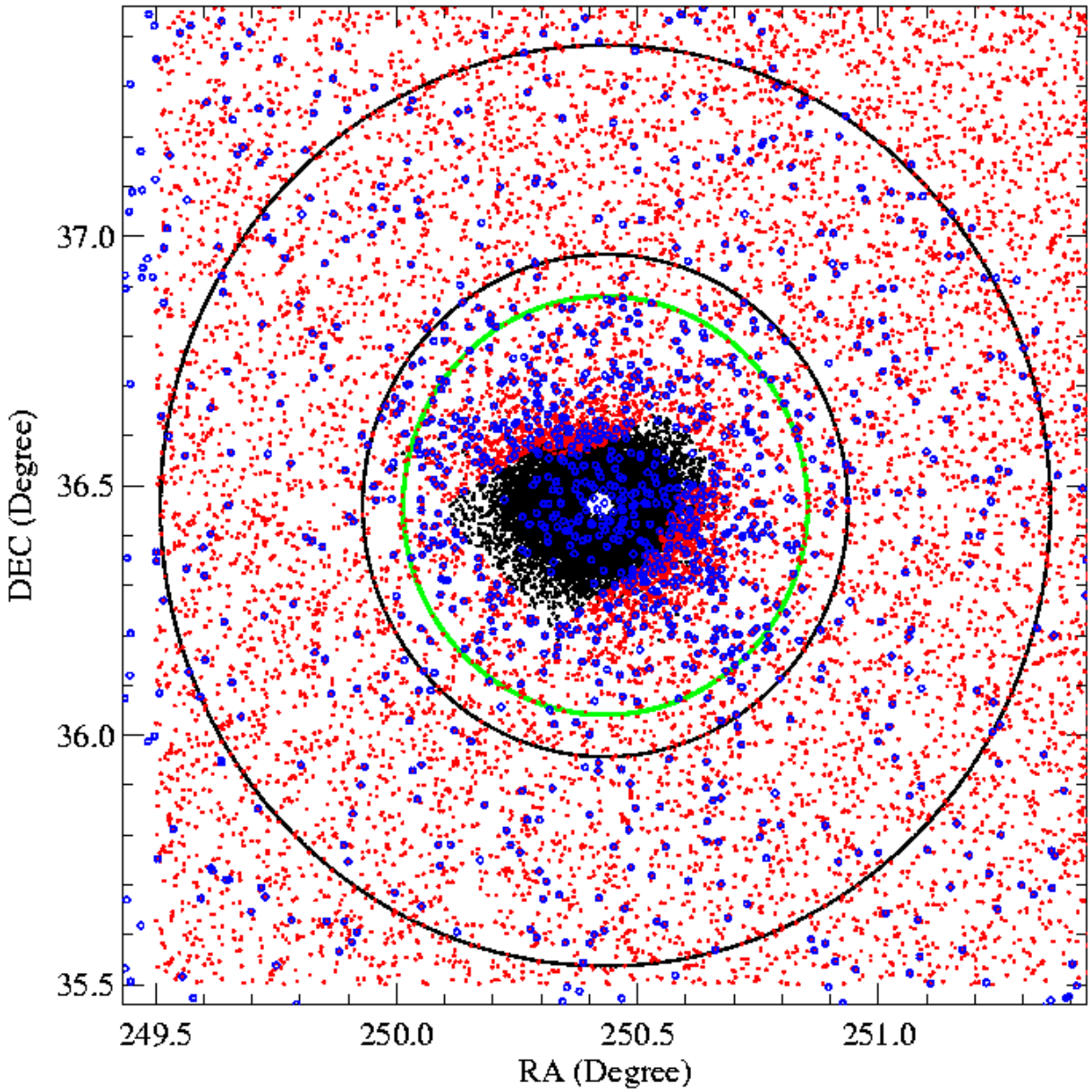

Fig. 1.— Stars with available photometry in the field of M 13. The red dots represent photometry from the SDSS PHOTO pipeline, while the black dots are from the crowded-field photometry analysis. Blue open circles indicate stars with available SDSS spectroscopy. The green circle is the tidal radius. The region inside this radius is regarded as the cluster region; the annulus between the two black circles is considered the field region.

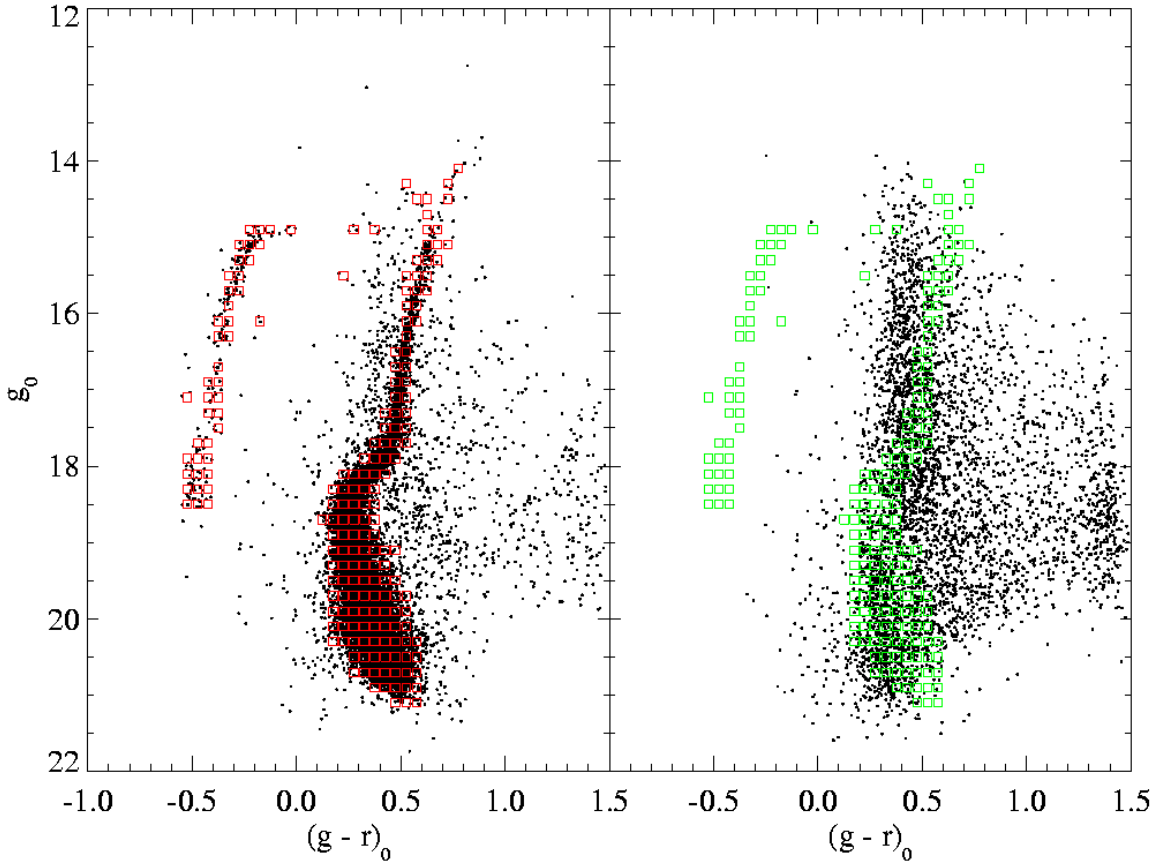

Fig. 2.— Color-Magnitude Diagrams of the M 13 stars inside the tidal radius (left panel), and inside the field region (right panel), shown as black dots. The selected sub-grids from the S/N cut are shown as red squares in the left panel and green squares in the right panel. These selected sub-grids are used in the analysis.

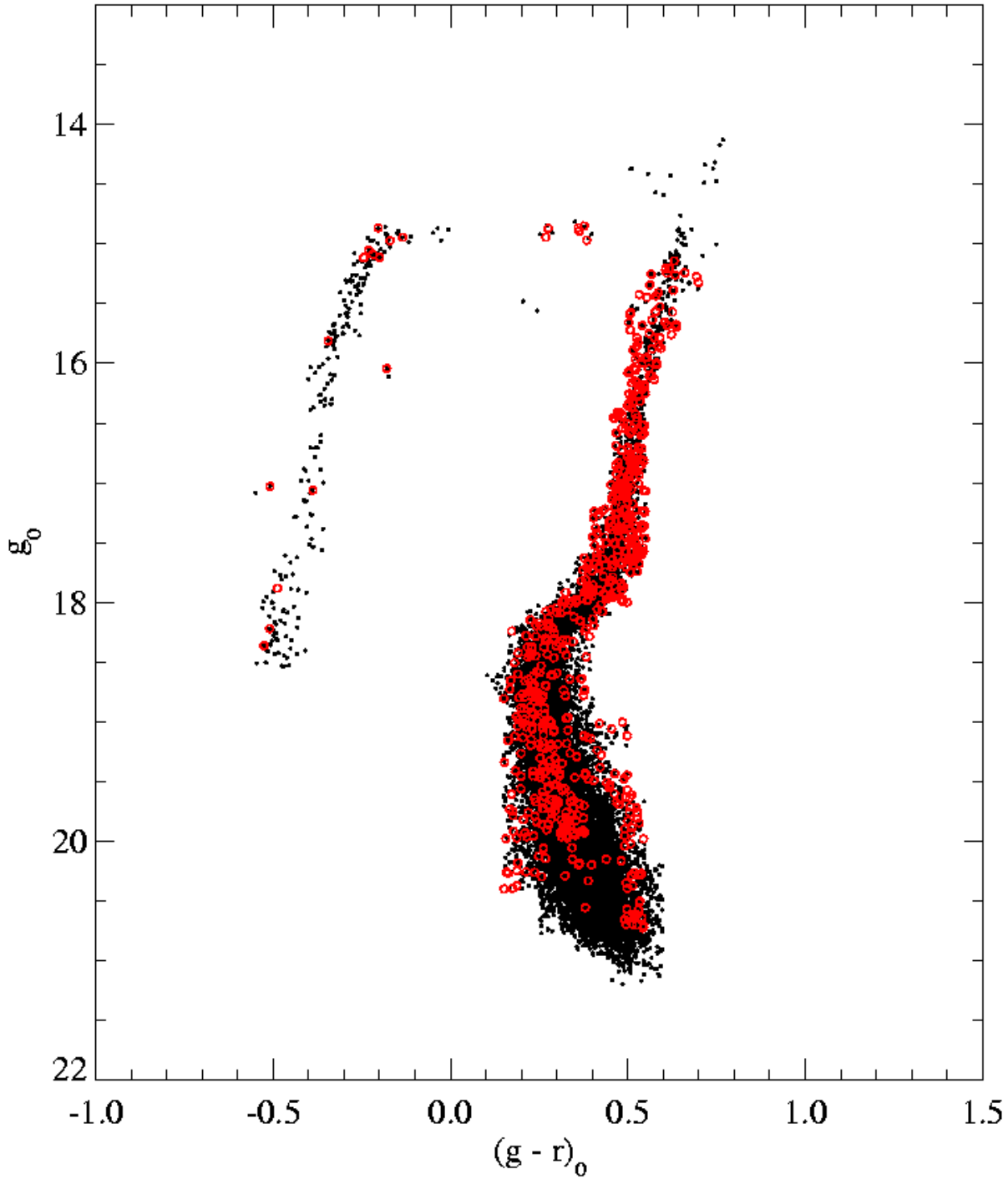

Fig. 3.— The M 13 Color-Magnitude Diagram based on the likely member stars (black dots) selected from the photometric sample. The likely members identified from the spectroscopic sample are indicated with red circles.

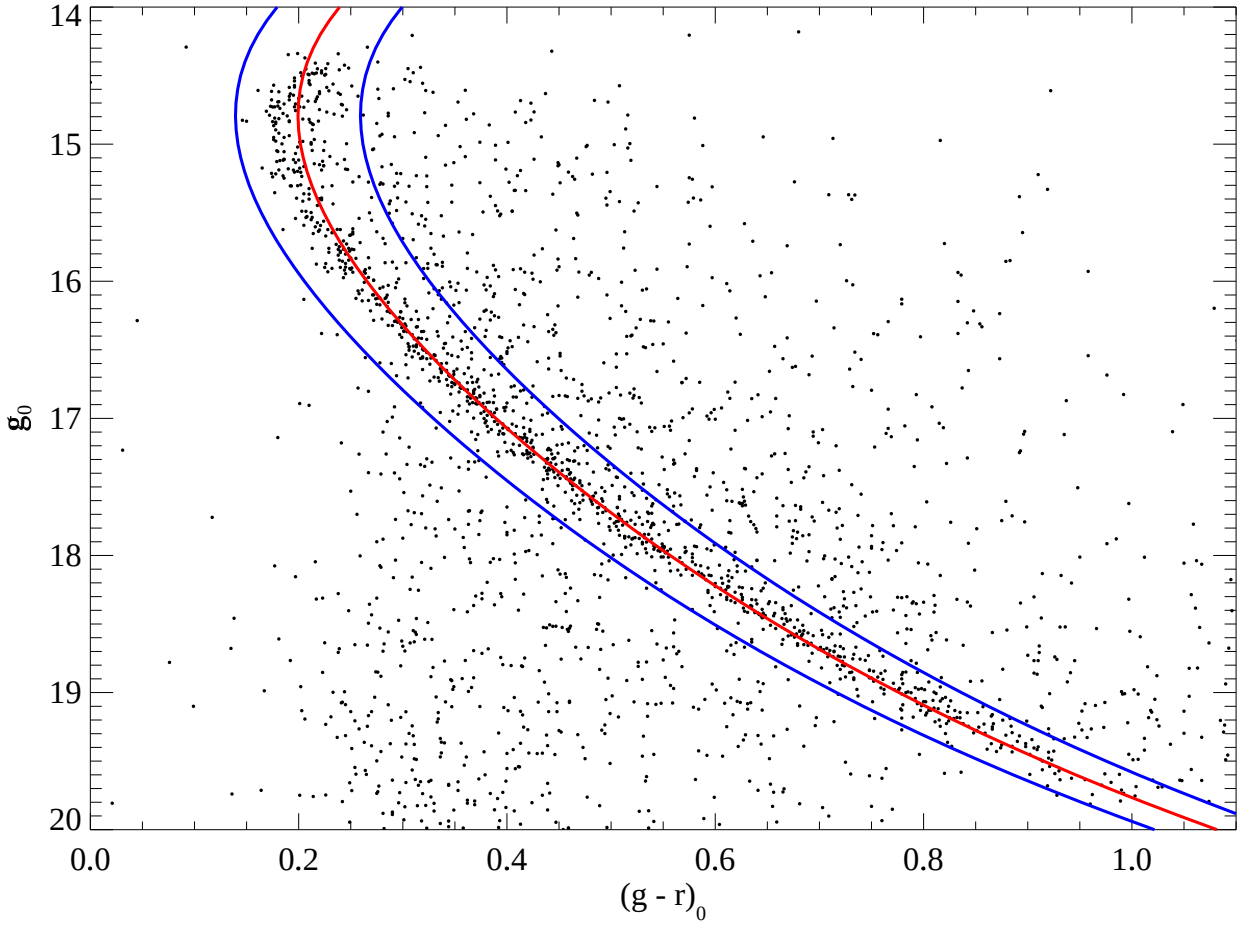

Fig. 4.— Color-Magnitude Diagram of the NGC 2420 field. The red line is the fiducial line obtained by application of a robust fourth-order polynomial fit. The stars inside the blue lines (fiducial $\pm$ 0.06 mag in $(g-r)_0$) are regarded as likely member stars from the photometric sample.

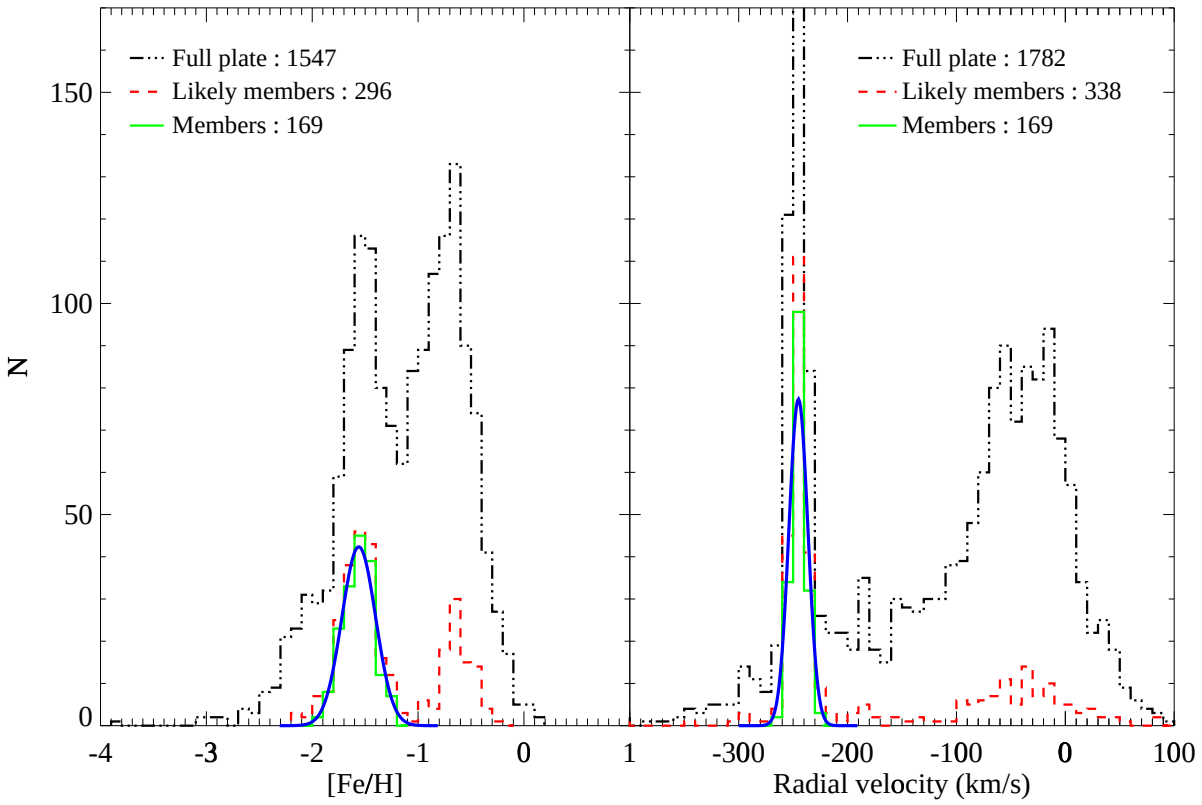

Fig. 5.— [Fe/H] and radial velocity distributions for stars in the direction of M 13. Gaussian fits (blue solid curves) to the distribution of the selected true members, shown in the green histograms, are over-plotted.

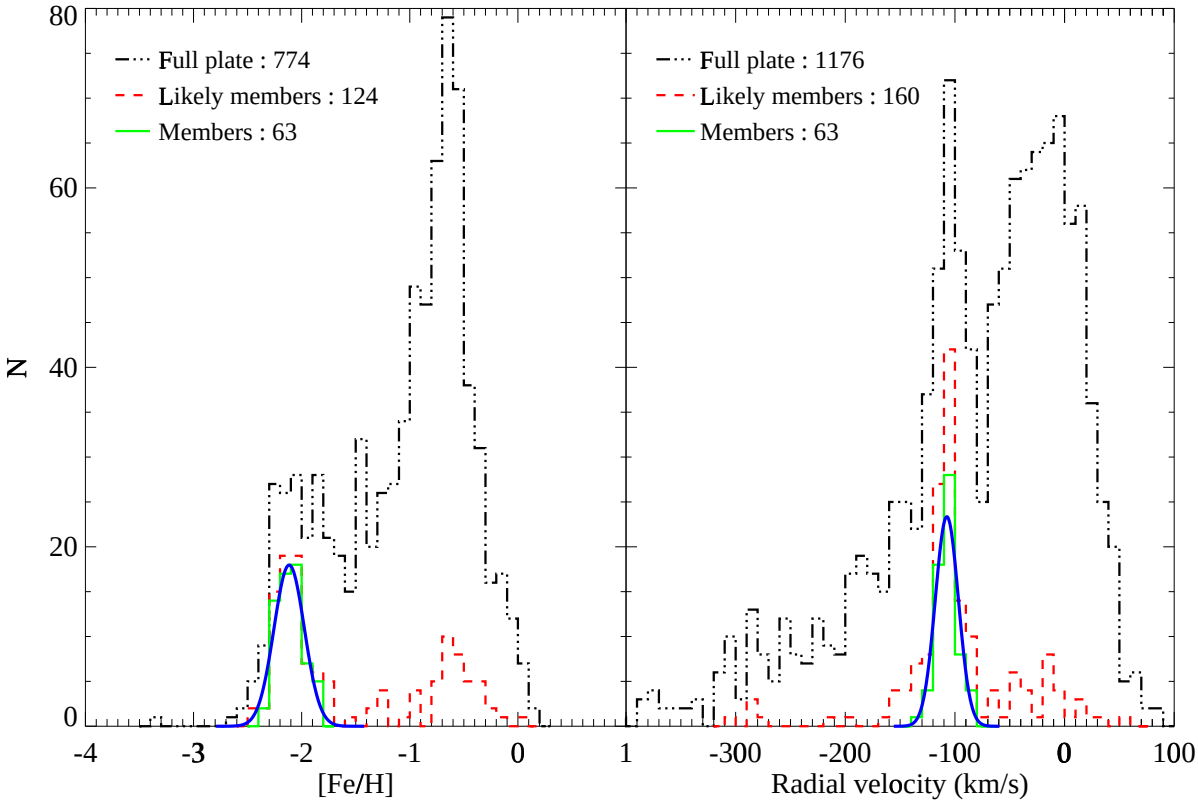

Fig. 6.— Same as Fig. 5 but for M 15.

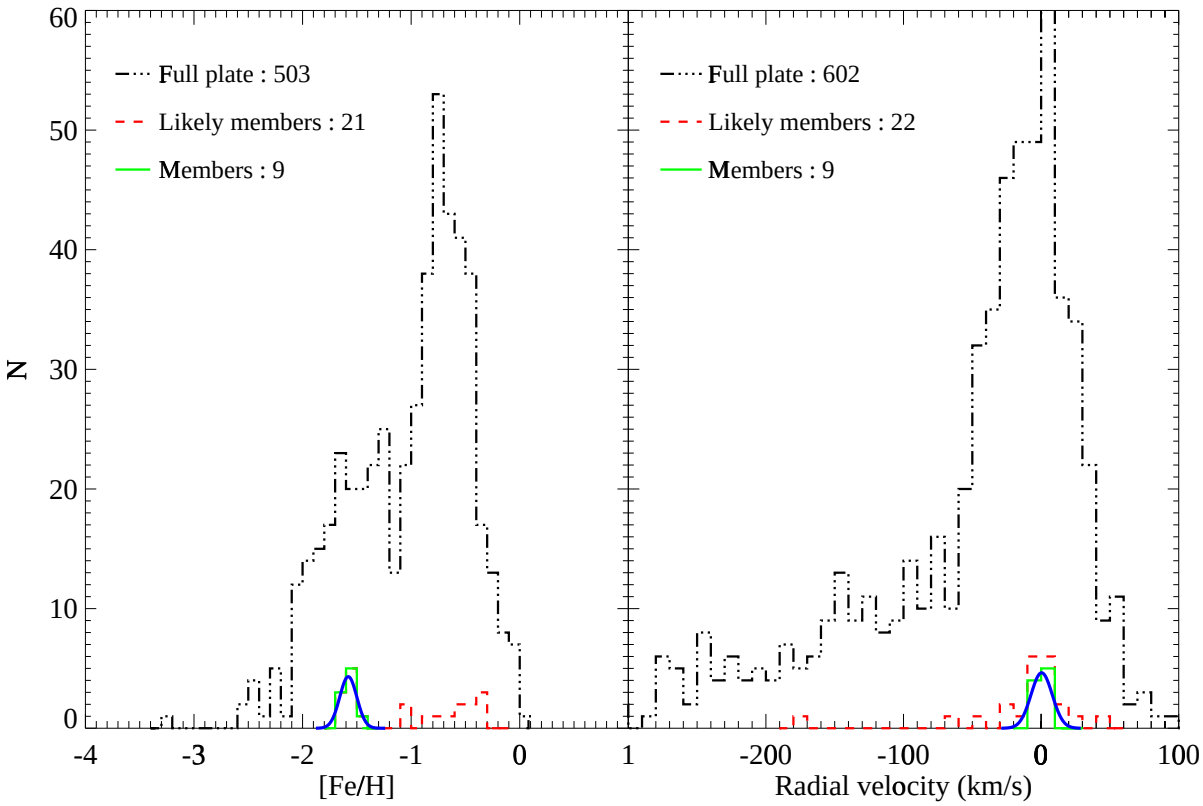

Fig. 7.— Same as Fig. 5 but for M 2.

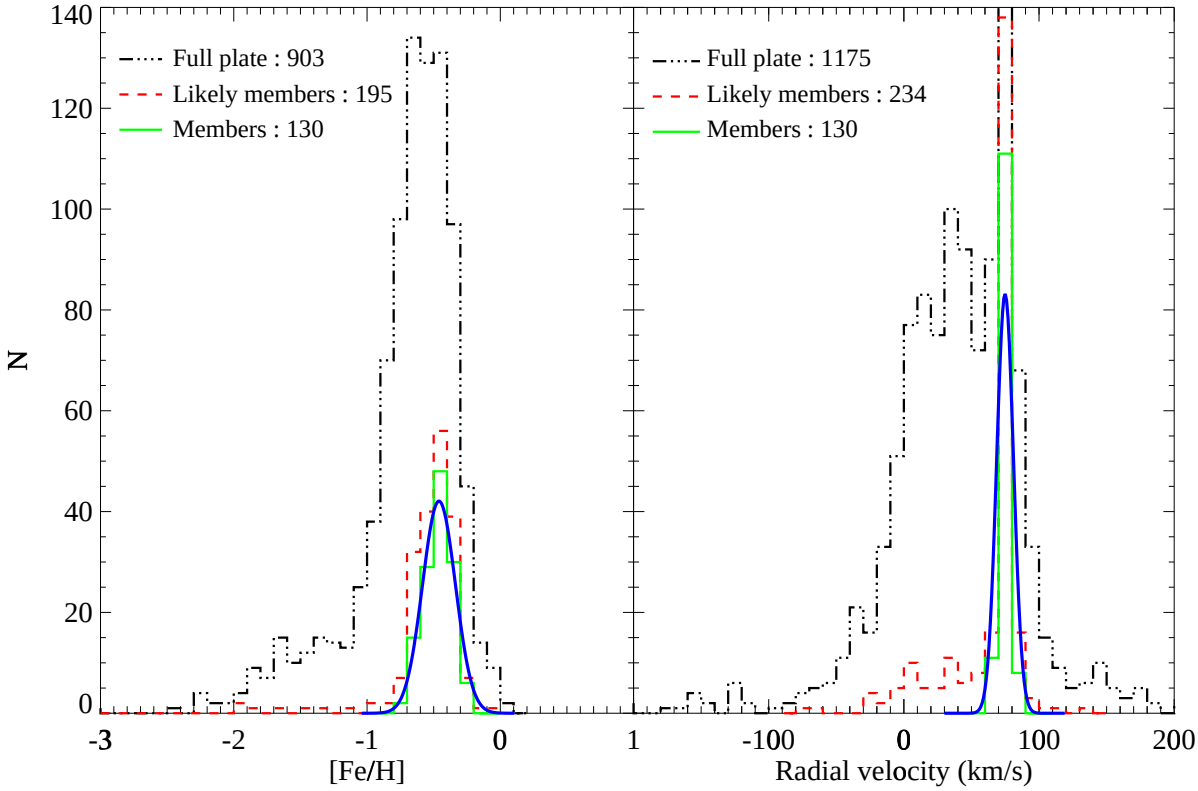

Fig. 8.— Same as Fig. 5 but for NGC 2420.

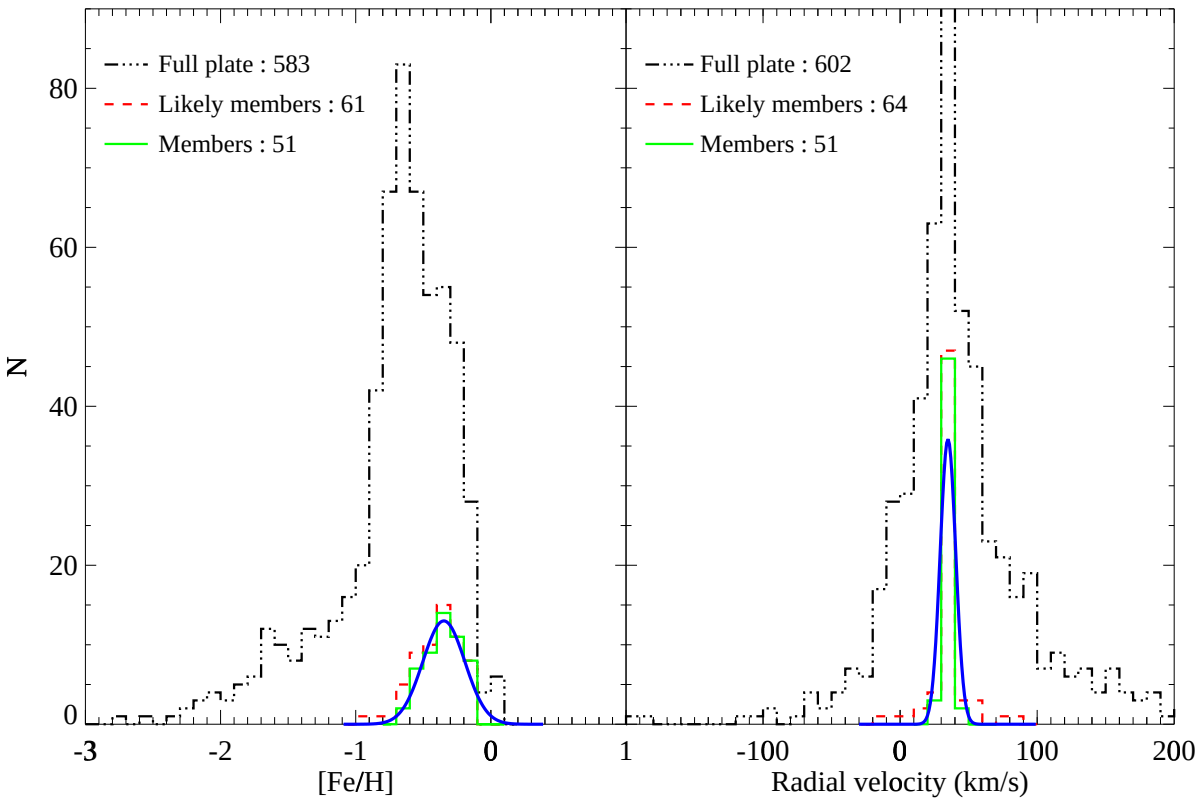

Fig. 9.— Same as Fig. 5 but for M 67.

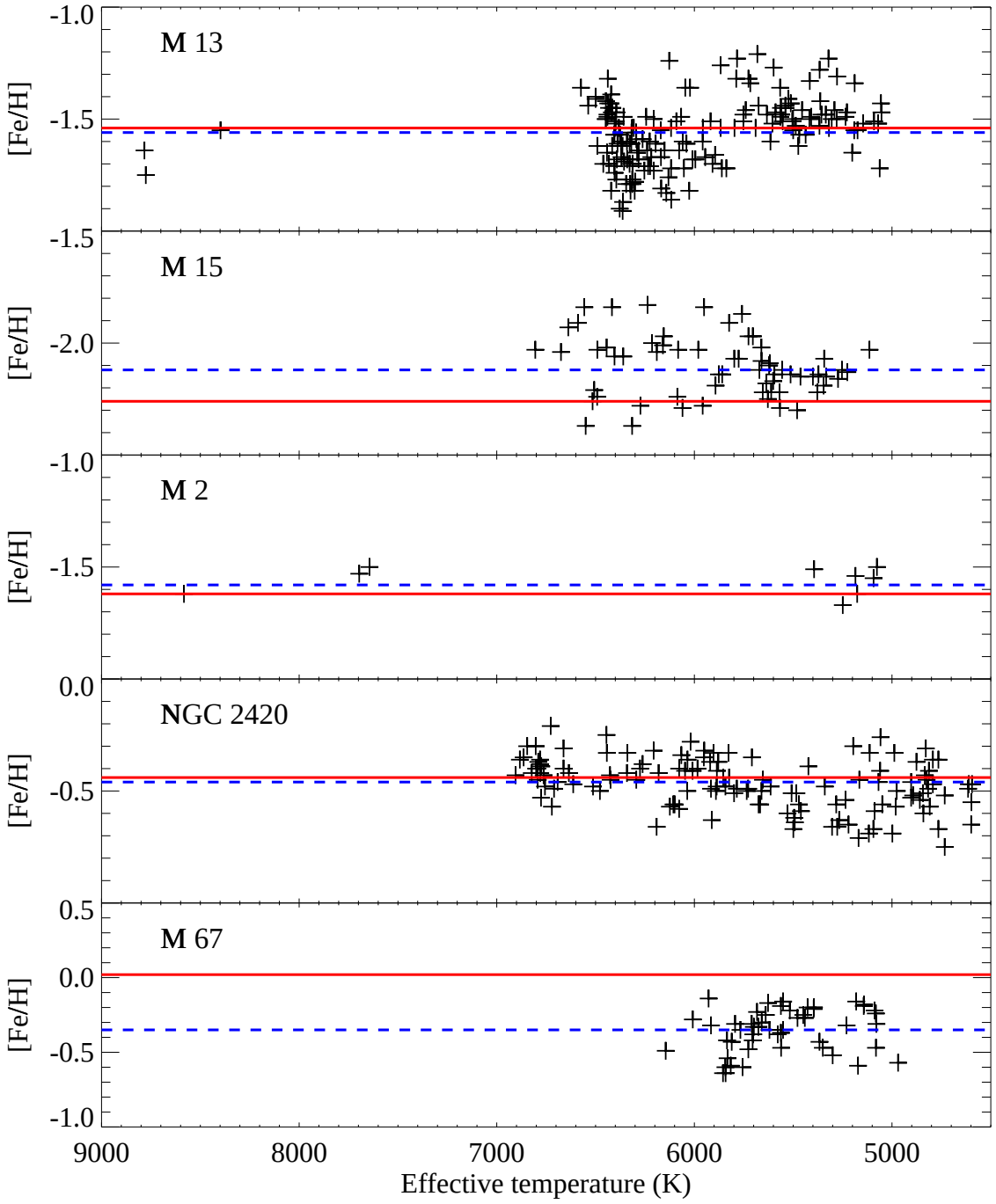

Fig. 10.— Distribution of [Fe/H] as a function of effective temperature for selected true member stars of M 13, M 15, M 2, NGC 2420, and M 67. The mean [Fe/H] determined for each cluster based on these estimates is shown with the blue dashed line; the red solid line represents the adopted literature value in each panel.

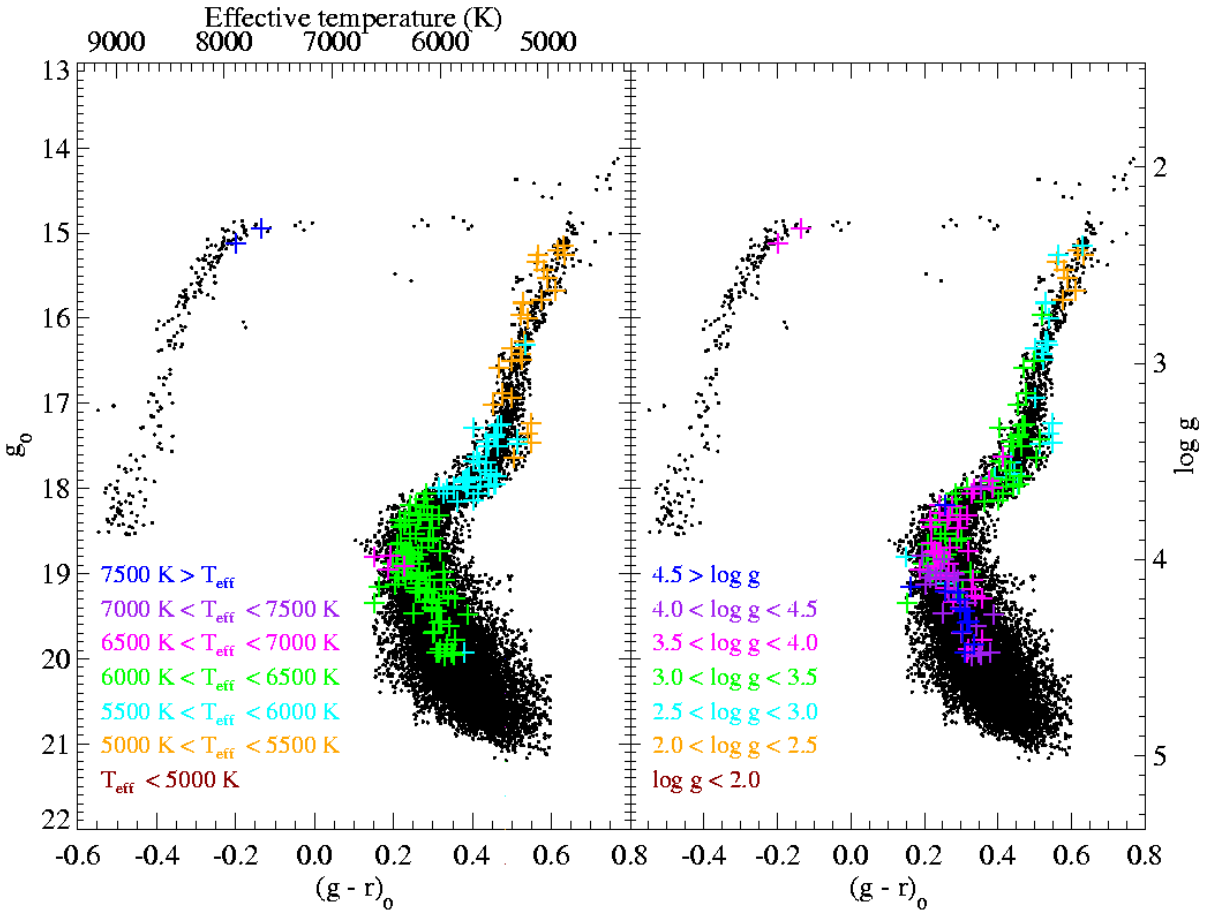

Fig. 11.— Temperature and gravity distributions of the selected true member stars for M 13. Each color represents a temperature range of width 500 K, and a surface gravity range of 0.5 dex, respectively. The temperature scales on the top of the left hand panel come from a linear relation between $(g - r)_0$ color and $T_{\rm eff}$ by performing a least squares fit to the theoretical models of Girardi et al. (2004). A similar procedure is applied for transforming the g_0 magnitude to a theoretical log g scale on the ordinate in the right-hand panel.

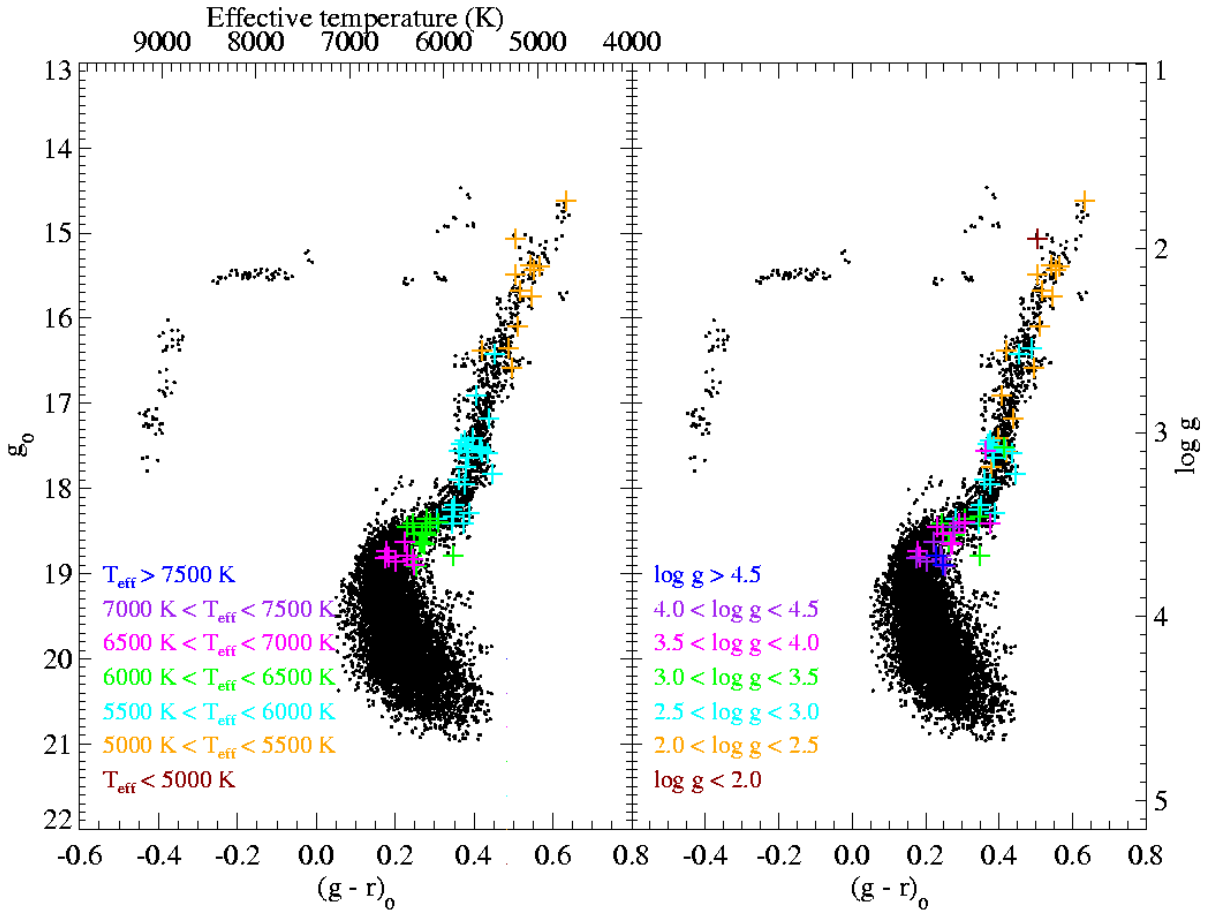

Fig. 12.— Same as Fig. 11 but for M 15.

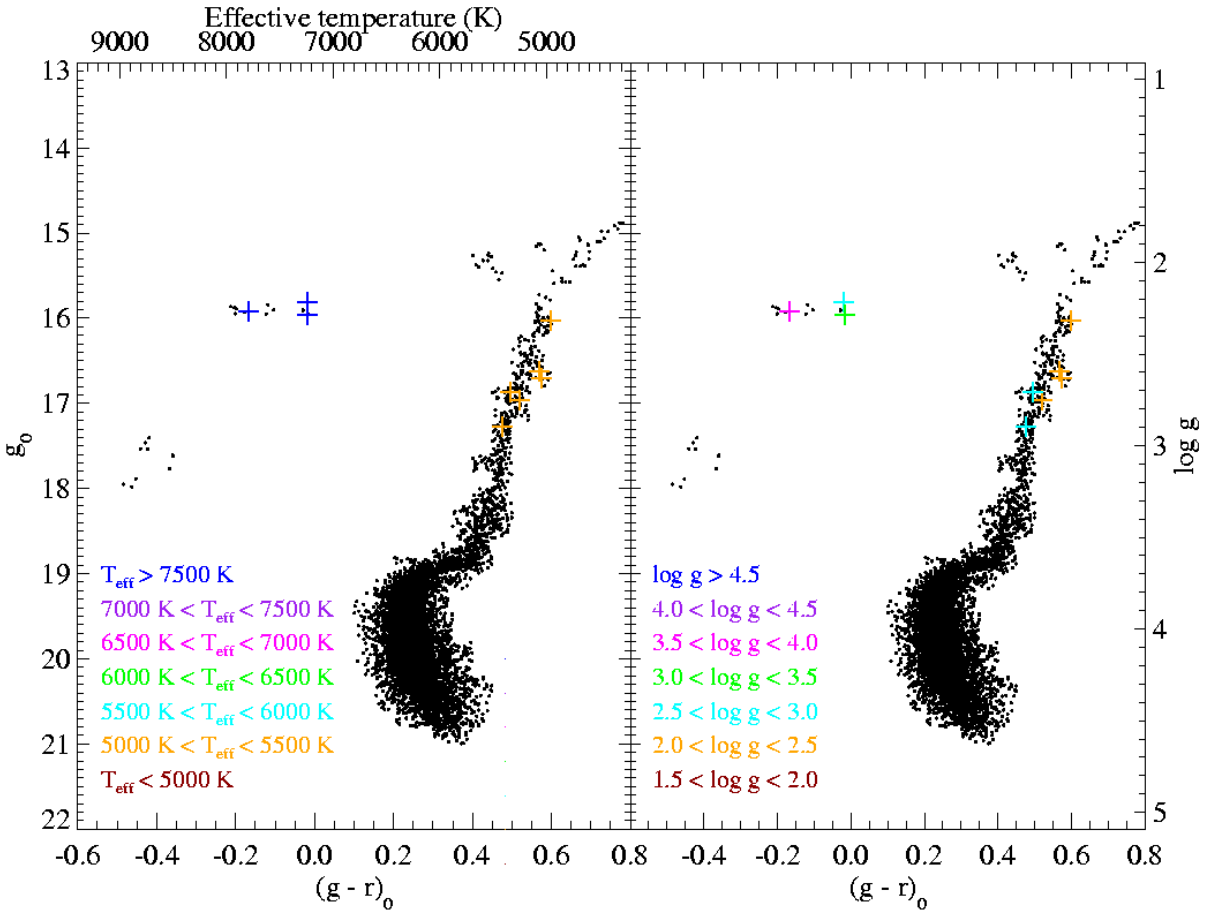

Fig. 13.— Same as Fig. 11 but for M 2.

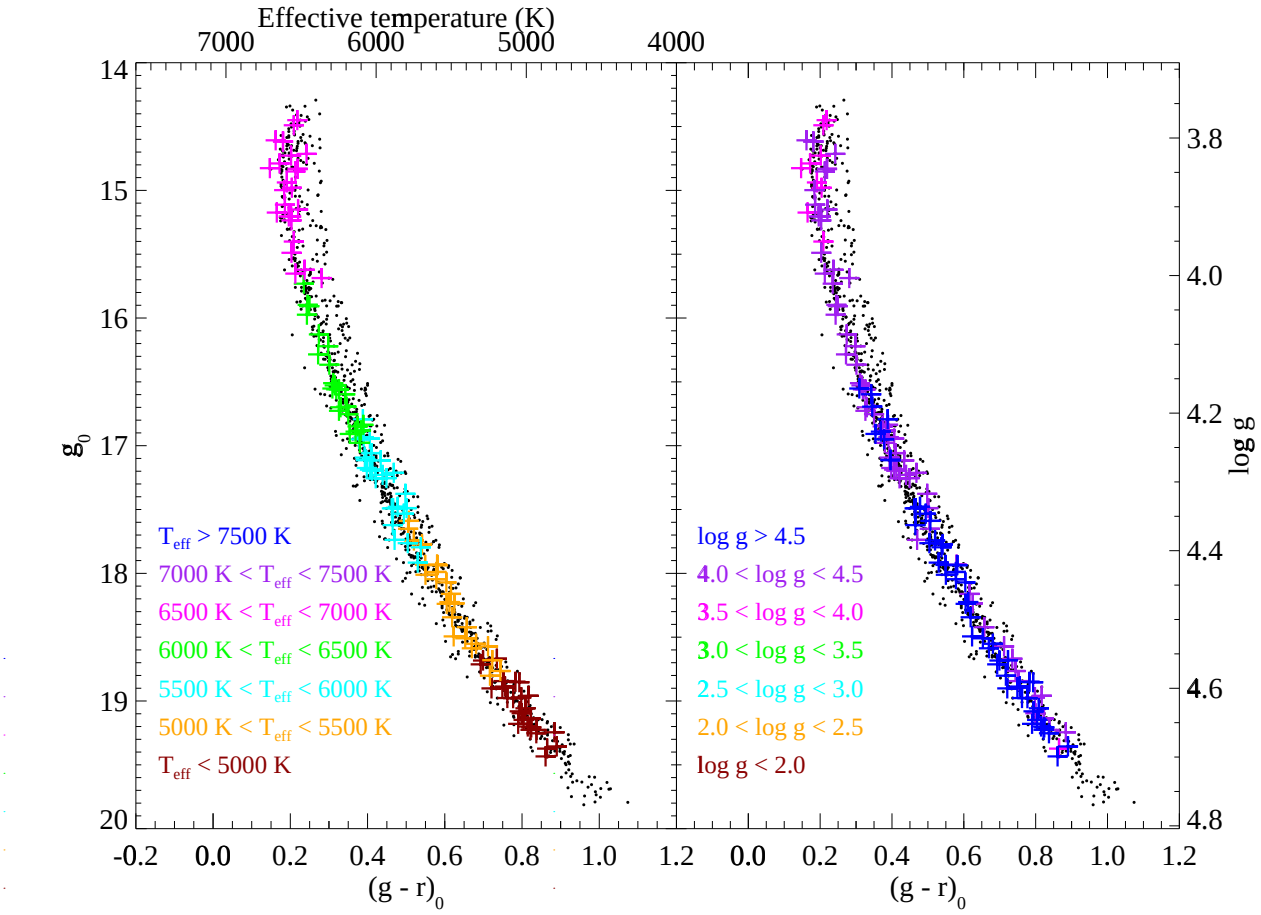

Fig. 14.— Same as Fig. 11 but for NGC 2420.

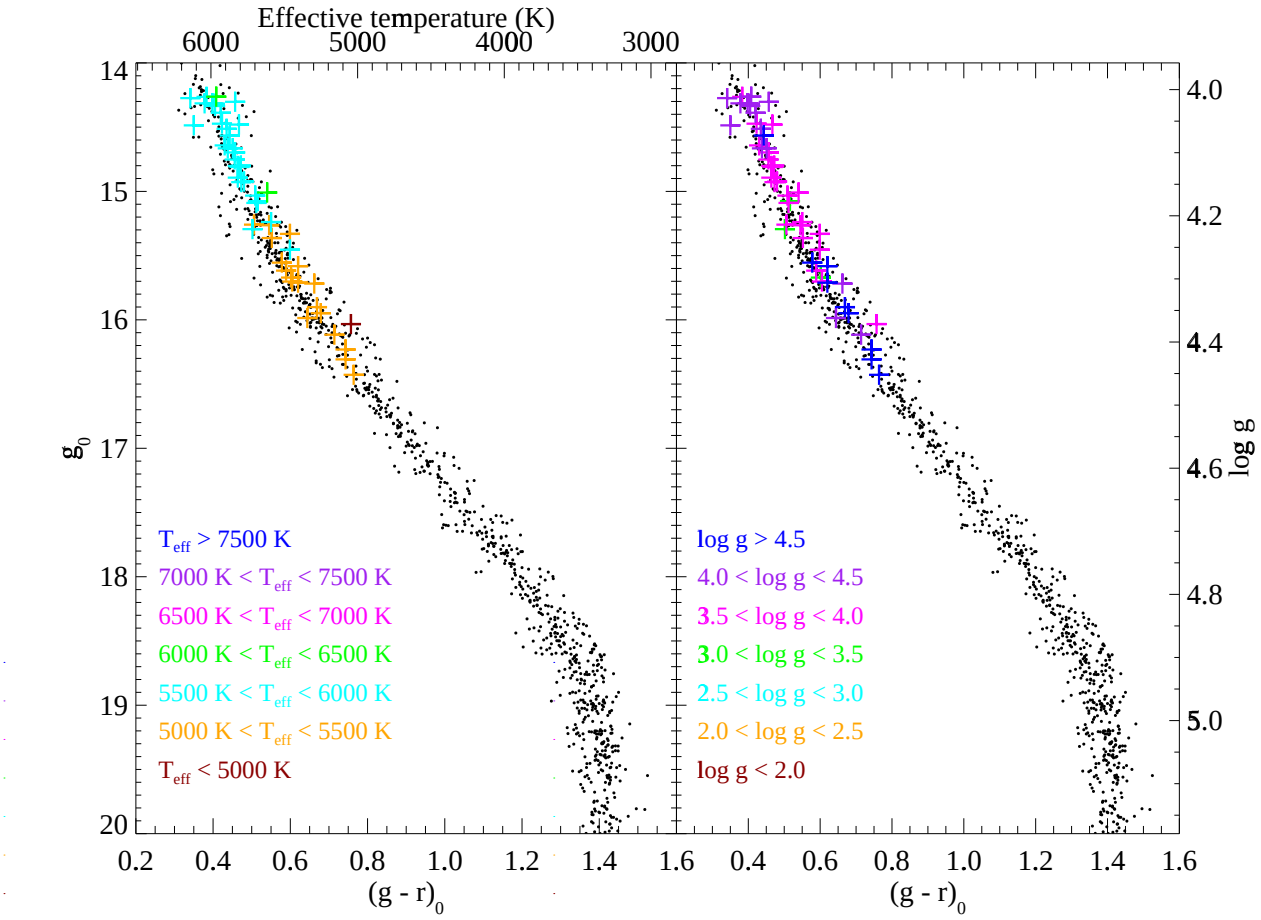

Fig. 15.— Same as Fig. 11 but for M 67.

Table 1. Properties of the Clusters

	M 15 (NGC 7078)	M 2 (NGC 7089)	M 13 (NGC 6205)	NGC 2420	M 67 (NGC 2682)
RA (J2000)	21:29:58.3	21:33:29.3	16:41:41.5	07:38:23	08:51:18
DEC (J2000)	+12:10:01	−00:49:23	+36:27:37	+21:34:24	+11:48:00
(l, b)	(65.0, −27.3)	(58.4, −35.8)	(59.0, +40.9)	(198.1, +19.6)	(215.7, +31.9)
[Fe/H]	−2.26	−1.62	−1.54	−0.44	+0.02
m - M	15.37	15.49	14.48	12.54	9.97
V_r(km s^{-1})	−107.0	−5.3	−245.6	74.0	32.9
E$(B-V)$	0.1	0.06	0.02	0.03	0.06
r_t	21.50	21.45	25.18	5[1]	25[1]

[1]This case is the apparent diameter of the cluster in arc minutes from Dias et al. (2002).

Note. — The parameter r_t is the tidal radius in arc minutes. The listed distance modulus, m−M, is corrected for extinction. The parameters for the globular clusters, M 13, M 15, and M 2 come from Harris (1996); those for the open clusters NGC 2420 and M 67 are from WEBDA (http://www.univie.ac.at/webda/). The radial velocity (V_r) listed for NGC 2420 and M 67 is the average of three literature values listed in WEBDA (see text). The [Fe/H] of NGC 2420 and M 67 is based on high- resolution spectroscopy described by Gratton (2000).

Table 2. Derived Radial Velocities and Metallicities of the Clusters

Cluster	$[Fe/H]_l$	$[Fe/H]_u$	RV_l	RV_u	<[Fe/H]>	σ ([Fe/H])	<RV>	σ (RV)	Mem_{tot}	$[Fe/H]_H$	RV_H	$[Fe/H]_{HR}$
	dex	dex	km s^{-1}	km s^{-1}	dex	dex	km s^{-1}	km s^{-1}		dex)	km s^{-1}	dex
(1)	(2)	(3)	(4)	(5)	(6)	(7)	(8)	(9)	(10)	(11)	(12)	(13)
M 13	−1.91	−1.20	−264.0	−226.1	−1.56	0.16	−245.1	8.7	169	−1.54	−245.6	−1.63
M 15	−2.42	−1.80	−132.8	−81.6	−2.12	0.14	−107.4	10.5	63	−2.26	−107.0	−2.42
M 2	−1.74	−1.40	−24.5	+25.3	−1.58	0.08	+0.4	7.7	9	−1.62	− 5.3	−1.56
NGC 2420	−0.77	−0.19	+60.5	+89.3	−0.46	0.12	+74.8	6.2	130	···	+ 74.0[1]	−0.44
M 67	−0.73	−0.02	+21.1	+48.6	−0.35	0.16	+34.9	5.6	51	···	+ 32.9[1]	+0.02

[1]This value is an average from the literature values. See §4.2 for more detail.

Note. — The subscripts u and l on [Fe/H] and RV are the upper and lower limits for the metallicity and radial velocity cuts used for choosing true members, as described in the text. The parameters for the globular clusters M 13, M 15, and M 2 come from Harris (1996); those for the open clusters NGC 2420 and M 67 are from WEBDA (http: //www.univie.ac.at/webda/). Values of $[Fe/H]_{HR}$, which are based on high-resolution spectroscopy, are from Kraft & Ivans (2003; M 13 and 15) from Ivans (private communication; M 2), and from Gratton (2000; NGC 2420 and M 67). The column labeled Mem_{tot} lists the total number of true members assigned to each cluster.

Table 3. Mean and 1σ Values of Residuals of $T_{\rm eff}$ and $\log g$ Between SSPP and Model Fits.

Cluster	N	$T_{\rm eff}$ $<\Delta>$ (K)	σ (K)	$\log g$ $<\Delta>$ (dex)	σ (dex)
M 13	169	+51	125	−0.07	0.44
M 15	63	+110	94	−0.17	0.40
M 2	9	+190	293	+0.19	0.55
NGC 2420	130	+12	105	+0.15	0.42
M 67	51	−119	104	−0.27	0.43

Note. — These values are 5σ clipped averages and standard deviations.

Table 4. Properties of Selected Member Stars of M 13

spSpec name	RA (degree)	DEC (degree)	RV (km s^{-1})	σ_{RV} (km s^{-1})	T_{eff} (K)	$\sigma_{T_{eff}}$ (K)	log g (dex)	$\sigma_{\log g}$ (dex)	[Fe/H] (dex)	$\sigma_{[Fe/H]}$ (dex)	u	σ_u	g	σ_g	r	σ_r	i	σ_i	z	σ_z	< S/N >
53521−2174−054	250.8113861	36.380367	−240.4	5.2	5605	2	2.98	0.22	−1.52	0.09	19.00	0.03	17.83	0.01	17.39	0.02	17.23	0.02	17.17	0.02	17.1
53521−2174−082	250.6566925	36.292824	−244.1	2.0	5146	44	2.35	0.23	−1.52	0.06	16.88	0.02	15.43	0.01	14.85	0.02	14.63	0.02	14.50	0.02	51.2
53521−2174−087	250.5986176	36.141987	−236.8	3.5	5500	31	3.11	0.21	−1.55	0.06	18.42	0.02	17.26	0.02	16.79	0.02	16.62	0.02	16.54	0.02	24.3
53521−2174−094	250.6187286	36.193378	−241.2	3.4	5553	25	3.14	0.27	−1.51	0.02	18.42	0.02	17.25	0.02	16.78	0.02	16.56	0.02	16.47	0.02	24.9
53521−2174−126	250.4946899	36.287205	−235.8	3.8	5487	60	3.02	0.12	−1.53	0.03	18.25	0.03	17.01	0.01	16.56	0.01	16.31	0.03	16.28	0.02	27.1
53521−2174−128	250.4741516	36.309807	−252.5	4.3	5524	77	3.34	0.24	−1.41	0.06	18.64	0.03	17.50	0.01	17.06	0.01	16.77	0.03	16.75	0.02	19.2
53521−2174−133	250.5125122	36.321091	−245.7	3.4	5418	64	3.16	0.11	−1.50	0.08	18.10	0.03	16.88	0.01	16.40	0.01	16.14	0.03	16.11	0.04	31.8
53521−2174−134	250.5464020	36.344273	−244.2	3.2	5455	79	2.88	0.38	−1.46	0.06	18.45	0.02	17.35	0.02	16.82	0.02	16.64	0.01	16.53	0.01	24.5
53521−2174−146	250.3612061	36.200855	−248.3	4.4	5633	2	2.96	0.27	−1.48	0.06	18.83	0.04	17.69	0.01	17.25	0.01	17.06	0.03	17.03	0.02	19.8
53521−2174−149	250.3400269	36.200890	−244.1	4.8	5681	43	3.39	0.20	−1.21	0.10	18.88	0.04	17.78	0.01	17.35	0.01	17.15	0.03	17.12	0.02	16.7
53521−2174−155	250.3851166	36.147091	−242.8	2.5	5367	39	3.00	0.12	−1.53	0.05	17.77	0.02	16.50	0.01	16.01	0.02	15.81	0.02	15.73	0.01	35.1
53521−2174−174	250.1682281	36.190548	−252.8	7.8	5784	34	3.33	0.38	−1.23	0.42	18.85	0.03	17.90	0.02	17.48	0.02	17.35	0.02	17.28	0.02	16.1
53521−2174−215	250.0930939	36.313175	−244.3	1.8	5174	56	2.34	0.21	−1.55	0.09	16.76	0.02	15.34	0.02	14.78	0.02	14.56	0.03	14.42	0.02	52.2
53521−2174−217	250.0905457	36.281464	−232.8	6.9	5958	95	3.48	0.60	−1.60	0.17	19.01	0.03	17.99	0.02	17.68	0.02	17.52	0.03	17.46	0.02	14.7
53521−2174−368	250.1569672	36.596581	−254.4	3.5	5512	48	3.21	0.19	−1.43	0.05	18.64	0.02	17.51	0.02	17.04	0.01	16.87	0.03	16.78	0.02	22.4
53521−2174−371	250.0941315	36.500916	−241.8	3.5	5566	17	3.09	0.09	−1.36	0.03	18.50	0.02	17.36	0.02	16.91	0.01	16.70	0.03	16.64	0.02	26.1
53521−2174−376	250.1804047	36.558369	−251.6	1.8	5201	26	2.41	0.28	−1.65	0.06	17.10	0.02	15.78	0.01	15.21	0.01	14.99	0.03	14.93	0.02	48.7
53521−2174−379	250.1767273	36.542747	−250.1	1.9	8783	165	3.64	0.20	−1.64	0.10	16.18	0.01	15.11	0.01	15.31	0.01	15.53	0.03	15.65	0.02	56.1
53521−2174−403	250.2917633	36.632149	−259.5	5.2	5918	51	4.15	0.18	−1.51	0.01	18.95	0.03	17.98	0.02	17.62	0.01	17.45	0.02	17.40	0.02	18.3
53521−2174−406	250.2974548	36.656551	−250.2	4.6	5675	94	3.42	0.25	−1.44	0.10	18.94	0.03	17.89	0.02	17.50	0.01	17.30	0.02	17.26	0.02	20.1
53521−2174−407	250.2983246	36.606567	−252.6	1.9	5416	73	3.29	0.12	−1.33	0.14	17.78	0.02	16.58	0.02	16.11	0.01	15.89	0.02	15.78	0.01	39.1
53521−2174−412	250.2389069	36.587105	−244.1	3.7	5504	57	2.72	0.11	−1.51	0.09	18.61	0.02	17.47	0.02	16.96	0.01	16.80	0.03	16.74	0.02	23.5
53521−2174−414	250.2673035	36.586380	−241.6	3.5	5437	77	2.68	0.29	−1.57	0.05	18.60	0.02	17.46	0.02	16.91	0.01	16.79	0.03	16.71	0.02	26.0
53521−2174−418	250.2429047	36.708576	−247.5	1.9	5363	54	2.85	0.11	−1.42	0.08	17.65	0.02	16.36	0.02	15.86	0.02	15.64	0.01	15.56	0.02	41.6
53521−2174−445	250.3153534	36.581833	−244.6	4.5	5752	72	3.39	0.28	−1.48	0.10	18.96	0.03	17.90	0.02	17.52	0.01	17.39	0.02	17.23	0.02	19.6
53521−2174−447	250.3488159	36.637089	−244.5	4.0	5726	43	3.33	0.13	−1.32	0.05	18.72	0.03	17.67	0.02	17.27	0.01	17.06	0.02	17.03	0.02	23.0
53521−2174−456	250.3559265	36.608372	−248.6	3.0	5539	27	3.07	0.20	−1.45	0.04	18.50	0.02	17.39	0.02	16.94	0.01	16.78	0.02	16.63	0.02	27.5
53521−2174−461	250.4161987	36.592712	−246.4	3.0	5501	60	3.21	0.26	−1.50	0.06	18.44	0.03	17.42	0.02	16.91	0.01	16.79	0.02	16.58	0.02	25.1
53521−2174−471	250.4050598	36.680744	−250.7	1.9	5305	49	2.85	0.24	−1.50	0.08	17.51	0.02	16.27	0.02	15.74	0.01	15.50	0.02	15.42	0.01	43.5
53521−2174−474	250.4210815	36.630798	−240.3	3.7	5474	35	3.12	0.27	−1.62	0.06	18.73	0.03	17.64	0.02	17.14	0.01	17.02	0.02	16.89	0.02	23.0
53521−2174−480	250.3775940	36.560562	−244.6	2.5	5409	20	2.91	0.19	−1.49	0.01	18.03	0.02	16.94	0.02	16.44	0.01	16.31	0.02	15.99	0.02	34.2
53521−2174−481	250.4867401	36.625168	−246.2	5.6	5690	60	3.06	0.27	−1.54	0.12	18.97	0.03	17.95	0.02	17.50	0.01	20.01	1.24	17.23	0.02	17.1
53521−2174−529	250.6122742	36.650723	−246.7	1.9	5357	37	2.94	0.19	−1.48	0.08	17.70	0.02	16.49	0.02	15.96	0.02	15.75	0.02	15.66	0.02	41.6

Table 4—Continued

spSpec name	RA (degree)	DEC (degree)	RV (km s^{-1})	σ_{RV} (km s^{-1})	T_{eff} (K)	$\sigma_{T_{eff}}$ (K)	log g (dex)	$\sigma_{\log g}$ (dex)	[Fe/H] (dex)	$\sigma_{[Fe/H]}$ (dex)	u	σ_u	g	σ_g	r	σ_r	i	σ_i	z	σ_z	< S/N >
53521−2174−533	250.5825653	36.416344	−250.1	4.5	5615	27	3.16	0.24	−1.60	0.08	18.92	0.04	17.86	0.03	17.40	0.02	17.20	0.02	17.16	0.02	20.3
53521−2174−537	250.6071167	36.431816	−252.3	1.6	5291	41	2.70	0.23	−1.46	0.09	17.27	0.01	16.00	0.02	15.46	0.02	15.19	0.01	15.08	0.01	49.0
53521−2174−539	250.6033020	36.480679	−251.2	3.2	5539	96	3.39	0.14	−1.44	0.02	18.78	0.03	17.70	0.02	17.28	0.02	16.99	0.01	16.87	0.02	23.6
53521−2174−542	250.4867096	36.697521	−250.9	1.3	5070	28	2.14	0.22	−1.52	0.07	16.78	0.02	15.26	0.02	14.63	0.01	14.38	0.02	14.27	0.01	55.1
53521−2174−554	250.4524536	36.731075	−250.2	1.6	5280	44	2.77	0.03	−1.50	0.06	17.20	0.02	15.81	0.02	15.29	0.01	15.04	0.02	14.92	0.01	49.7
53521−2174−560	250.4494934	36.746979	−248.1	3.4	5565	62	3.23	0.16	−1.49	0.02	18.49	0.02	17.45	0.02	17.02	0.01	16.80	0.02	16.70	0.02	25.8
53521−2174−563	250.7275696	36.537083	−247.3	2.0	5319	45	2.87	0.23	−1.54	0.10	17.66	0.02	16.42	0.01	15.90	0.01	15.69	0.01	15.58	0.02	38.5
53521−2174−565	250.6674805	36.541718	−247.8	5.0	5797	59	3.24	0.32	−1.54	0.06	18.87	0.03	17.92	0.01	17.54	0.01	17.35	0.01	17.28	0.02	20.6
53521−2174−573	250.7793579	36.401161	−245.5	5.7	5788	51	3.41	0.52	−1.32	0.09	19.09	0.03	17.98	0.01	17.59	0.02	17.45	0.02	17.38	0.02	19.6
53521−2174−577	250.6542358	36.559769	−250.0	4.1	5562	24	2.98	0.17	−1.45	0.06	18.97	0.03	17.95	0.01	17.50	0.01	17.33	0.01	17.26	0.02	20.7
53532−2185−111	250.6518555	36.315819	−246.0	4.9	6398	94	3.14	0.54	−1.51	0.08	19.47	0.04	18.58	0.02	18.34	0.04	18.32	0.05	18.37	0.04	20.7
53532−2185−120	250.6814728	36.301613	−229.4	6.2	6395	53	4.43	0.06	−1.47	0.09	20.02	0.05	19.20	0.02	18.92	0.02	18.81	0.02	18.68	0.04	15.3
53532−2185−141	250.5120239	36.217281	−238.8	4.0	6364	78	3.20	0.34	−1.62	0.06	19.35	0.04	18.39	0.01	18.16	0.01	18.04	0.03	18.08	0.03	26.6
53532−2185−143	250.5701752	36.201962	−235.4	4.9	6341	36	3.44	0.18	−1.60	0.10	19.46	0.04	18.53	0.01	18.28	0.01	18.16	0.03	18.21	0.03	23.4
53532−2185−148	250.6033325	36.234558	−243.2	5.4	6404	87	4.08	0.41	−1.74	0.01	19.84	0.05	18.99	0.01	18.75	0.02	18.63	0.03	18.69	0.04	18.3
53532−2185−150	250.6054077	36.200813	−241.7	5.2	6403	66	3.40	0.30	−1.54	0.07	19.71	0.04	18.79	0.02	18.56	0.02	18.44	0.02	18.41	0.04	20.6
53532−2185−152	250.6186066	36.331161	−235.4	5.5	6392	53	3.37	0.43	−1.68	0.13	19.70	0.04	18.81	0.02	18.56	0.02	18.49	0.01	18.47	0.03	20.9
53532−2185−153	250.5179138	36.306831	−243.9	3.0	5861	19	3.48	0.22	−1.72	0.03	19.08	0.04	18.14	0.01	17.74	0.01	17.56	0.03	17.52	0.02	33.6
53532−2185−156	250.5538483	36.304375	−245.1	7.1	6340	48	4.07	0.32	−1.68	0.11	19.87	0.05	19.05	0.01	18.79	0.02	18.70	0.03	18.71	0.04	17.9
53532−2185−158	250.5086365	36.321423	−240.5	5.8	6389	99	3.92	0.38	−1.61	0.14	19.90	0.05	18.93	0.01	18.70	0.02	18.56	0.03	18.58	0.04	19.4
53532−2185−160	250.5746155	36.340302	−240.8	6.5	6253	38	4.71	0.08	−1.73	0.14	20.01	0.05	19.23	0.02	18.93	0.02	18.89	0.02	18.89	0.04	15.2
53532−2185−167	250.3744202	36.210903	−248.3	4.4	6404	58	3.53	0.49	−1.57	0.08	19.73	0.05	18.75	0.01	18.51	0.02	18.40	0.03	18.39	0.04	22.2
53532−2185−169	250.3382111	36.202835	−238.7	5.7	6295	59	3.49	0.54	−1.56	0.06	19.96	0.06	19.01	0.01	18.75	0.02	18.65	0.03	18.67	0.04	18.6
53532−2185−172	250.4851227	36.205223	−247.0	5.1	6448	35	3.51	0.33	−1.42	0.07	19.75	0.05	18.77	0.01	18.53	0.02	18.41	0.03	18.41	0.04	21.5
53532−2185−175	250.4423218	36.258049	−250.9	5.2	6537	76	2.96	0.66	−1.44	0.23	19.80	0.05	18.81	0.01	18.66	0.02	18.45	0.03	18.51	0.04	19.9
53532−2185−176	250.4879761	36.319519	−235.4	4.7	6358	73	3.46	0.37	−1.49	0.09	19.80	0.05	18.82	0.01	18.59	0.02	18.38	0.03	18.41	0.04	21.8
53532−2185−177	250.4530029	36.298698	−245.6	5.1	6440	97	3.48	0.67	−1.48	0.13	19.73	0.05	18.89	0.01	18.68	0.02	18.48	0.03	18.58	0.04	20.6
53532−2185−178	250.4822845	36.300014	−243.8	6.3	6425	132	4.09	0.16	−1.43	0.13	19.99	0.06	19.13	0.03	18.93	0.03	18.78	0.04	18.79	0.05	18.3
53532−2185−179	250.4799957	36.221458	−239.4	4.0	6406	85	3.44	0.31	−1.57	0.08	19.33	0.05	18.43	0.01	18.20	0.01	18.10	0.03	18.16	0.03	26.7
53532−2185−181	250.2265778	36.218925	−246.9	4.9	6440	67	3.55	0.31	−1.49	0.13	19.59	0.05	18.74	0.02	18.51	0.02	18.44	0.02	18.37	0.04	21.8
53532−2185−185	250.2001953	36.208260	−263.6	5.7	6421	87	4.08	0.54	−1.82	0.09	19.60	0.05	18.83	0.02	18.58	0.02	18.53	0.02	18.45	0.04	19.9
53532−2185−196	250.1731720	36.201431	−249.1	5.9	6302	60	3.93	0.58	−1.82	0.08	19.83	0.05	19.02	0.02	18.76	0.02	18.69	0.02	18.73	0.05	17.5
53532−2185−197	250.1752930	36.316170	−245.3	6.8	6363	59	2.72	0.59	−1.91	0.11	20.09	0.06	19.11	0.02	18.85	0.02	18.80	0.03	18.82	0.05	15.6
53532−2185−198	250.2095490	36.280247	−241.3	5.5	6319	1	3.97	0.44	−1.61	0.11	19.57	0.04	18.89	0.02	18.62	0.02	18.52	0.03	18.52	0.04	20.8

Table 4—Continued

spSpec name	RA (degree)	DEC (degree)	RV (km s^{-1})	σ_{RV} (km s^{-1})	T_{eff} (K)	$\sigma_{T_{eff}}$ (K)	log g (dex)	$\sigma_{\log g}$ (dex)	[Fe/H] (dex)	$\sigma_{[Fe/H]}$ (dex)	u	σ_u	g	σ_g	r	σ_r	i	σ_i	z	σ_z	< S/N >
53532−2185−237	250.1001129	36.310001	−239.1	3.2	6059	99	3.41	0.21	−1.60	0.06	19.04	0.03	18.06	0.02	17.78	0.02	17.64	0.03	17.61	0.03	33.0
53532−2185−388	250.0598145	36.565910	−250.1	3.5	6377	65	3.75	0.19	−1.57	0.05	19.18	0.03	18.28	0.02	18.04	0.01	17.94	0.03	17.89	0.03	29.9
53532−2185−423	250.1191559	36.614777	−247.8	4.8	6318	76	3.44	0.44	−1.56	0.13	19.80	0.04	18.88	0.02	18.63	0.01	18.56	0.03	18.57	0.04	21.6
53532−2185−424	250.1623840	36.546970	−242.6	4.8	6328	69	4.40	0.28	−1.70	0.06	19.95	0.10	19.23	0.11	18.96	0.10	18.80	0.09	19.00	0.16	22.6
53532−2185−425	250.1024933	36.708916	−248.3	3.3	6282	36	3.65	0.14	−1.68	0.03	19.23	0.03	18.31	0.02	18.05	0.01	17.98	0.02	17.94	0.03	31.6
53532−2185−426	250.1142273	36.579521	−246.0	2.8	5945	58	3.73	0.21	−1.67	0.05	19.02	0.03	18.01	0.02	17.67	0.01	17.54	0.03	17.49	0.02	35.6
53532−2185−427	250.1687622	36.572681	−243.5	2.9	5908	38	3.65	0.22	−1.70	0.03	19.01	0.03	18.00	0.02	17.65	0.01	17.52	0.03	17.49	0.02	36.2
53532−2185−428	250.2005005	36.620838	−247.8	6.1	6168	95	3.37	0.91	−1.81	0.05	20.09	0.05	19.19	0.02	18.90	0.01	18.80	0.03	18.85	0.05	17.1
53532−2185−430	250.1428375	36.630520	−253.7	10.1	6262	49	4.44	0.26	−1.59	0.14	20.49	0.07	19.69	0.02	19.39	0.01	19.26	0.03	19.25	0.06	11.7
53532−2185−431	250.1810608	36.514454	−239.5	9.4	6091	44	3.99	0.32	−1.51	0.16	20.83	0.09	19.89	0.02	19.57	0.02	19.49	0.03	19.35	0.07	10.3
53532−2185−433	250.0788116	36.418709	−261.8	9.7	5895	27	4.43	0.38	−1.66	0.31	20.56	0.10	19.93	0.02	19.55	0.03	19.43	0.04	19.37	0.08	10.3
53532−2185−435	250.1384125	36.391571	−238.6	5.6	6416	69	4.17	0.27	−1.62	0.08	19.99	0.06	19.05	0.02	18.82	0.02	18.77	0.03	18.73	0.05	19.2
53532−2185−439	250.0806732	36.503437	−240.9	2.8	6151	71	3.06	0.22	−1.64	0.05	19.08	0.03	18.13	0.02	17.86	0.01	17.71	0.03	17.73	0.03	34.9
53532−2185−461	250.3284149	36.700005	−240.6	3.6	6307	86	3.11	0.47	−1.54	0.11	19.26	0.03	18.37	0.02	18.14	0.01	18.02	0.02	18.06	0.03	29.9
53532−2185−462	250.2369232	36.717884	−246.8	2.9	6196	61	3.51	0.25	−1.61	0.04	19.08	0.04	18.20	0.02	17.93	0.02	17.84	0.01	17.85	0.03	33.9
53532−2185−466	250.2878876	36.725266	−244.6	5.1	6500	112	4.04	0.26	−1.40	0.19	19.67	0.05	18.80	0.02	18.60	0.02	18.46	0.02	18.53	0.04	19.9
53532−2185−469	250.2945404	36.606640	−246.0	6.0	6447	106	4.38	0.27	−1.50	0.14	19.84	0.05	18.98	0.02	18.77	0.02	18.68	0.02	18.64	0.04	17.2
53532−2185−473	250.2791901	36.576611	−234.8	6.8	6131	120	3.90	0.56	−1.76	0.18	20.24	0.06	19.29	0.02	18.93	0.01	18.93	0.03	18.99	0.06	17.1
53532−2185−475	250.2398529	36.588871	−248.3	4.0	6314	47	3.35	0.25	−1.77	0.06	19.47	0.04	18.59	0.02	18.29	0.01	18.24	0.03	18.30	0.03	26.6
53532−2185−476	250.2485657	36.574799	−243.4	5.7	6117	62	3.99	0.25	−1.86	0.07	19.95	0.05	19.07	0.02	18.74	0.01	18.69	0.04	18.63	0.05	19.1
53532−2185−477	250.2305450	36.610828	−243.4	7.8	6077	92	4.76	0.76	−1.64	0.16	20.60	0.07	19.58	0.02	19.26	0.01	19.18	0.03	19.35	0.07	13.0
53532−2185−478	250.2751617	36.618698	−244.5	5.1	6327	37	4.09	0.26	−1.61	0.15	19.82	0.05	19.01	0.02	18.73	0.02	18.62	0.02	18.61	0.04	20.7
53532−2185−479	250.2099609	36.532490	−248.9	7.0	6026	98	4.43	0.20	−1.82	0.20	20.31	0.06	19.48	0.02	19.09	0.01	19.08	0.03	19.04	0.06	14.6
53532−2185−480	250.2232056	36.626942	−241.2	7.6	6244	70	4.74	0.10	−1.49	0.14	20.52	0.07	19.68	0.02	19.38	0.01	19.25	0.03	19.43	0.08	12.0
53532−2185−481	250.3259277	36.655441	−245.2	3.4	6315	65	3.60	0.33	−1.54	0.07	19.12	0.03	18.20	0.02	17.95	0.01	17.81	0.02	17.77	0.02	32.1
53532−2185−482	250.4379120	36.601913	−234.5	2.9	5995	17	3.35	0.25	−1.68	0.04	19.06	0.03	18.15	0.02	17.79	0.01	17.71	0.02	17.60	0.02	34.9
53532−2185−483	250.4119263	36.610191	−252.0	5.9	6234	47	3.31	0.37	−1.71	0.09	20.15	0.06	19.19	0.02	18.89	0.03	18.92	0.03	18.75	0.04	18.0
53532−2185−485	250.3427429	36.637764	−247.6	3.7	6442	91	3.78	0.44	−1.65	0.10	19.25	0.03	18.45	0.02	18.24	0.02	18.10	0.02	18.13	0.03	28.2
53532−2185−487	250.3905029	36.591457	−244.1	3.4	6281	40	3.77	0.31	−1.64	0.07	19.20	0.03	18.36	0.02	18.06	0.01	18.07	0.02	17.92	0.03	30.7
53532−2185−489	250.3863983	36.711922	−243.9	5.2	6449	116	4.41	0.06	−1.50	0.15	19.89	0.05	19.04	0.02	18.83	0.02	18.68	0.02	18.58	0.04	19.8
53532−2185−490	250.4195862	36.592098	−242.5	7.0	6206	28	4.62	0.11	−1.50	0.11	20.26	0.07	19.43	0.03	19.12	0.02	19.12	0.04	19.02	0.05	16.1
53532−2185−492	250.3582611	36.607357	−239.8	3.3	6169	71	3.43	0.37	−1.67	0.04	19.06	0.05	18.22	0.05	17.93	0.07	17.88	0.08	17.82	0.04	34.3
53532−2185−493	250.3370056	36.581230	−236.1	3.3	6399	82	3.71	0.03	−1.52	0.09	19.28	0.04	18.37	0.02	18.16	0.01	18.11	0.02	18.01	0.03	31.2
53532−2185−494	250.4333649	36.619698	−241.8	7.4	6118	31	3.97	0.04	−1.72	0.11	20.12	0.06	19.26	0.02	18.92	0.02	18.90	0.02	18.91	0.05	17.5

Table 4—Continued

spSpec name	RA (degree)	DEC (degree)	RV (km s^{-1})	σ_{RV} (km s^{-1})	T_{eff} (K)	$\sigma_{T_{eff}}$ (K)	log g (dex)	$\sigma_{\log g}$ (dex)	[Fe/H] (dex)	$\sigma_{[Fe/H]}$ (dex)	u	σ_u	g	σ_g	r	σ_r	i	σ_i	z	σ_z	< S/N >
53532−2185−495	250.3131714	36.642708	−240.4	4.4	6461	83	3.45	0.02	−1.70	0.12	19.40	0.04	18.66	0.02	18.45	0.02	18.33	0.02	18.34	0.03	25.3
53532−2185−496	250.3283539	36.603851	−237.2	7.8	6046	96	3.86	0.41	−1.36	0.16	20.94	0.18	19.92	0.14	19.61	0.05	19.57	0.04	19.58	0.08	10.2
53532−2185−497	250.3796539	36.606239	−234.8	8.5	6053	17	4.20	0.18	−1.72	0.10	20.50	0.08	19.62	0.02	19.28	0.02	19.25	0.03	19.11	0.05	12.9
53532−2185−498	250.4183960	36.693439	−233.7	4.5	6325	36	3.83	0.32	−1.79	0.04	19.44	0.04	18.70	0.02	18.43	0.02	18.33	0.02	18.37	0.03	25.0
53532−2185−499	250.3423157	36.618721	−229.1	4.6	6418	75	3.79	0.29	−1.47	0.07	19.52	0.04	18.74	0.02	18.52	0.02	18.44	0.02	18.41	0.03	24.1
53532−2185−500	250.3634491	36.578873	−243.9	3.1	6395	52	4.51	0.25	−1.77	0.04	18.96	0.03	18.20	0.02	17.94	0.02	17.97	0.03	17.84	0.02	36.5
53532−2185−504	250.5587463	36.680569	−249.5	4.1	6378	99	3.55	0.54	−1.90	0.07	19.55	0.03	18.74	0.02	18.51	0.02	18.41	0.02	18.44	0.03	24.9
53532−2185−506	250.5240936	36.660801	−245.6	2.5	5838	38	3.35	0.12	−1.72	0.03	19.02	0.03	18.06	0.02	17.65	0.01	17.53	0.02	17.48	0.02	39.0
53532−2185−507	250.4723969	36.677731	−241.8	5.4	6142	60	3.75	0.20	−1.83	0.06	20.07	0.06	19.18	0.02	18.85	0.02	18.79	0.02	18.77	0.04	18.5
53532−2185−511	250.5202179	36.342960	−246.6	6.9	6170	12	4.59	0.15	−1.55	0.12	20.75	0.13	19.93	0.13	19.62	0.18	19.35	0.18	19.35	0.08	14.0
53532−2185−512	250.5370789	36.365250	−249.0	3.3	6224	36	3.71	0.17	−1.71	0.06	19.19	0.03	18.32	0.02	18.00	0.02	17.92	0.02	17.92	0.04	33.7
53532−2185−513	250.5628357	36.372688	−245.5	4.8	6218	71	3.30	0.56	−1.67	0.11	19.78	0.04	18.97	0.02	18.65	0.02	18.61	0.02	18.58	0.03	22.8
53532−2185−514	250.5161896	36.359978	−237.4	5.4	6205	40	4.19	0.31	−1.73	0.14	20.26	0.07	19.35	0.03	19.03	0.04	19.02	0.03	19.02	0.06	18.6
53532−2185−515	250.5661469	36.400230	−244.2	5.1	6361	30	3.63	0.21	−1.87	0.06	19.81	0.05	18.99	0.02	18.71	0.02	18.65	0.02	18.68	0.04	21.8
53532−2185−516	250.4558868	36.613400	−238.0	10.0	6040	27	4.22	0.26	−1.61	0.20	20.75	0.10	19.93	0.03	19.59	0.04	19.48	0.03	19.37	0.06	10.8
53532−2185−517	250.4772949	36.625591	−249.2	10.6	6067	105	4.42	0.03	−1.49	0.18	20.81	0.10	19.95	0.02	19.60	0.02	19.47	0.03	19.43	0.07	10.5
53532−2185−519	250.5725555	36.425186	−243.5	4.9	6369	92	3.97	0.35	−1.67	0.05	19.87	0.06	19.06	0.14	18.83	0.12	18.67	0.13	18.72	0.04	22.7
53532−2185−534	250.3009644	36.802814	−251.6	4.0	6345	35	3.49	0.29	−1.79	0.11	19.46	0.04	18.61	0.02	18.32	0.02	18.26	0.02	18.24	0.03	26.7
53532−2185−537	250.4304962	36.822891	−240.2	4.8	6371	22	3.41	0.33	−1.60	0.10	19.59	0.04	18.78	0.02	18.52	0.02	18.46	0.02	18.42	0.03	24.1
53532−2185−540	250.3366394	36.751308	−232.3	6.7	6406	60	4.88	0.22	−1.71	0.10	19.98	0.06	19.21	0.02	18.96	0.02	18.85	0.02	18.92	0.05	16.8
53532−2185−542	250.6344757	36.460258	−235.6	7.2	6300	79	4.10	0.54	−1.78	0.10	20.41	0.07	19.46	0.02	19.21	0.02	19.01	0.02	19.05	0.05	15.4
53532−2185−543	250.6009674	36.613602	−250.8	3.3	6290	45	3.49	0.18	−1.65	0.04	19.22	0.03	18.30	0.02	18.03	0.02	17.91	0.02	17.91	0.02	32.8
53532−2185−544	250.6094360	36.447392	−249.4	5.3	6415	96	3.09	0.47	−1.45	0.09	19.85	0.05	18.88	0.02	18.68	0.02	18.54	0.01	18.53	0.03	21.9
53532−2185−545	250.6271667	36.714451	−240.3	5.6	6382	65	4.35	0.29	−1.54	0.13	19.95	0.04	19.07	0.02	18.78	0.02	18.70	0.02	18.70	0.04	18.9
53532−2185−549	250.5913239	36.461399	−234.6	6.1	6127	88	4.78	0.19	−1.24	0.07	20.45	0.07	19.56	0.03	19.24	0.07	19.02	0.02	19.05	0.05	14.7
53532−2185−551	250.5914764	36.413662	−232.8	10.1	6022	72	4.39	0.06	−1.36	0.16	20.82	0.09	19.97	0.03	19.64	0.03	19.48	0.03	19.49	0.07	10.4
53532−2185−552	250.6224670	36.431900	−251.6	5.5	6432	82	3.66	0.36	−1.70	0.11	19.71	0.04	18.94	0.02	18.70	0.02	18.59	0.02	18.60	0.03	20.2
53532−2185−553	250.6461029	36.350220	−245.7	3.1	5957	70	3.86	0.24	−1.54	0.06	18.98	0.03	18.06	0.02	17.74	0.02	17.57	0.01	17.56	0.02	36.9
53532−2185−554	250.6182556	36.410843	−246.2	3.7	6312	36	3.93	0.12	−1.70	0.04	19.20	0.03	18.37	0.02	18.11	0.02	17.97	0.01	17.94	0.02	30.9
53532−2185−555	250.6027374	36.400173	−241.2	7.8	6239	32	4.04	0.13	−1.64	0.13	20.27	0.07	19.40	0.04	19.10	0.04	18.97	0.04	18.98	0.06	16.1
53532−2185−556	250.6363068	36.383652	−249.0	6.9	6226	49	4.51	0.84	−1.60	0.07	20.23	0.06	19.41	0.02	19.12	0.02	19.00	0.02	18.98	0.05	15.7
53532−2185−557	250.6013031	36.364738	−243.7	4.4	6314	71	3.71	0.16	−1.79	0.11	19.58	0.04	18.73	0.02	18.41	0.02	18.35	0.01	18.36	0.03	24.8
53532−2185−558	250.5827942	36.475479	−250.1	3.8	6421	83	3.74	0.29	−1.39	0.10	19.49	0.04	18.64	0.02	18.42	0.03	18.25	0.02	18.25	0.03	27.0
53532−2185−559	250.6181030	36.472069	−246.1	4.7	6574	94	3.87	0.46	−1.36	0.14	19.81	0.05	18.95	0.02	18.77	0.02	18.57	0.02	18.57	0.03	21.5

Table 4—Continued

spSpec name	RA (degree)	DEC (degree)	RV (km s^{-1})	σ_{RV} (km s^{-1})	T_{eff} (K)	$\sigma_{T_{eff}}$ (K)	log g (dex)	$\sigma_{\log g}$ (dex)	[Fe/H] (dex)	$\sigma_{[Fe/H]}$ (dex)	u	σ_u	g	σ_g	r	σ_r	i	σ_i	z	σ_z	< S/N >
53532−2185−560	250.5843353	36.379768	−239.5	3.4	6323	39	3.58	0.40	−1.82	0.03	19.27	0.03	18.46	0.02	18.17	0.02	18.10	0.01	18.09	0.02	30.0
53532−2185−575	250.6388245	36.796120	−227.9	10.0	6009	35	3.93	0.13	−1.68	0.14	20.67	0.07	19.78	0.02	19.42	0.02	19.33	0.03	19.19	0.05	11.8
53532−2185−577	250.5796356	36.790611	−259.0	5.4	6313	43	4.00	0.08	−1.71	0.05	20.02	0.04	19.17	0.02	18.91	0.02	18.81	0.02	18.85	0.04	18.3
53532−2185−581	250.7305756	36.608727	−245.7	5.7	6294	47	4.70	0.25	−1.59	0.10	20.18	0.05	19.31	0.02	19.01	0.02	18.92	0.02	18.87	0.04	16.9
53532−2185−582	250.7253876	36.503780	−234.4	8.2	6118	3	4.77	0.12	−1.54	0.10	20.69	0.07	19.84	0.02	19.50	0.02	19.38	0.02	19.19	0.05	11.8
53532−2185−583	250.6839142	36.503529	−244.0	6.8	6432	177	3.44	0.18	−1.45	0.19	20.25	0.06	19.34	0.02	19.19	0.02	18.99	0.02	18.98	0.05	16.1
53532−2185−584	250.6747742	36.539852	−255.6	6.8	6356	25	3.94	0.85	−1.69	0.03	20.13	0.05	19.33	0.02	19.05	0.02	18.91	0.02	18.83	0.04	16.5
53532−2185−585	250.6607666	36.504436	−233.6	6.1	6438	182	4.55	0.70	−1.32	0.02	20.14	0.06	19.16	0.02	18.99	0.02	18.77	0.02	18.76	0.04	18.6
53532−2185−589	250.7702637	36.421120	−244.5	5.8	6436	83	3.06	0.39	−1.43	0.10	19.93	0.05	18.98	0.02	18.76	0.02	18.63	0.02	18.59	0.04	20.1
53532−2185−591	250.6871948	36.405094	−253.3	4.5	6491	74	3.49	0.35	−1.62	0.13	19.69	0.04	18.79	0.02	18.59	0.02	18.44	0.01	18.40	0.03	23.6
53532−2185−593	250.6662598	36.387859	−239.5	4.8	6500	55	3.82	0.41	−1.41	0.09	19.75	0.04	18.92	0.02	18.69	0.02	18.59	0.02	18.59	0.03	21.4
53565−2255−103	250.6466827	36.307610	−249.4	5.3	5867	4	3.58	0.34	−1.54	0.05	19.01	0.03	17.99	0.01	17.60	0.02	17.48	0.02	17.40	0.02	17.3
53565−2255−112	250.6735535	36.331844	−241.6	4.1	5056	36	2.14	0.22	−1.43	0.12	16.67	0.02	15.20	0.01	14.58	0.02	14.35	0.02	14.23	0.02	14.6
53565−2255−113	250.6521149	36.330883	−253.0	5.1	5278	89	2.14	0.26	−1.31	0.19	16.86	0.01	15.52	0.02	14.93	0.02	14.70	0.01	14.59	0.01	12.1
53565−2255−115	250.6161957	36.345905	−248.0	4.7	5752	75	3.08	0.19	−1.51	0.09	18.99	0.03	17.97	0.02	17.53	0.02	17.37	0.01	17.32	0.02	19.3
53565−2255−116	250.5545197	36.267830	−251.5	1.8	5335	51	2.87	0.25	−1.48	0.08	17.55	0.03	16.27	0.01	15.74	0.01	15.52	0.03	15.41	0.02	44.6
53565−2255−120	250.6273346	36.330883	−252.9	2.0	5191	1	2.30	0.25	−1.55	0.08	16.86	0.01	15.52	0.02	14.93	0.02	14.70	0.01	14.59	0.01	55.3
53565−2255−143	250.5123444	36.306122	−231.4	3.3	5366	37	3.07	0.46	−1.28	0.18	17.34	0.03	15.96	0.01	15.44	0.01	15.16	0.03	15.09	0.02	50.5
53565−2255−148	250.4909821	36.308311	−244.3	1.7	5228	72	2.52	0.13	−1.47	0.11	17.22	0.03	15.83	0.01	15.30	0.01	14.99	0.03	14.94	0.02	51.9
53565−2255−173	250.3810425	36.249397	−236.1	4.0	5560	102	3.80	0.20	−1.48	0.09	18.76	0.04	17.63	0.01	17.21	0.01	16.94	0.03	16.90	0.02	22.0
53565−2255−394	250.0941315	36.500916	−259.0	3.5	5599	24	3.00	0.09	−1.27	0.06	18.50	0.02	17.36	0.02	16.91	0.01	16.70	0.03	16.64	0.02	25.9
53565−2255−423	250.1767273	36.542747	−250.7	1.9	8776	172	3.70	0.20	−1.75	0.10	16.18	0.01	15.11	0.01	15.31	0.01	15.53	0.03	15.65	0.02	59.6
53565−2255−425	250.2703552	36.638271	−257.8	4.6	5867	30	3.73	0.26	−1.26	0.13	18.95	0.03	17.91	0.02	17.54	0.01	17.33	0.02	17.28	0.02	19.2
53565−2255−466	250.8296051	36.382706	−259.3	4.8	5740	47	2.83	0.08	−1.46	0.07	18.92	0.03	17.87	0.02	17.48	0.02	17.28	0.02	17.19	0.02	20.0
53565−2255−476	250.5411072	36.356194	−247.4	3.0	5469	76	2.80	0.35	−1.57	0.05	18.35	0.02	17.24	0.02	16.69	0.02	16.51	0.01	16.40	0.01	29.8
53565−2255−483	250.3755646	36.591225	−256.3	1.4	5189	66	2.37	0.28	−1.34	0.08	16.54	0.01	15.14	0.02	14.51	0.01	14.34	0.02	14.08	0.01	60.3
53565−2255−484	250.4003448	36.591225	−250.0	4.1	5091	78	2.62	0.07	−1.51	0.15	16.54	0.01	15.14	0.02	14.51	0.01	14.34	0.02	14.08	0.01	16.1
53565−2255−490	250.3626251	36.566055	−245.5	1.9	5589	131	2.98	0.35	−1.47	0.08	17.52	0.13	16.32	0.09	15.78	0.03	15.67	0.03	15.35	0.02	45.5
53565−2255−492	250.4226074	36.604641	−239.8	7.7	8398	76	3.80	0.20	−1.55	0.10	16.08	0.01	14.94	0.02	15.08	0.01	15.30	0.02	15.30	0.01	18.5
53565−2255−507	250.4755554	36.594837	−246.9	5.7	5062	13	2.14	0.31	−1.72	0.15	16.99	0.02	15.68	0.02	15.07	0.01	14.87	0.02	14.66	0.01	11.3
53565−2255−510	250.4507599	36.594837	−252.3	1.5	5235	61	2.26	0.25	−1.49	0.08	16.99	0.02	15.68	0.02	15.07	0.01	14.87	0.02	14.66	0.01	53.6
53565−2255−546	250.6332245	36.451298	−240.7	4.6	5053	203	2.26	0.36	−1.47	0.09	16.62	0.01	15.25	0.02	14.69	0.02	14.37	0.01	14.21	0.01	16.9
53565−2255−551	250.6084442	36.451298	−245.5	1.4	5321	2	2.62	0.21	−1.23	0.05	16.62	0.01	15.25	0.02	14.69	0.02	14.37	0.01	14.21	0.01	60.8
53565−2255−556	250.5987854	36.482475	−247.5	2.9	5717	50	3.28	0.20	−1.34	0.06	18.42	0.02	17.29	0.02	16.89	0.02	16.61	0.01	16.50	0.01	30.5

Table 4—Continued

spSpec name	RA (degree)	DEC (degree)	RV (km s^{-1})	σ_{RV} (km s^{-1})	T_{eff} (K)	$\sigma_{T_{eff}}$ (K)	log g (dex)	$\sigma_{\log g}$ (dex)	[Fe/H] (dex)	$\sigma_{[Fe/H]}$ (dex)	u	σ_u	g	σ_g	r	σ_r	i	σ_i	z	σ_z	< S/N >

Note. — The column labeled spSpec name is constructed from the Modified Julian Date (5 digits), the spectroscopic plug plate number (four digits), and the fiber used (three digits). The error in the listed RV is computed from ELODIE template matching. The atmospheric parameter estimates ($T_{\rm eff}$, log g, and [Fe/H]) are the adopted values from the SSPP (Lee et al. 2007a); the quoted internal error is the listed uncertainty in each value. The photometric errors in each band are based on the PHOTO pipeline (Lupton et al. 2001). In the last column, <S/N> is the average signal-to-noise per pixel of the spectra, calculated over the range 3850–6000 Å.

Table 5. Properties of Selected Member Stars of M 15

spSpec name	RA (degree)	DEC (degree)	RV (km s^{-1})	σ_{RV} (km s^{-1})	T_{eff} (K)	$\sigma_{T_{eff}}$ (K)	log g (dex)	$\sigma_{\log g}$ (dex)	[Fe/H] (dex)	$\sigma_{[Fe/H]}$ (dex)	u	σ_u	g	σ_g	r	σ_r	i	σ_i	z	σ_z	< S/N >
53289−1960−401	322.4521790	12.338844	−107.5	2.8	5372	18	2.36	0.36	−2.14	0.05	17.24	0.02	16.09	0.01	15.58	0.01	15.35	0.01	15.28	0.01	48.2
53289−1960−402	322.4679565	12.327691	−107.1	2.4	5226	20	2.10	0.31	−2.13	0.05	16.71	0.02	15.39	0.01	14.83	0.01	14.56	0.01	14.48	0.01	54.3
53289−1960−406	322.4168396	12.266688	−100.7	2.1	5253	18	2.09	0.26	−2.12	0.04	16.69	0.02	15.38	0.01	14.83	0.01	14.57	0.01	14.48	0.01	58.2
53289−1960−411	322.4046326	12.227963	−107.9	3.8	5480	5	2.34	0.13	−2.30	0.05	17.48	0.02	16.38	0.01	15.96	0.01	15.71	0.01	15.60	0.01	41.2
53289−1960−413	322.4143066	12.305798	−104.5	3.1	5346	36	2.11	0.27	−2.19	0.04	16.89	0.02	15.67	0.01	15.16	0.01	14.93	0.01	14.86	0.01	49.9
53289−1960−419	322.4579773	12.303373	−110.3	2.1	5273	28	2.25	0.37	−2.16	0.05	16.70	0.02	15.44	0.01	14.88	0.01	14.62	0.01	14.54	0.01	58.3
53289−1960−441	322.5975342	12.257596	−118.9	7.3	5759	132	3.53	0.56	−1.87	0.18	18.49	0.03	17.55	0.01	17.19	0.01	17.00	0.01	16.94	0.02	18.7
53289−1960−442	322.5028076	12.375646	−119.2	3.6	5400	34	2.66	0.24	−2.15	0.03	17.45	0.02	16.35	0.01	15.86	0.01	15.66	0.01	15.57	0.01	38.5
53289−1960−459	322.7053528	12.125361	−107.3	2.3	5378	8	2.00	0.14	−2.22	0.02	16.25	0.02	15.07	0.01	14.57	0.01	14.35	0.01	14.25	0.01	62.8
53289−1960−460	322.7267761	12.119604	−98.5	3.6	5513	51	2.63	0.32	−2.14	0.04	17.46	0.02	16.42	0.01	15.97	0.01	15.79	0.01	15.68	0.02	40.6
53289−1960−500	322.4296570	12.004886	−105.7	4.3	5661	38	2.41	0.34	−2.02	0.07	18.17	0.02	17.18	0.01	16.74	0.01	16.55	0.01	16.51	0.02	29.6
53289−1960−501	322.5649414	11.992488	−81.6	11.4	5798	6	2.88	0.46	−2.07	0.12	19.25	0.04	18.29	0.01	17.91	0.01	17.74	0.01	17.67	0.02	13.5
53289−1960−506	322.5260010	11.946434	−104.4	2.6	5333	34	2.12	0.33	−2.15	0.04	17.00	0.02	15.74	0.01	15.20	0.01	14.94	0.01	14.83	0.02	50.5
53289−1960−511	322.5564575	12.010468	−112.4	4.3	5463	38	2.30	0.35	−2.15	0.07	17.73	0.02	16.58	0.01	16.08	0.01	15.89	0.01	15.79	0.01	36.5
53289−1960−522	322.6466675	12.302749	−110.9	4.9	5556	91	2.44	0.33	−2.12	0.08	17.94	0.02	16.91	0.01	16.50	0.01	16.31	0.01	16.23	0.01	25.0
53289−1960−523	322.5946350	12.299892	−99.5	1.7	5114	39	2.04	0.28	−2.03	0.05	16.13	0.02	14.62	0.01	13.99	0.01	13.76	0.00	13.57	0.01	62.9
53289−1960−529	322.5634155	12.329430	−100.4	2.5	5343	26	2.08	0.24	−2.07	0.03	16.77	0.02	15.48	0.01	14.98	0.01	14.75	0.01	14.67	0.01	56.9
53321−1962−323	322.3222656	12.281335	−99.0	7.0	6159	61	3.97	0.33	−2.01	0.07	19.26	0.04	18.41	0.01	18.12	0.01	18.02	0.01	17.99	0.03	19.9
53321−1962−329	322.4080811	12.358446	−97.9	7.3	6155	102	3.90	0.38	−1.97	0.11	19.41	0.05	18.52	0.01	18.24	0.01	18.16	0.01	18.17	0.03	18.0
53321−1962−335	322.3918152	12.275231	−125.2	7.4	6060	70	3.51	0.59	−2.29	0.15	19.37	0.04	18.40	0.01	18.09	0.01	18.00	0.01	17.95	0.03	19.8
53321−1962−364	322.4689941	12.278071	−104.3	3.6	5671	73	2.50	0.50	−2.12	0.08	18.62	0.03	17.58	0.01	17.19	0.01	16.99	0.01	16.94	0.02	33.6
53321−1962−370	322.4340820	12.294349	−121.5	8.4	6273	53	4.29	0.44	−2.28	0.13	19.33	0.04	18.44	0.01	18.17	0.01	18.05	0.01	18.03	0.03	18.7
53321−1962−371	322.4648743	12.303191	−130.9	7.3	6214	78	3.15	0.51	−2.00	0.08	19.47	0.05	18.52	0.01	18.26	0.01	18.12	0.01	18.09	0.03	17.7
53321−1962−372	322.4102173	12.272476	−119.7	7.2	6082	101	2.53	0.71	−2.03	0.15	19.29	0.04	18.36	0.01	18.08	0.01	17.95	0.01	17.94	0.03	20.4
53321−1962−375	322.4530640	12.260857	−108.3	4.4	5654	84	2.29	0.22	−2.22	0.09	18.79	0.03	17.75	0.01	17.37	0.01	17.17	0.01	17.14	0.02	31.0
53321−1962−376	322.4066772	12.290338	−107.6	3.6	5618	51	3.13	0.27	−2.09	0.04	18.52	0.03	17.52	0.01	17.10	0.01	16.92	0.01	16.86	0.02	34.9
53321−1962−399	322.2647400	12.088030	−129.3	8.7	6805	103	4.13	0.45	−2.03	0.26	19.68	0.06	18.82	0.02	18.64	0.02	18.65	0.02	18.57	0.04	15.0
53321−1962−402	322.5315247	12.312680	−101.6	4.4	5726	81	2.97	0.30	−1.97	0.08	18.87	0.03	17.89	0.01	17.53	0.01	17.33	0.01	17.27	0.02	27.6
53321−1962−406	322.5553284	12.353999	−104.6	4.9	5776	56	2.93	0.52	−2.07	0.08	18.93	0.04	17.94	0.01	17.57	0.01	17.41	0.01	17.34	0.02	26.8
53321−1962−407	322.5682373	12.340600	−113.8	7.7	6444	108	3.96	0.58	−2.02	0.09	19.33	0.04	18.45	0.01	18.22	0.01	18.12	0.02	18.10	0.03	17.6
53321−1962−413	322.4278564	12.366820	−108.3	3.6	5567	68	2.22	0.41	−2.29	0.09	18.65	0.03	17.57	0.01	17.15	0.01	17.04	0.01	16.90	0.02	34.2
53321−1962−414	322.5430603	12.254919	−86.8	7.4	6237	115	3.56	0.40	−1.83	0.10	19.38	0.05	18.53	0.02	18.28	0.01	18.14	0.02	18.08	0.03	18.9
53321−1962−415	322.4989014	12.316244	−109.1	3.5	5660	62	2.49	0.62	−2.08	0.04	18.44	0.03	17.41	0.01	17.01	0.01	16.83	0.01	16.77	0.02	36.0
53321−1962−421	322.3530884	12.238419	−110.1	5.8	5951	104	3.12	0.50	−1.84	0.14	19.27	0.04	18.36	0.01	18.05	0.02	17.89	0.02	17.84	0.03	20.7

Table 5—Continued

spSpec name	RA (degree)	DEC (degree)	RV (km s^{-1})	$\sigma_{\rm RV}$ (km s^{-1})	$T_{\rm eff}$ (K)	$\sigma_{T_{\rm eff}}$ (K)	log g (dex)	$\sigma_{\log g}$ (dex)	[Fe/H] (dex)	$\sigma_{\rm [Fe/H]}$ (dex)	u	σ_u	g	σ_g	r	σ_r	i	σ_i	z	σ_z	< S/N >
53321−1962−423	322.3211060	12.217339	−115.0	5.2	5824	65	2.99	0.53	−1.91	0.11	19.18	0.04	18.20	0.01	17.85	0.01	17.69	0.01	17.61	0.02	22.3
53321−1962−427	322.3056030	12.249682	−107.2	3.9	5622	115	2.72	0.51	−2.10	0.08	18.63	0.03	17.64	0.01	17.25	0.01	17.09	0.01	17.00	0.02	32.4
53321−1962−438	322.3101501	12.185511	−108.6	3.2	5569	57	2.63	0.38	−2.22	0.04	18.56	0.03	17.55	0.01	17.13	0.02	16.90	0.01	16.82	0.02	35.2
53321−1962−442	322.6037598	12.366948	−103.6	9.2	6557	140	3.84	0.39	−1.84	0.11	19.58	0.05	18.74	0.01	18.56	0.01	18.47	0.03	18.50	0.05	15.1
53321−1962−454	322.5975342	12.257596	−114.4	3.9	5704	123	2.52	0.51	−1.97	0.07	18.49	0.03	17.55	0.01	17.19	0.01	17.00	0.01	16.94	0.02	31.2
53321−1962−466	322.3733521	12.240548	−116.1	3.6	5601	118	2.68	0.02	−2.17	0.06	18.52	0.03	17.50	0.01	17.12	0.01	16.92	0.01	16.85	0.02	38.6
53321−1962−470	322.3207092	12.106877	−119.8	6.4	6589	65	4.25	0.43	−1.91	0.02	19.34	0.05	18.62	0.02	18.40	0.02	18.34	0.02	18.34	0.04	19.9
53321−1962−471	322.4016724	12.009658	−104.7	8.1	6638	109	4.40	0.19	−1.93	0.09	19.68	0.05	18.85	0.01	18.65	0.01	18.61	0.02	18.59	0.04	16.5
53321−1962−474	322.3290100	12.039521	−111.9	3.2	5628	112	2.96	0.45	−2.25	0.08	18.36	0.03	17.44	0.01	17.06	0.02	16.91	0.01	16.84	0.02	37.6
53321−1962−482	322.5291748	12.030179	−120.9	8.2	6492	55	4.39	0.51	−2.24	0.14	19.60	0.05	18.92	0.01	18.66	0.01	18.62	0.02	18.59	0.04	15.7
53321−1962−487	322.5066223	11.983128	−117.1	8.0	6086	58	3.36	0.71	−2.24	0.12	19.61	0.05	18.79	0.04	18.44	0.03	18.30	0.03	18.28	0.03	17.4
53321−1962−488	322.4795532	12.013686	−101.3	8.0	6417	112	3.91	0.24	−1.84	0.28	19.52	0.05	18.65	0.02	18.38	0.02	18.36	0.02	18.37	0.04	16.0
53321−1962−490	322.4822083	11.986870	−113.8	9.0	6515	46	4.50	0.33	−2.26	0.11	19.69	0.05	18.90	0.01	18.65	0.01	18.55	0.02	18.58	0.04	15.9
53321−1962−493	322.5000610	11.843804	−109.9	5.7	5876	51	3.18	0.52	−2.14	0.10	19.19	0.04	18.32	0.01	17.98	0.01	17.82	0.01	17.78	0.03	23.7
53321−1962−495	322.4521179	11.955274	−97.7	8.1	6491	91	4.17	0.60	−2.03	0.16	19.60	0.05	18.80	0.01	18.55	0.01	18.46	0.02	18.48	0.04	16.9
53321−1962−496	322.4375000	11.972004	−82.6	7.8	6550	77	4.67	0.06	−2.37	0.17	19.52	0.04	18.78	0.01	18.56	0.01	18.48	0.02	18.53	0.04	17.0
53321−1962−497	322.4447021	12.011971	−112.7	8.5	6507	30	4.18	0.55	−2.21	0.13	19.64	0.05	18.82	0.01	18.58	0.01	18.50	0.02	18.57	0.04	16.1
53321−1962−500	322.4923096	11.963464	−108.3	6.5	6404	68	3.44	0.44	−2.06	0.15	19.23	0.04	18.41	0.01	18.16	0.01	18.07	0.01	18.08	0.03	23.0
53321−1962−510	322.6307373	12.017861	−90.7	6.4	6190	56	3.05	0.51	−2.04	0.19	19.53	0.04	18.54	0.01	18.26	0.01	18.16	0.01	18.12	0.03	20.4
53321−1962−515	322.5826111	11.990081	−104.7	3.1	5611	51	2.53	0.42	−2.22	0.02	18.54	0.03	17.58	0.01	17.15	0.01	16.95	0.01	16.86	0.02	36.3
53321−1962−516	322.5649414	11.992488	−99.1	5.8	5859	32	2.88	0.58	−2.14	0.13	19.25	0.04	18.29	0.01	17.91	0.01	17.74	0.01	17.67	0.02	24.0
53321−1962−518	322.6694946	12.089317	−96.7	5.1	5893	76	2.88	0.68	−2.19	0.11	19.10	0.04	18.25	0.01	17.90	0.01	17.78	0.01	17.74	0.03	25.8
53321−1962−520	322.5625916	12.011796	−109.2	5.8	6360	64	3.46	0.35	−2.06	0.09	19.50	0.04	18.63	0.01	18.37	0.08	18.28	0.01	18.24	0.03	20.6
53321−1962−532	322.6614685	12.270009	−114.3	3.3	5636	111	2.92	0.32	−2.18	0.03	18.46	0.03	17.48	0.01	17.11	0.01	16.94	0.01	16.84	0.02	37.1
53321−1962−533	322.6655579	12.248962	−107.5	7.2	6315	81	3.57	0.54	−2.37	0.08	19.48	0.05	18.64	0.01	18.37	0.01	18.32	0.02	18.38	0.04	18.7
53321−1962−535	322.6758423	12.262588	−100.5	3.7	5595	45	2.88	0.42	−2.14	0.07	18.79	0.04	17.82	0.01	17.38	0.01	17.21	0.01	17.17	0.02	31.7
53321−1962−539	322.7539978	12.195694	−86.9	8.1	6675	104	3.95	0.56	−2.04	0.11	19.73	0.06	18.81	0.01	18.62	0.01	18.57	0.02	18.51	0.04	17.9
53321−1962−550	322.6591187	12.145007	−104.1	6.5	5980	19	2.94	0.52	−2.03	0.13	19.24	0.04	18.41	0.01	18.07	0.01	17.99	0.01	17.96	0.03	21.0
53321−1962−558	322.6465759	12.128071	−112.9	5.8	5958	43	3.69	0.40	−2.28	0.09	19.23	0.04	18.42	0.01	18.04	0.01	17.95	0.01	17.93	0.03	21.7

Table 6. Properties of Selected Member Stars of M 2

spSpec name	RA (degree)	DEC (degree)	RV (km s^{-1})	$\sigma_{\rm RV}$ (km s^{-1})	$T_{\rm eff}$ (K)	$\sigma_{T_{\rm eff}}$ (K)	log g (dex)	$\sigma_{\log g}$ (dex)	[Fe/H] (dex)	$\sigma_{\rm [Fe/H]}$ (dex)	u	σ_u	g	σ_g	r	σ_r	i	σ_i	z	σ_z	< S/N >
53299−1961−123	323.3084412	−1.018151	9.5	2.3	7644	176	2.57	0.20	−1.50	0.10	16.97	0.02	15.81	0.02	15.83	0.01	15.84	0.01	15.88	0.01	44.6
53299−1961−125	323.3046265	−0.900651	−4.4	1.6	5076	52	2.17	0.21	−1.50	0.07	17.48	0.02	16.03	0.02	15.43	0.01	15.21	0.01	15.06	0.01	46.8
53299−1961−131	323.4663696	−0.819519	2.2	1.9	5185	34	2.40	0.25	−1.54	0.08	18.03	0.02	16.71	0.01	16.13	0.01	15.88	0.01	15.81	0.01	37.0
53299−1961−140	323.3161316	−0.936875	−9.1	3.0	5394	64	2.85	0.14	−1.51	0.08	18.53	0.02	17.27	0.03	16.79	0.01	16.59	0.01	16.52	0.01	27.9
53299−1961−144	323.4824524	−0.780800	3.2	2.8	5249	68	2.40	0.33	−1.67	0.06	18.28	0.02	16.96	0.01	16.44	0.01	16.24	0.01	16.13	0.01	30.7
53299−1961−148	323.4711914	−0.799086	−5.0	1.9	7696	74	3.31	0.20	−1.53	0.10	17.14	0.02	15.95	0.01	15.97	0.01	16.01	0.01	16.08	0.01	46.9
53299−1961−152	323.5119629	−0.501376	2.1	2.0	5176	38	2.38	0.26	−1.62	0.06	17.99	0.02	16.62	0.02	16.05	0.01	15.84	0.01	15.72	0.02	37.8
53299−1961−159	323.5318298	−0.781852	−0.9	2.3	5093	304	2.78	0.41	−1.55	0.10	18.19	0.02	16.87	0.01	16.37	0.01	16.17	0.01	16.05	0.01	32.7
53299−1961−202	323.2455750	−0.889511	1.9	2.1	8583	119	3.58	0.20	−1.62	0.10	17.06	0.02	15.92	0.02	16.09	0.01	16.26	0.01	16.38	0.01	48.1

Table 7. Properties of Selected Member Stars of NGC 2420

spSpec name	RA (degree)	DEC (degree)	RV (km s^{-1})	σ_{RV} (km s^{-1})	T_{eff} (K)	$\sigma_{T_{eff}}$ (K)	log g (dex)	$\sigma_{\log g}$ (dex)	[Fe/H] (dex)	$\sigma_{[Fe/H]}$ (dex)	u	σ_u	g	σ_g	r	σ_r	i	σ_i	z	σ_z	< S/N >
53378−2078−101	114.7240067	21.321098	81.7	2.0	6191	36	4.13	0.17	−0.66	0.06	17.62	0.02	16.56	0.01	16.24	0.01	16.13	0.01	16.14	0.01	35.1
53378−2078−110	114.7332535	21.459303	87.1	1.8	6124	46	4.37	0.11	−0.57	0.18	17.68	0.02	16.56	0.01	16.23	0.01	16.12	0.01	16.11	0.01	38.2
53378−2078−111	114.7337723	21.533043	75.9	1.8	5887	36	4.44	0.09	−0.48	0.07	18.26	0.02	17.06	0.01	16.65	0.01	16.52	0.01	16.52	0.01	28.2
53378−2078−114	114.7632294	21.450647	74.0	1.7	6100	69	4.32	0.05	−0.56	0.12	17.82	0.02	16.70	0.01	16.37	0.01	16.24	0.01	16.28	0.01	36.1
53378−2078−116	114.7709503	21.494595	78.4	3.1	5117	77	4.54	0.07	−0.69	0.09	19.90	0.05	18.34	0.01	17.73	0.01	17.45	0.01	17.40	0.02	13.3
53378−2078−118	114.7212982	21.550411	74.6	2.6	5303	37	4.74	0.10	−0.66	0.08	19.56	0.04	18.05	0.01	17.47	0.01	17.27	0.01	17.21	0.02	16.6
53378−2078−120	114.7709274	21.527533	61.4	2.5	5529	107	4.16	0.09	−0.60	0.11	19.00	0.03	17.74	0.01	17.27	0.01	17.10	0.01	17.16	0.02	18.0
53378−2078−142	114.6714630	21.474438	73.3	2.0	5843	67	4.39	0.10	−0.48	0.10	18.43	0.02	17.20	0.01	16.78	0.01	16.67	0.01	16.61	0.01	26.9
53378−2078−149	114.6430588	21.448729	72.1	1.2	6781	52	4.06	0.16	−0.36	0.06	16.07	0.01	15.00	0.01	14.81	0.01	14.75	0.01	14.83	0.01	59.9
53378−2078−150	114.6955032	21.390019	76.7	1.9	5912	32	4.44	0.08	−0.63	0.10	18.11	0.02	16.93	0.01	16.54	0.01	16.38	0.01	16.36	0.02	30.9
53378−2078−151	114.6724091	21.539541	75.1	1.6	6106	51	4.54	0.01	−0.56	0.10	17.78	0.02	16.69	0.01	16.35	0.01	16.25	0.01	16.26	0.01	36.3
53378−2078−152	114.6924210	21.552748	74.5	2.0	5282	56	4.54	0.11	−0.56	0.09	19.67	0.04	18.07	0.01	17.47	0.01	17.23	0.01	17.13	0.02	17.5
53378−2078−154	114.6604004	21.508270	71.1	2.1	5461	60	4.70	0.06	−0.59	0.10	19.39	0.04	17.93	0.01	17.39	0.01	17.21	0.01	17.13	0.02	19.1
53378−2078−155	114.7134628	21.373636	68.3	1.9	5499	71	4.67	0.08	−0.67	0.07	19.02	0.03	17.59	0.01	17.08	0.01	16.89	0.01	16.83	0.02	22.5
53378−2078−156	114.7031097	21.515936	74.2	1.6	6047	59	4.29	0.13	−0.41	0.08	17.90	0.02	16.75	0.01	16.40	0.01	16.30	0.01	16.30	0.01	35.6
53378−2078−157	114.6541367	21.529306	71.6	1.7	5891	73	4.43	0.05	−0.50	0.12	18.25	0.02	17.09	0.01	16.70	0.01	16.56	0.01	16.54	0.01	30.1
53378−2078−158	114.6927338	21.469568	76.9	2.2	5277	38	4.76	0.07	−0.66	0.06	19.44	0.04	17.94	0.01	17.35	0.01	17.13	0.01	17.02	0.02	18.1
53378−2078−159	114.6708221	21.450685	73.4	1.2	6790	36	4.09	0.13	−0.37	0.06	16.27	0.02	15.23	0.01	15.03	0.01	15.01	0.01	15.06	0.01	57.7
53378−2078−161	114.5712433	21.543400	75.9	1.2	6823	8	3.75	0.29	−0.42	0.05	16.02	0.02	14.98	0.01	14.78	0.01	14.71	0.03	14.78	0.02	60.1
53378−2078−165	114.6024323	21.426910	75.3	2.8	5235	41	4.65	0.09	−0.54	0.05	19.91	0.05	18.24	0.01	17.63	0.01	17.43	0.01	17.34	0.02	14.8
53378−2078−166	114.5820389	21.519642	72.2	1.4	6513	46	4.29	0.09	−0.48	0.06	16.69	0.02	15.69	0.01	15.41	0.01	15.32	0.02	15.37	0.02	52.3
53378−2078−167	114.6017532	21.449791	71.9	1.6	5950	61	4.58	0.04	−0.32	0.09	18.18	0.02	16.95	0.01	16.57	0.01	16.43	0.01	16.41	0.02	31.5
53378−2078−168	114.6115570	21.318134	72.4	1.4	6478	93	4.29	0.13	−0.50	0.05	16.73	0.01	15.73	0.01	15.50	0.01	15.47	0.01	15.51	0.01	50.9
53378−2078−169	114.5819626	21.280655	77.1	1.2	6801	29	3.90	0.13	−0.40	0.06	15.54	0.02	14.49	0.01	14.28	0.01	14.26	0.01	14.33	0.01	64.5
53378−2078−171	114.6197968	21.561134	73.3	1.9	5675	44	4.43	0.14	−0.56	0.05	18.83	0.03	17.49	0.11	16.99	0.08	16.81	0.08	16.77	0.02	25.0
53378−2078−172	114.5688705	21.504910	72.2	1.7	5660	32	4.16	0.17	−0.50	0.06	18.60	0.02	17.38	0.01	16.88	0.01	16.72	0.02	16.70	0.02	26.1
53378−2078−174	114.6007996	21.527756	74.7	2.1	5471	79	4.42	0.27	−0.56	0.06	19.37	0.03	17.93	0.01	17.35	0.01	17.14	0.02	17.08	0.02	18.7
53378−2078−176	114.6416779	21.603819	72.2	1.2	6763	64	3.98	0.17	−0.43	0.08	16.01	0.02	14.94	0.01	14.75	0.01	14.71	0.02	14.74	0.02	60.5
53378−2078−177	114.6228180	21.586617	75.1	2.0	5495	44	4.67	0.09	−0.62	0.08	19.24	0.03	17.77	0.01	17.23	0.01	17.07	0.02	17.04	0.02	20.6
53378−2078−178	114.6506577	21.588242	76.9	2.3	5169	91	4.46	0.15	−0.71	0.10	19.73	0.04	18.16	0.01	17.55	0.01	17.35	0.02	17.24	0.02	16.0
53378−2078−179	114.5720901	21.569319	72.7	1.3	6775	37	4.10	0.13	−0.39	0.06	16.26	0.02	15.20	0.01	15.00	0.01	14.93	0.02	14.99	0.02	58.6
53378−2078−182	114.5458374	21.481653	70.7	1.3	6721	79	4.00	0.11	−0.57	0.06	15.85	0.01	14.83	0.01	14.61	0.01	14.60	0.01	14.66	0.01	61.1
53378−2078−186	114.5329285	21.496721	68.4	1.4	6756	57	4.18	0.15	−0.48	0.06	16.15	0.01	15.15	0.01	14.93	0.01	14.91	0.01	14.97	0.01	58.6
53378−2078−192	114.5202713	21.508390	70.3	1.7	5854	20	4.41	0.06	−0.44	0.06	18.29	0.02	17.12	0.01	16.68	0.01	16.57	0.01	16.56	0.02	29.5

Table 7—Continued

spSpec name	RA (degree)	DEC (degree)	RV (km s^{-1})	$\sigma_{\rm RV}$ (km s^{-1})	$T_{\rm eff}$ (K)	$\sigma_{T_{\rm eff}}$ (K)	log g (dex)	$\sigma_{\log g}$ (dex)	[Fe/H] (dex)	$\sigma_{\rm [Fe/H]}$ (dex)	u	σ_u	g	σ_g	r	σ_r	i	σ_i	z	σ_z	< S/N >
53378−2078−194	114.4920883	21.528856	75.1	2.5	5492	65	4.49	0.07	−0.64	0.08	19.00	0.03	17.65	0.01	17.15	0.01	17.00	0.01	16.93	0.02	21.4
53378−2078−195	114.5080185	21.480667	72.2	1.4	6710	38	3.98	0.11	−0.49	0.05	16.43	0.02	15.40	0.01	15.19	0.01	15.18	0.01	15.19	0.01	54.7
53378−2078−197	114.5511093	21.571732	71.0	1.9	5879	60	4.59	0.04	−0.37	0.09	18.32	0.02	17.11	0.01	16.72	0.01	16.56	0.02	16.55	0.02	28.3
53378−2078−199	114.5634613	21.418985	73.1	1.5	6427	96	4.08	0.28	−0.43	0.06	17.00	0.01	15.91	0.01	15.66	0.01	15.60	0.01	15.62	0.01	49.0
53378−2078−200	114.5384979	21.543732	72.7	2.1	5340	57	4.58	0.14	−0.48	0.03	19.45	0.03	17.99	0.01	17.41	0.01	17.18	0.02	17.11	0.02	17.6
53378−2078−223	114.3904495	21.523254	69.8	1.5	6424	103	4.11	0.19	−0.45	0.06	16.95	0.02	15.90	0.01	15.65	0.01	15.59	0.01	15.61	0.01	48.8
53378−2078−224	114.4638596	21.543934	73.4	1.2	6793	37	3.90	0.15	−0.45	0.06	15.76	0.01	14.73	0.01	14.53	0.01	14.52	0.01	14.55	0.01	62.9
53378−2078−227	114.4512711	21.468901	73.0	1.7	6036	67	4.56	0.04	−0.50	0.12	18.05	0.02	16.91	0.01	16.55	0.01	16.43	0.01	16.42	0.02	32.2
53378−2078−232	114.4003372	21.434925	74.9	1.3	6796	58	3.93	0.12	−0.40	0.07	16.22	0.01	15.17	0.01	15.01	0.01	14.94	0.01	14.99	0.01	58.2
53378−2078−233	114.3611526	21.547220	76.1	1.6	6077	83	4.37	0.02	−0.58	0.14	17.85	0.02	16.73	0.01	16.40	0.01	16.30	0.01	16.26	0.01	36.2
53378−2078−235	114.4902191	21.548447	75.6	1.7	5728	40	4.25	0.09	−0.49	0.06	18.46	0.02	17.23	0.01	16.79	0.01	16.66	0.02	16.60	0.02	27.5
53378−2078−273	114.3406677	21.562317	74.7	3.1	6009	37	4.27	0.16	−0.41	0.10	18.00	0.02	16.84	0.01	16.45	0.01	16.37	0.02	16.32	0.02	13.8
53378−2078−277	114.3005371	21.531923	86.5	2.7	5220	27	4.52	0.11	−0.65	0.06	19.78	0.05	18.23	0.01	17.61	0.01	17.43	0.01	17.37	0.02	14.2
53378−2078−422	114.4277878	21.642904	72.4	1.7	5508	40	4.56	0.12	−0.51	0.09	19.25	0.04	17.80	0.01	17.26	0.01	17.11	0.02	17.06	0.02	22.2
53378−2078−427	114.4302673	21.777519	74.0	1.7	6019	34	4.47	0.05	−0.28	0.08	18.17	0.02	16.98	0.01	16.60	0.01	16.46	0.01	16.49	0.02	33.8
53378−2078−431	114.4749222	21.663054	69.5	1.1	6635	86	4.16	0.03	−0.42	0.07	15.73	0.02	14.71	0.01	14.47	0.01	14.40	0.02	14.44	0.02	65.3
53378−2078−435	114.4620132	21.588032	73.9	1.7	5484	35	4.54	0.07	−0.51	0.08	19.11	0.03	17.74	0.01	17.22	0.01	17.06	0.02	17.00	0.02	23.0
53378−2078−440	114.4428024	21.680481	73.3	1.5	5827	74	4.52	0.14	−0.33	0.10	18.75	0.03	17.49	0.01	17.02	0.01	16.89	0.01	16.84	0.02	27.6
53378−2078−462	114.5509872	21.740852	71.2	1.4	6339	4	4.33	0.10	−0.33	0.08	17.37	0.02	16.28	0.02	16.01	0.01	15.92	0.01	15.93	0.01	46.3
53378−2078−463	114.5498276	21.721819	71.8	1.1	6727	46	4.25	0.13	−0.21	0.06	16.52	0.07	15.49	0.06	15.29	0.07	15.28	0.07	15.23	0.07	58.0
53378−2078−465	114.5717773	21.840559	74.8	1.6	5653	34	4.53	0.16	−0.45	0.06	18.82	0.03	17.53	0.01	17.04	0.01	16.91	0.01	16.86	0.02	25.9
53378−2078−466	114.5513763	21.821871	72.5	1.1	6846	8	4.18	0.07	−0.30	0.06	16.15	0.01	15.11	0.01	14.93	0.01	14.91	0.01	14.94	0.01	59.7
53378−2078−468	114.5113068	21.658003	73.9	1.6	5824	4	4.70	0.01	−0.44	0.08	18.76	0.03	17.48	0.01	17.00	0.01	16.84	0.02	16.81	0.02	26.9
53378−2078−469	114.5523911	21.648226	73.9	1.0	6613	55	3.60	0.23	−0.47	0.01	15.57	0.02	14.45	0.01	14.23	0.01	14.17	0.02	14.20	0.02	64.8
53378−2078−470	114.5214005	21.710367	73.3	1.5	5785	23	4.36	0.17	−0.49	0.06	18.51	0.02	17.25	0.01	16.81	0.01	16.68	0.02	16.61	0.02	31.1
53378−2078−471	114.5303192	21.614901	76.6	1.3	6294	6	4.38	0.04	−0.45	0.07	17.41	0.02	16.37	0.01	16.06	0.01	16.02	0.02	15.96	0.02	45.3
53378−2078−472	114.5822067	21.598427	72.9	1.2	6780	44	4.01	0.08	−0.42	0.05	15.71	0.02	14.62	0.01	14.44	0.01	14.38	0.02	14.43	0.02	65.7
53378−2078−473	114.5220795	21.600906	73.2	1.4	6262	35	4.37	0.03	−0.38	0.07	17.61	0.02	16.53	0.01	16.21	0.01	16.09	0.02	16.11	0.02	42.3
53378−2078−475	114.4970779	21.644300	72.6	1.9	5267	54	4.37	0.22	−0.63	0.12	19.85	0.04	18.24	0.01	17.61	0.03	17.38	0.04	17.28	0.02	17.8
53378−2078−476	114.5061035	21.610609	75.1	1.6	5614	71	4.68	0.08	−0.48	0.14	19.35	0.03	17.92	0.01	17.39	0.01	17.18	0.02	17.12	0.02	21.6
53378−2078−477	114.5529404	21.628851	76.1	1.5	5952	36	4.63	0.04	−0.35	0.07	18.38	0.02	17.11	0.01	16.72	0.01	16.56	0.02	16.55	0.02	33.0
53378−2078−478	114.5313034	21.647833	79.2	1.5	5735	66	4.76	0.09	−0.50	0.12	19.06	0.03	17.62	0.01	17.16	0.01	16.97	0.02	16.93	0.02	25.3
53378−2078−480	114.5518036	21.664013	74.5	1.5	5903	23	4.49	0.15	−0.33	0.08	18.51	0.02	17.26	0.01	16.84	0.01	16.69	0.02	16.65	0.02	30.7
53378−2078−481	114.5914230	21.674248	67.6	1.9	6445	36	4.35	0.10	−0.25	0.07	17.20	0.02	16.13	0.02	15.85	0.01	15.79	0.01	15.79	0.01	47.5

Table 7—Continued

spSpec name	RA (degree)	DEC (degree)	RV (km s^{-1})	$\sigma_{\rm RV}$ (km s^{-1})	$T_{\rm eff}$ (K)	$\sigma_{T_{\rm eff}}$ (K)	log g (dex)	$\sigma_{\log g}$ (dex)	[Fe/H] (dex)	$\sigma_{\rm [Fe/H]}$ (dex)	u	σ_u	g	σ_g	r	σ_r	i	σ_i	z	σ_z	< S/N >
53378−2078−485	114.6053772	21.694122	78.0	1.3	5984	32	4.56	0.04	−0.40	0.08	17.98	0.02	16.79	0.02	16.40	0.01	16.30	0.01	16.28	0.01	36.8
53378−2078−491	114.6300507	21.615072	73.4	1.2	6692	65	4.37	0.04	−0.46	0.08	15.94	0.02	14.85	0.01	14.64	0.01	14.58	0.02	14.61	0.02	62.7
53378−2078−492	114.6291809	21.672440	74.4	1.4	6035	29	4.42	0.08	−0.36	0.07	18.07	0.02	16.88	0.02	16.50	0.01	16.39	0.01	16.38	0.01	35.8
53378−2078−493	114.5901718	21.628422	77.6	1.7	5667	53	4.70	0.14	−0.56	0.16	19.26	0.03	17.76	0.01	17.26	0.01	17.08	0.02	17.03	0.02	22.9
53378−2078−496	114.6028900	21.614571	73.1	1.5	6066	31	4.66	0.06	−0.34	0.08	18.12	0.02	16.89	0.01	16.52	0.01	16.38	0.02	16.36	0.02	34.9
53378−2078−499	114.5844727	21.697393	76.1	1.5	5920	43	4.46	0.05	−0.37	0.08	18.40	0.02	17.17	0.02	16.78	0.01	16.64	0.01	16.62	0.02	31.0
53378−2078−503	114.6588974	21.779421	70.0	1.1	6803	51	4.14	0.04	−0.30	0.06	15.69	0.01	14.61	0.02	14.45	0.01	14.41	0.01	14.46	0.01	65.2
53378−2078−510	114.7120285	21.617662	64.4	1.5	5916	27	4.32	0.14	−0.49	0.12	18.17	0.02	16.94	0.02	16.54	0.01	16.35	0.01	16.36	0.01	35.3
53378−2078−511	114.6601486	21.613201	72.6	1.2	6883	30	4.22	0.10	−0.36	0.05	16.24	0.01	15.20	0.02	15.01	0.01	14.93	0.01	15.02	0.01	60.2
53378−2078−512	114.6719818	21.630064	72.3	1.2	6662	28	4.32	0.03	−0.40	0.07	16.66	0.01	15.62	0.02	15.38	0.01	15.29	0.01	15.38	0.01	55.2
53378−2078−513	114.6427383	21.634518	75.4	1.3	6206	69	4.69	0.07	−0.32	0.09	17.64	0.02	16.55	0.02	16.24	0.01	16.14	0.01	16.16	0.02	42.9
53378−2078−514	114.7189484	21.580208	73.0	1.5	6077	51	4.43	0.09	−0.40	0.07	17.98	0.09	16.85	0.10	16.48	0.16	16.34	0.01	16.38	0.21	36.2
53378−2078−515	114.7006531	21.605631	72.6	1.4	6181	27	4.53	0.04	−0.42	0.07	17.69	0.02	16.60	0.02	16.26	0.01	16.09	0.01	16.18	0.01	41.0
53378−2078−516	114.6420288	21.651564	71.9	1.3	6341	26	4.43	0.05	−0.42	0.05	17.28	0.02	16.22	0.02	15.92	0.01	15.84	0.01	15.88	0.01	47.5
53378−2078−517	114.6432877	21.728846	75.9	1.4	5709	46	4.55	0.14	−0.35	0.10	18.81	0.02	17.49	0.02	17.03	0.01	16.89	0.01	16.86	0.02	27.1
53378−2078−518	114.6788712	21.703911	66.2	1.2	6662	43	4.19	0.06	−0.31	0.07	16.66	0.01	15.65	0.02	15.44	0.01	15.38	0.01	15.41	0.01	54.6
53378−2078−519	114.7201385	21.600649	73.3	1.4	5799	40	4.33	0.16	−0.51	0.07	18.48	0.03	17.21	0.01	16.74	0.01	16.64	0.01	16.55	0.01	32.0
53378−2078−520	114.6900711	21.580940	73.5	1.3	6275	35	4.41	0.05	−0.40	0.06	17.58	0.02	16.51	0.02	16.20	0.01	15.98	0.01	16.08	0.01	42.7
53378−2078−548	114.7715225	21.684803	71.7	1.2	6905	25	3.75	0.35	−0.43	0.05	15.85	0.01	14.79	0.02	14.62	0.01	14.58	0.01	14.66	0.01	63.5
53378−2078−552	114.7907104	21.658455	83.1	2.4	5165	46	4.47	0.16	−0.45	0.13	20.16	0.06	18.42	0.01	17.77	0.01	17.57	0.01	17.51	0.02	13.3
53378−2078−553	114.7563171	21.637693	79.2	1.8	5423	49	4.86	0.10	−0.39	0.17	19.65	0.04	18.01	0.03	17.46	0.01	17.28	0.01	17.22	0.02	18.8
53378−2078−554	114.7373505	21.682465	68.9	1.3	6864	103	3.75	0.37	−0.35	0.07	15.87	0.01	14.83	0.02	14.68	0.01	14.64	0.01	14.70	0.01	62.7
53378−2078−557	114.7612228	21.602289	73.3	1.3	6443	77	4.39	0.05	−0.33	0.06	17.06	0.02	15.97	0.01	15.73	0.01	15.67	0.01	15.66	0.01	49.2
53378−2078−560	114.7902832	21.615337	76.3	1.6	5886	54	4.44	0.12	−0.41	0.11	18.42	0.03	17.19	0.01	16.78	0.01	16.67	0.01	16.67	0.02	30.3
53379−2079−076	114.8654022	21.591274	76.3	1.4	5113	43	4.26	0.44	−0.33	0.15	20.29	0.07	18.57	0.01	17.86	0.01	17.65	0.01	17.58	0.02	21.2
53379−2079−141	114.7252884	21.498737	75.9	1.9	4765	76	4.82	0.09	−0.36	0.14	21.75	0.22	19.25	0.01	18.42	0.01	18.09	0.01	17.94	0.02	13.4
53379−2079−148	114.6623688	21.491985	74.5	1.9	4733	66	4.55	0.02	−0.52	0.12	21.56	0.19	19.20	0.01	18.39	0.01	18.07	0.01	17.95	0.02	14.9
53379−2079−149	114.7246323	21.518278	76.1	1.6	4903	16	4.71	0.18	−0.46	0.08	20.82	0.10	18.89	0.01	18.14	0.01	17.85	0.01	17.76	0.02	17.4
53379−2079−152	114.7128296	21.469206	78.4	2.1	4765	71	4.42	0.25	−0.67	0.08	21.25	0.14	19.23	0.01	18.39	0.01	18.10	0.01	17.95	0.02	13.7
53379−2079−158	114.6514664	21.519800	77.2	2.0	4598	99	5.05	0.34	−0.55	0.08	21.79	0.23	19.43	0.01	18.57	0.01	18.26	0.01	18.09	0.03	12.2
53379−2079−159	114.6842728	21.541288	79.7	1.9	4595	155	4.80	0.28	−0.47	0.08	21.29	0.15	19.36	0.01	18.47	0.01	18.14	0.01	18.02	0.02	13.2
53379−2079−162	114.6411285	21.466083	75.7	1.4	5068	60	4.89	0.23	−0.46	0.17	20.60	0.09	18.68	0.01	17.96	0.01	17.74	0.01	17.69	0.02	20.8
53379−2079−163	114.6339798	21.310768	68.7	2.4	4599	65	4.74	0.24	−0.65	0.07	21.11	0.13	19.21	0.01	18.38	0.01	18.09	0.01	17.93	0.02	11.6
53379−2079−166	114.5640030	21.557892	74.7	1.4	4981	71	4.55	0.16	−0.57	0.11	20.63	0.07	18.68	0.01	17.98	0.01	17.72	0.02	17.61	0.02	20.6

Table 7—Continued

spSpec name	RA (degree)	DEC (degree)	RV (km s^{-1})	σ_{RV} (km s^{-1})	T_{eff} (K)	$\sigma_{T_{eff}}$ (K)	log g (dex)	$\sigma_{\log g}$ (dex)	[Fe/H] (dex)	$\sigma_{[Fe/H]}$ (dex)	u	σ_u	g	σ_g	r	σ_r	i	σ_i	z	σ_z	< S/N >
53379−2079−169	114.5825729	21.549602	75.7	1.7	4903	17	4.02	0.19	−0.53	0.04	20.93	0.09	18.84	0.01	18.09	0.01	17.81	0.02	17.70	0.02	16.7
53379−2079−181	114.5458374	21.481653	71.0	1.0	6776	57	4.09	0.11	−0.53	0.07	15.85	0.01	14.83	0.01	14.61	0.01	14.60	0.01	14.66	0.01	77.2
53379−2079−182	114.5021820	21.350065	78.8	1.9	4793	60	4.93	0.20	−0.47	0.15	21.08	0.12	19.15	0.02	18.34	0.01	18.05	0.01	17.87	0.02	12.5
53379−2079−191	114.5309906	21.548798	80.8	2.1	4829	74	4.45	0.20	−0.31	0.08	21.06	0.09	19.14	0.01	18.32	0.01	18.02	0.02	17.87	0.02	13.9
53379−2079−192	114.5139694	21.403902	74.3	1.6	4976	76	4.56	0.10	−0.50	0.08	20.58	0.06	18.71	0.01	18.02	0.01	17.77	0.02	17.68	0.02	19.5
53379−2079−194	114.5345688	21.444080	74.1	1.4	5094	56	4.57	0.09	−0.67	0.08	20.24	0.05	18.51	0.01	17.86	0.01	17.64	0.01	17.50	0.02	22.7
53379−2079−195	114.5383835	21.459230	77.6	1.7	4893	1	4.58	0.23	−0.52	0.09	20.87	0.08	18.89	0.01	18.13	0.01	17.88	0.02	17.74	0.02	17.1
53379−2079−198	114.5100632	21.580110	75.7	1.5	5088	18	4.64	0.16	−0.59	0.11	20.27	0.05	18.59	0.01	17.92	0.01	17.66	0.02	17.56	0.02	22.0
53379−2079−200	114.5501785	21.515902	78.8	1.8	4841	62	4.53	0.11	−0.60	0.11	21.05	0.09	19.06	0.01	18.25	0.01	17.96	0.02	17.87	0.02	15.2
53379−2079−237	114.3715134	21.576729	73.2	1.8	4615	163	4.20	0.03	−0.49	0.08	21.14	0.14	19.25	0.01	18.36	0.01	18.11	0.02	17.97	0.03	14.3
53379−2079−238	114.4818726	21.496136	73.9	1.7	5060	69	4.79	0.29	−0.41	0.13	20.64	0.07	18.80	0.01	18.08	0.01	17.84	0.02	17.68	0.02	17.7
53379−2079−270	114.3305511	21.473141	77.4	1.6	4817	58	4.52	0.42	−0.49	0.09	20.77	0.07	18.85	0.01	18.06	0.01	17.79	0.01	17.65	0.02	17.0
53379−2079−431	114.3533020	21.674223	71.2	1.3	4813	27	4.72	0.50	−0.41	0.09	20.62	0.10	18.85	0.01	18.07	0.01	17.79	0.02	17.71	0.02	18.9
53379−2079−434	114.3718185	21.656651	86.0	1.6	4733	72	4.05	0.29	−0.75	0.06	20.88	0.12	18.96	0.01	18.14	0.01	17.84	0.02	17.69	0.02	18.0
53379−2079−477	114.5016327	21.681393	76.8	1.5	4859	109	4.23	0.54	−0.54	0.08	21.11	0.10	18.97	0.01	18.17	0.01	17.91	0.02	17.78	0.02	18.0
53379−2079−480	114.5439606	21.591728	73.1	1.5	4843	31	4.55	0.31	−0.51	0.10	21.20	0.11	19.08	0.01	18.29	0.01	17.94	0.02	17.80	0.02	16.9
53379−2079−483	114.5822067	21.598427	67.3	1.0	6781	43	4.15	0.08	−0.38	0.04	15.71	0.02	14.62	0.01	14.44	0.01	14.38	0.02	14.43	0.02	81.0
53379−2079−495	114.5839233	21.631277	77.6	1.6	4988	19	4.87	0.37	−0.33	0.11	21.01	0.09	18.90	0.01	18.18	0.01	17.90	0.02	17.79	0.02	17.8
53379−2079−496	114.6000900	21.607351	79.3	1.4	4998	85	4.18	0.09	−0.69	0.06	20.48	0.06	18.67	0.01	17.93	0.01	17.72	0.02	17.63	0.02	22.6
53379−2079−498	114.6408386	21.609079	80.1	1.6	4876	18	4.72	0.42	−0.37	0.09	20.95	0.09	18.98	0.01	18.22	0.01	17.93	0.02	17.77	0.02	17.3
53379−2079−500	114.5563812	21.802401	79.6	1.9	4793	71	4.94	0.04	−0.36	0.08	21.34	0.16	19.23	0.01	18.40	0.01	18.11	0.01	17.94	0.03	14.7
53379−2079−502	114.6971817	21.661120	77.8	1.7	4825	75	4.35	0.35	−0.45	0.11	21.18	0.11	19.10	0.02	18.30	0.01	18.00	0.01	17.88	0.02	15.4
53379−2079−507	114.7510529	21.611731	82.2	1.9	4611	121	3.81	0.60	−0.47	0.09	21.39	0.15	19.37	0.01	18.51	0.02	18.22	0.01	18.08	0.02	13.7
53379−2079−511	114.7137070	21.664612	78.1	1.7	4834	30	4.55	0.56	−0.43	0.07	20.84	0.08	18.98	0.02	18.20	0.01	17.91	0.01	17.82	0.02	17.1
53379−2079−512	114.6809235	21.718416	76.3	1.3	5196	95	4.76	0.09	−0.30	0.23	20.12	0.05	18.49	0.02	17.87	0.01	17.64	0.01	17.52	0.02	23.6
53379−2079−516	114.6617126	21.614836	76.0	1.4	5058	17	4.39	0.14	−0.26	0.07	20.68	0.07	18.76	0.02	18.02	0.01	17.70	0.01	17.66	0.02	20.2
53379−2079−519	114.6623764	21.765589	79.0	1.7	4809	2	4.89	0.45	−0.57	0.11	21.18	0.11	19.18	0.02	18.39	0.01	18.09	0.01	17.92	0.02	14.8
53379−2079−558	114.7901764	21.681410	78.2	1.5	5049	75	4.69	0.12	−0.56	0.12	20.21	0.05	18.55	0.02	17.87	0.01	17.65	0.01	17.60	0.02	22.0

Table 8. Properties of Selected Member Stars of M 67

spSpec name	RA (degree)	DEC (degree)	RV (km s^{-1})	$\sigma_{\rm RV}$ (km s^{-1})	$T_{\rm eff}$ (K)	$\sigma_{T_{\rm eff}}$ (K)	log g (dex)	$\sigma_{\log g}$ (dex)	[Fe/H] (dex)	$\sigma_{\rm [Fe/H]}$ (dex)	u	σ_u	g	σ_g	r	σ_r	i	σ_i	z	σ_z	< S/N >
54142−2667−361	132.6933289	11.871265	35.4	0.8	5350	96	3.99	0.29	−0.47	0.14	16.92	0.01	15.33	0.00	14.73	0.00	14.49	0.00	14.40	0.01	58.1
54142−2667−363	132.5890350	11.985747	32.4	0.8	5395	116	3.86	0.39	−0.20	0.28	16.78	0.02	15.26	0.01	14.75	0.02	14.57	0.01	14.56	0.01	57.3
54142−2667−364	132.6169128	11.913978	33.3	0.9	5855	167	4.45	0.17	−0.64	0.31	15.58	0.02	14.31	0.01	13.94	0.02	13.77	0.01	13.79	0.01	62.4
54142−2667−372	132.6952972	11.897903	33.9	0.8	5172	261	3.38	0.44	−0.59	0.07	17.33	0.01	15.67	0.00	15.07	0.00	14.86	0.01	14.80	0.01	54.0
54142−2667−378	132.6899872	11.926571	38.2	0.8	5079	124	4.83	0.15	−0.31	0.14	18.21	0.01	16.23	0.01	15.49	0.00	15.24	0.01	15.13	0.01	45.0
54142−2667−379	132.5899200	11.839747	35.4	0.9	5699	158	4.07	0.52	−0.33	0.14	15.96	0.01	14.66	0.02	14.23	0.01	14.13	0.02	14.09	0.02	61.4
54142−2667−402	132.7021637	12.014961	35.0	0.8	5551	43	3.41	0.65	−0.16	0.27	16.83	0.02	15.29	0.01	14.79	0.02	14.58	0.01	14.52	0.01	56.4
54142−2667−404	132.7532043	11.886464	34.3	0.8	5517	257	3.37	0.66	−0.22	0.18	16.53	0.01	15.08	0.00	14.56	0.01	14.38	0.01	14.34	0.01	58.8
54142−2667−406	132.7005005	11.913181	32.9	0.9	5842	175	4.38	0.16	−0.64	0.34	15.59	0.01	14.32	0.01	13.91	0.01	13.78	0.00	13.77	0.00	62.4
54142−2667−407	132.7347107	11.858081	34.1	0.9	5916	148	3.81	0.36	−0.32	0.11	15.46	0.01	14.26	0.02	13.88	0.01	13.74	0.01	13.75	0.01	62.7
54142−2667−408	132.7437439	11.994214	33.2	0.9	5835	135	3.85	0.37	−0.42	0.17	15.78	0.01	14.47	0.01	14.05	0.00	13.89	0.00	13.84	0.01	61.8
54142−2667−409	132.7742462	11.886261	34.5	0.8	5367	153	3.76	0.47	−0.43	0.14	16.89	0.01	15.36	0.01	14.81	0.01	14.62	0.01	14.56	0.01	56.8
54142−2667−410	132.7377930	11.947349	31.3	0.8	5441	145	3.73	0.45	−0.27	0.19	16.76	0.01	15.26	0.00	14.72	0.01	14.55	0.01	14.49	0.01	57.5
54142−2667−411	132.8010254	11.787528	27.8	0.8	5562	42	3.61	0.58	−0.19	0.25	17.03	0.01	15.45	0.00	14.86	0.01	14.68	0.01	14.58	0.01	57.1
54142−2667−412	132.7361145	11.831808	33.7	0.8	5562	174	3.54	0.49	−0.37	0.16	16.32	0.01	14.92	0.00	14.44	0.00	14.29	0.00	14.25	0.00	60.4
54142−2667−415	132.7000732	11.828167	34.6	0.8	5659	157	3.76	0.44	−0.30	0.15	16.17	0.01	14.80	0.01	14.34	0.01	14.18	0.01	14.14	0.01	61.0
54142−2667−417	132.7567139	11.937789	33.3	0.8	5627	44	3.65	0.56	−0.17	0.16	16.80	0.01	15.24	0.00	14.69	0.01	14.51	0.01	14.44	0.01	58.4
54142−2667−418	132.7534637	11.814725	35.1	0.9	5620	161	3.70	0.43	−0.35	0.15	16.30	0.01	14.89	0.00	14.43	0.00	14.27	0.00	14.23	0.01	60.6
54142−2667−419	132.7431183	11.970697	31.8	1.0	5727	141	3.76	0.46	−0.48	0.17	16.10	0.01	14.75	0.01	14.30	0.01	14.14	0.00	14.11	0.01	60.8
54142−2667−429	132.3948822	11.788092	34.7	1.0	5756	158	4.40	0.17	−0.60	0.28	15.78	0.01	14.49	0.02	14.14	0.01	13.97	0.02	13.97	0.01	61.6
54142−2667−441	132.8041229	11.950172	35.4	0.9	5710	165	3.71	0.46	−0.31	0.15	16.04	0.01	14.70	0.00	14.24	0.01	14.09	0.00	14.06	0.01	60.2
54142−2667−444	132.8395844	11.984572	31.0	1.0	5928	159	4.45	0.15	−0.14	0.09	15.65	0.01	14.34	0.00	13.93	0.01	13.80	0.00	13.80	0.01	61.9
54142−2667−445	132.7831726	11.981397	34.1	0.8	5551	170	3.60	0.48	−0.35	0.16	16.48	0.01	15.03	0.00	14.52	0.00	14.36	0.00	14.32	0.01	58.4
54142−2667−451	132.8012543	11.906319	34.7	0.9	5832	158	4.37	0.15	−0.54	0.29	15.69	0.01	14.39	0.00	13.97	0.00	13.82	0.00	13.81	0.01	62.1
54142−2667−452	132.7928009	12.025431	36.9	0.9	5088	67	5.09	0.26	−0.22	0.13	18.46	0.02	16.43	0.02	15.66	0.01	15.44	0.01	15.32	0.02	44.3
54142−2667−453	132.8423767	11.807839	22.6	0.8	5081	92	4.22	0.34	−0.47	0.12	17.97	0.01	16.12	0.01	15.40	0.01	15.13	0.01	15.01	0.01	50.2
54142−2667−454	132.8407745	11.861747	34.7	0.9	5794	155	4.13	0.34	−0.31	0.14	15.59	0.01	14.30	0.00	13.85	0.01	13.72	0.03	13.66	0.01	62.5
54142−2667−455	132.9283295	11.991872	32.9	0.9	6008	62	4.39	0.14	−0.28	0.14	15.53	0.01	14.26	0.01	13.85	0.00	13.72	0.00	13.69	0.01	62.3
54142−2667−457	132.9065857	11.945644	35.1	0.9	5767	118	4.05	0.31	−0.35	0.15	16.02	0.01	14.66	0.00	14.21	0.00	14.06	0.00	14.03	0.01	60.8
54142−2667−458	132.8022461	12.188075	34.4	0.8	5683	153	4.50	0.18	−0.23	0.16	15.90	0.02	14.56	0.02	14.12	0.01	13.99	0.02	13.99	0.01	60.3
54142−2667−460	132.7881317	11.950017	35.4	0.9	5676	143	3.83	0.43	−0.33	0.14	16.17	0.01	14.81	0.00	14.34	0.00	14.19	0.00	14.16	0.01	59.9
54142−2667−463	132.5035400	11.702733	34.5	0.9	5816	171	4.39	0.15	−0.59	0.31	15.56	0.01	14.31	0.02	13.91	0.01	13.82	0.02	13.81	0.01	62.8
54142−2667−466	132.6327057	11.502099	36.7	0.8	5181	32	4.61	0.14	−0.16	0.17	17.71	0.03	15.90	0.01	15.23	0.02	15.04	0.01	14.97	0.01	52.0
54142−2667−469	132.6607056	11.776742	33.9	0.9	5143	153	3.84	0.38	−0.19	0.27	17.37	0.01	15.70	0.02	15.10	0.01	14.88	0.02	14.83	0.02	54.6

Table 8—Continued

spSpec name	RA (degree)	DEC (degree)	RV (km s^{-1})	σ_{RV} (km s^{-1})	T_{eff} (K)	$\sigma_{T_{eff}}$ (K)	log g (dex)	$\sigma_{\log g}$ (dex)	[Fe/H] (dex)	$\sigma_{[Fe/H]}$ (dex)	u	σ_u	g	σ_g	r	σ_r	i	σ_i	z	σ_z	< S/N >
54142−2667−479	132.7179260	11.750975	35.3	0.9	5578	177	3.62	0.49	−0.38	0.16	16.13	0.01	14.80	0.02	14.33	0.01	14.22	0.01	14.24	0.01	60.9
54142−2667−481	132.7949219	11.664139	40.3	0.9	5561	172	3.59	0.47	−0.47	0.11	16.30	0.02	14.93	0.01	14.46	0.01	14.28	0.01	14.24	0.01	60.3
54142−2667−486	132.7528229	11.678155	36.6	0.8	5396	37	4.80	0.08	−0.21	0.09	17.35	0.02	15.71	0.00	15.09	0.01	14.88	0.01	14.82	0.01	55.3
54142−2667−488	132.7667389	11.706717	45.1	1.1	6145	50	3.67	0.35	−0.49	0.10	15.40	0.03	15.01	0.03	14.47	0.03	14.06	0.03	14.08	0.03	61.3
54142−2667−500	132.7791290	11.697017	34.8	0.8	4969	157	3.85	0.19	−0.57	0.01	17.85	0.02	16.03	0.00	15.28	0.01	15.00	0.01	14.87	0.01	53.5
54142−2667−508	132.8550415	11.637817	33.6	0.7	5478	26	4.75	0.04	−0.27	0.14	17.16	0.01	15.56	0.00	14.98	0.00	14.78	0.01	14.72	0.01	55.7
54142−2667−522	133.0017548	11.935228	37.0	1.0	5811	118	4.01	0.28	−0.43	0.10	15.79	0.01	14.51	0.02	14.08	0.01	13.95	0.01	13.93	0.01	61.7
54142−2667−533	132.9949951	11.804089	34.2	0.9	5230	43	4.71	0.05	−0.32	0.14	17.75	0.02	15.95	0.01	15.27	0.01	15.06	0.01	14.95	0.01	54.0
54142−2667−537	132.9948730	11.833992	33.2	0.9	5702	173	3.72	0.40	−0.38	0.15	15.75	0.01	14.48	0.02	14.01	0.01	13.89	0.01	13.84	0.01	62.2
54142−2667−538	132.9619751	11.869030	34.2	0.8	5082	73	4.82	0.14	−0.24	0.09	18.29	0.01	16.31	0.00	15.57	0.00	15.31	0.00	15.19	0.01	48.3
54142−2667−539	133.0189972	11.980183	36.4	0.8	5141	43	4.12	0.42	−0.18	0.12	17.83	0.02	15.99	0.02	15.34	0.01	15.11	0.01	15.01	0.01	51.4
54142−2667−540	132.9941711	11.870869	33.8	0.9	5449	26	3.54	0.59	−0.25	0.18	17.31	0.01	15.62	0.01	15.03	0.01	14.83	0.01	14.77	0.01	55.6
54142−2667−549	133.0392914	11.646603	33.9	0.8	5427	84	4.20	0.22	−0.20	0.18	15.99	0.03	15.72	0.03	15.06	0.03	14.76	0.03	14.78	0.03	57.3
54142−2667−552	133.0268097	11.670785	32.4	0.8	5300	25	4.74	0.07	−0.52	0.11	17.25	0.01	15.58	0.00	14.96	0.01	14.74	0.01	14.64	0.01	55.5
54142−2667−561	133.0414581	12.175214	34.2	0.9	5843	166	4.42	0.16	−0.60	0.32	15.55	0.02	14.27	0.02	13.93	0.01	13.81	0.02	13.78	0.01	61.3
54142−2667−566	133.2035370	12.046594	28.8	0.8	5639	53	3.64	0.61	−0.25	0.16	16.60	0.02	15.09	0.02	14.58	0.01	14.43	0.02	14.35	0.01	58.9
54142−2667−575	133.0644226	11.883697	34.6	0.9	5705	145	3.89	0.39	−0.42	0.17	15.93	0.01	14.64	0.02	14.21	0.01	14.10	0.01	14.08	0.01	60.8